GRAPHENE NANOPLATELET BASED POLYMER COMPOSITES AND THEIR MULTIPLE APPLICATIONS

By

Zeyang Yu

A DISSERTATION

Submitted to
Michigan State University
in partial fulfillment of the requirements
for the degree of

Chemical Engineering - Doctor of Philosophy

2019

ABSTRACT

GRAPHENE NANOPLATELET BASED POLYMER COMPOSITES AND THEIR MULTIPLE APPLICATIONS

By

Zeyang Yu

Graphene nanoplatelets (GnP) consist of a few layers of graphene with thicknesses in the nanometer range. GnP is considered a multifunctional nanomaterial since it possesses excellent mechanical, electrical and thermal properties and as a result of its 2D structure, it offers the possibility of improving the barrier properties of a polymer matrix by reducing the permeability of small molecules through the polymer matrix. The aromatic planar basal surface of GnP consisting of carbon in the sp^2 state is inert and the carbon atoms at the GnP edges are the few sites at which functional groups can be added to GnP. When GnP is treated with strong acids, graphene oxide (GO) is formed. The carbon atoms are changed from sp^2 to sp^3 bonding and the basal plane surface has a large population of oxygen groups which change the surface from hydrophobic to hydrophilic. The GO has the potential to act as a coupling agent to improve the interfacial interaction between GnP and the polymer matrix. Besides adding GnP to a polymer to form a multifunctional polymer composite, the GnP can be fabricated into thin 'paper' electrodes by vacuum filtration of a GnP suspension. This GnP thin film has in-plane electrical conductivity similar to metals and when coated with an insulating polymer layer can function as an electrode in an electrostatic actuator. This dissertation investigates the interaction of GnP with polymer matrices, modifying the surface chemistry to improve the interfacial interaction between filler and matrix, and exploring new applications for multifunctional GnP-polymer composites.

The dispersion of GnP into a thermoplastic polyurethane (TPU) through melt blending has been investigated. The dispersion and alignment of GnP plays a key role in attaining the

multifunctional properties of the composite. 25wt% GnP was incorporated into TPU through an extrusion process, wherein the dispersion and alignment of GnP was controlled by the film extrusion speed. The effect of three film extrusion speeds of 2, 3 and 5 ft/min on the dispersion and alignment of GnP were investigated. The optimum extrusion conditions gave 350% improvement in through-plane thermal conductivity; 75% reduction in oxygen permeability; and the tensile modulus and strength increased by 950% and 470% respectively.

Graphene oxide (GO) was selected as a possible modifier to improve the interaction between GnP and an epoxy matrix. The rich oxygen based functional groups on the GO surface could function as reaction sites for chemical bonding directly or sites for adding other chemical groups such as diamines or epoxy. GO and GnP were sonicated together in a water phase forming a GO-GnP complex, followed by treatment with two different diamines ((p-phenylenediamine (PPDA) and Jeffamine D2000) with different chain lengths. The functionalized GO-GnP complex was added to the GnP-epoxy composite at a 0.86wt% loading. An increase in tensile modulus of ~60% was measured as a result.

The GnP was also investigated as a thin ‘paper’ electrode fabricated through vacuum filtration of a GnP suspension. GnP electrodes were fabricated from the compressed GnP paper and then coated on both sides with a thin epoxy layer. An electrostatic actuator was constructed from two parallel-aligned composite GnP paper electrodes fixed at the anode of the high power supply and with the cathode connected to the ground. The two composite electrodes would separate at the free end when a voltage was applied. The actuating performance was shown to be improved based on either increasing the surface area of electrode or enhancing the relative permittivity of the insulating layer between two electrodes.

ACKNOWLEDGEMETNS

There are many people that made earning my PhD degree possible. Firstly. I would like to thank my advisor Dr. Lawrence Drzal for taking me into his research group and giving me the guidance throughout my graduate studies. His knowledge, enthusiasm and support encourage me to overcome the difficulties, broaden the view of research area and achieve my goals in my PhD journey.

I would like to thank my committee members, Dr. Andre. Lee, Dr. Krishnamurthy. Jayaraman, and Dr. Ranjan. Mukherjee for being on my committee to help me test my knowledge and understanding.

I would like to acknowledge Mike Rich, Brian Rook, Per Askeland and Ed Drown for guidance in instruments and share their experience with me in designation for experiments and understanding for the results.

All of my lab colleagues, who were always there to discuss the results and support each other in research and career: Markus, Nick, Dee, Keith, Yan, Mariana, Chris, Mario, Eric. I also appreciate all my friends I got to know at Michigan State University. Your support always gave me the encouragements and motivations to carry on.

Last but not least, I want to thank my parents, Zhiqiang Yu and Jing Zhao, and my girlfriend Yusi Cheng, their love, support and patience while I pursued my PhD degree. All of you are always willing to listen to my complaint, encourage me and help me to solve the problems. I love you all forever.

It is a long journey to achieve my PhD degree, but with all of you, it is an important and meaningful period of life.

TABLE OF CONTENTS

LIST OF TABLES

LIST OF FIGURES

CHAPTER 1 - INTRODUCTION AND LITERATURE REVIEW

1.1 Motivation

Polymer systems are widely used due to their unique attributes: ease of production, light weight, and often ductile nature. However, polymers have lower modulus and strength compared to metals and ceramics [1]. One route to improve their intrinsic properties is to synthesize a polymer composite by incorporation of different fillers (fibers, whiskers, platelets or particles) into the host matrix, which has opened a new dimension in the field of materials science [2]. Polymer nanocomposites are composites in which at least one of the phases has dimensions in the nanometer range [3]. Introduction of polymer nanocomposites was through the research of the Toyota research group, which incorporated nanoclay into nylon-6 achieving an extraordinary set of mechanical, thermal and physical properties [4,5]. With the fast growing of availability of competing nanofillers (such as carbon based (carbon nanotubes, carbon black, graphene); oxides (clay, zirconium phosphate, silica, etc.); metal and intermetallic (silver, platinum, palladium, etc.) [6], it can be seen that the properties of nanocomposites are adjustable based on the incorporation of the nanoparticle in order to meet requirements from different applications.

First isolated in 2004 [7], graphene sheet, one atom thick two dimensional of sp^2-bonded carbon layer, stands out among many nanofillers. Its 2D structure not only provides a large aspect ratio but also various outstanding properties, which can modify the polymer to which they are added. Epoxy and polyurethane polymers are examples of thermoset and thermoplastic polymers respectively, which are some of the most widely used matrices in industrial production. However, either low tensile strength and modulus, poor thermal and electrical conductivity, and low gas barrier performance of thermoplastic polyurethane or low toughness, strength, and

resistance to crack propagation of a thermoset epoxy limits their applications in different areas. Few-layer Graphene Nanoplatelet sheets have the potential to function as a nano-filler for improving the weakness of above two polymer matrices, and many results have been documented in past publications [8-14]. However, the improvements in the physicochemical properties of the nanocomposites depends on the distribution and orientation of the graphene layers in the polymer matrix as well as interfacial bonding between the graphene layers and the host matrix. Pristine graphene is primarily hydrophobic with few chemical sites at the edges of the platelets which are compatible with polymers and therefore the reinforcing effect is less than desired and deteriorates at high filler loading. As a result, non-covalent or covalent functionalized graphene are necessary as the most effective filler for polymer nanocomposite. Graphene oxide, which is a heavily oxygenated graphene (with hydroxyl, epoxide, carboxyl, ketones functional groups) on the basal plane and edges overcomes many of the interaction and dispersion issues but lacks the mechanical, electrical and other properties intrinsic in the graphene. One possible approach would be to utilize graphene oxide as a coupling agent or surfactant to help disperse other carbon materials into the polymer for improving the dispersion and interfacial properties between fillers and host [15-16].

This dissertation investigates the nano-engineering of graphene in particular polymers to improve their mechanical properties, thermal conductivity, gas barrier properties, etc. by utilizing graphene oxide as the coupling agent for enhancing the properties of graphene-epoxy composite.

1.2 Epoxy polymers

Epoxy resins are an important class of polymeric materials, characterized by presence of more than one three-membered ring known as epoxide [17]. The vast majority of industrially important epoxy resins are bi- or multifunctional epoxides. The monofunctional epoxides are primarily used as reactive dilutes, viscosity modifiers, or adhesion promoter [18]. Epoxies are widely used as coatings, automotive primer, semiconductor packaging, adhesives, and aerospace composites. A common epoxy resin is diglycidyl ether of bisphenol-A (DGEBA), which is formed by reaction between bisphenol-A and epichlorohydrin under basic conditions. The structure of DGEBA is shown in Figure 1.1(a). When the n is at the very low value(n≈0.2), it is the liquid epoxy resin. Pure DGEBA is a crystalline solid with an epoxide equivalent weight (EEW) of 170. The typical commercial unmodified liquid resins are viscous liquids with EEW ~188 and viscosity of 11000-16000 mPa-s [18]. Solid epoxy resins with higher molecular weight, which contains repeating units and the degree of polymerization values vary from 2 to ~35 for commercial products.

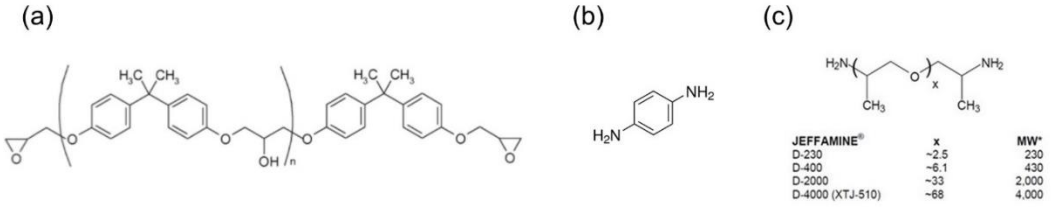

Figure 1.1. Chemical Structure of (a) DGEBA, (b) p-phenylenediamine, (c) JEFFAMINE series

The epoxy resins-curing agent systems exhibit the same features as other polymeric system during the curing process. These features include: extensive branching, passing through gel point, formation of a giant macromolecule with closed circuits, and eventually formation of a dense network [19]. For a curing process with amine based curing agents, the epoxide group is

activated by the formation of hydrogen bonds between the ring oxygen and hydrogen atom from amine. This process is considered as an auto-catalytic reaction as new forming hydroxyl group worked as catalyst [20,21]. The major reactions that occur between amine and epoxide in the curing process are shown in Figure 1.2. Nucleophilic attack by the primary amine on the less hindered methylene oxygen leads to formation of hydroxyl group and the primary amine transfers to secondary amine. Then a second nucleophilic attack by the secondary amine formed in last step on second epoxide ring. This process is usually slower compared to the first process, because of steric hinderance and the decrease in molecular mobility due to crosslink formation. Another possible reaction is between the hydroxyl group converted from the first and second step with the epoxide group, which is an etherification reaction [22-25]. The process and final properties of cured epoxy are determined by several factors: curing mechanism: kind of functional groups of curing agents; number of functional groups in resins and curing agent: density of crosslinking; chemical structures of epoxy resins and curing agent; molar ratio between resins and curing agent: degree of curing [26]. Depending on the actual requirement and application, the properties of cured epoxy can be easily adjusted. However, improvements in toughness, strength, resistance to crack propagation are still being sought in order to satisfy the increasing demands for high-performance applications. To address this issue, the nanofillers has been considered as an efficient way to modify its performance [27-32].

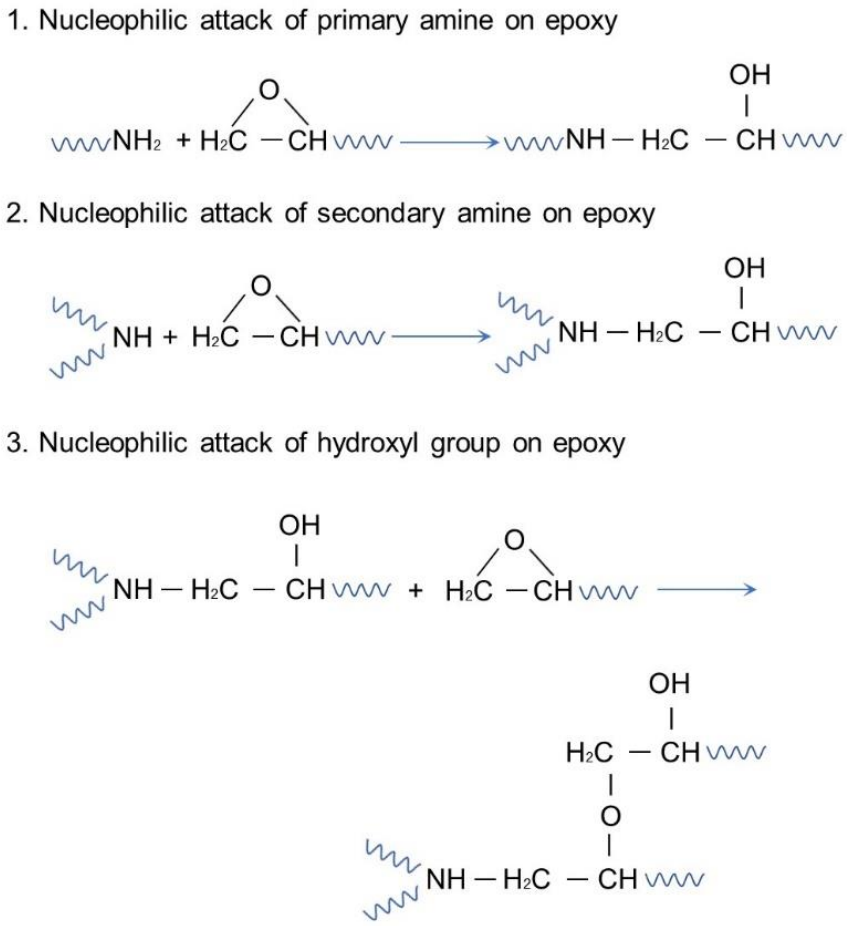

Figure 1.2. Curing reaction in epoxy/diamine [22]

1.3 Polyurethane Polymers

Thermoplastic polyurethane (TPU) elastomers are linear copolymers consisting of alternative blocks of hard and soft segments. TPUs are usually prepared through the reaction between three components, the long chain diols (polyester or polyether based), diisocyanates (aromatic or aliphatic based) and a small amount of short chain diols (function as chain extender) [33]. The formation of polyurethane elastomer is shown in Figure 1.3. The hard segments contain alternative sequences of isocyanate and chain extender, while the soft segment is formed by polyol and diisocyanate [34]. Because of different polarity and chemical structure of these

two segments, they form the hard domains and soft domains. Figure 1.4 represents the schematic illustration of this micro-structure.

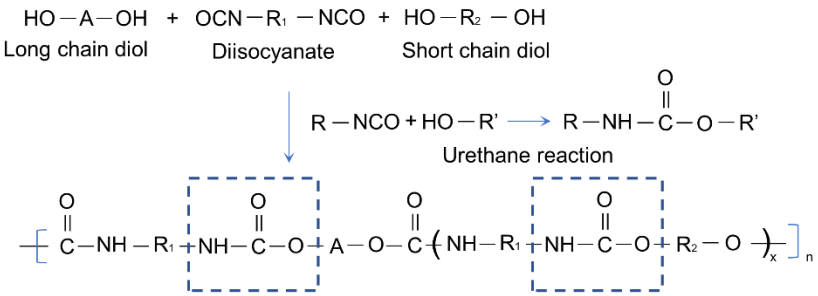

Figure 1.3. Formation of polyurethane elastomer [34]

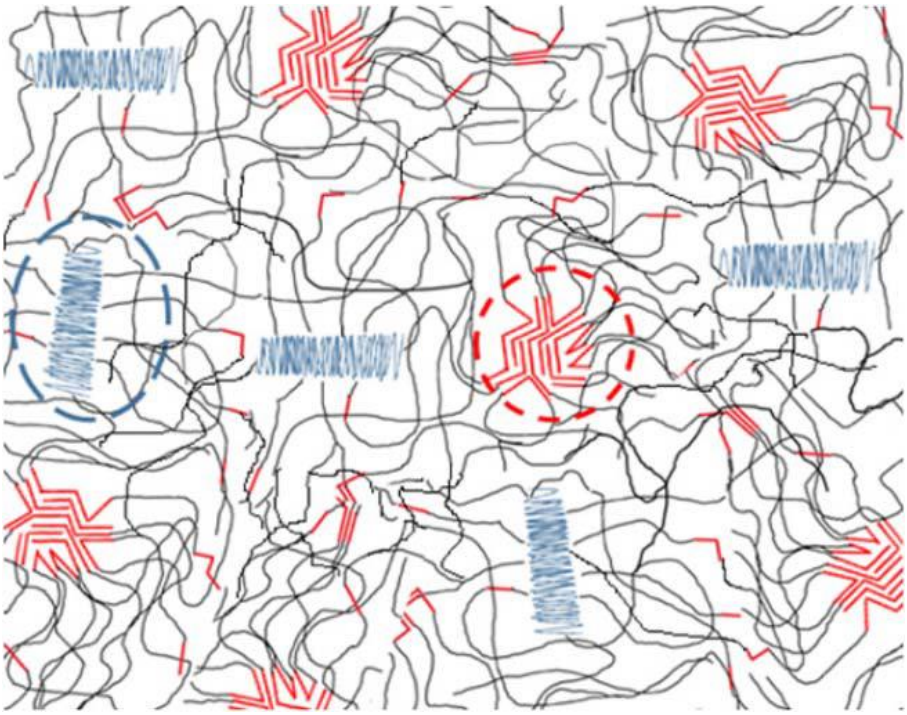

Figure 1.4. Microphase separated morphology of TPU. Red solid lines represent the hard segments and the blue region is soft segment. The black solid lines represent the amorphous part of soft segment blocks [35]

In linear polyurethane, the hard segments function as crosslinks, which lead to linear polyurethane showing elastomeric properties at low temperature but being processable at elevated temperature (above the melting point). The properties of thermoplastic polyurethane can be easily controlled by varying the chemical structure and content of each phase [36-41] or modifying on preparation procedures [42,43]. Currently, polyurethane is one of most widely used thermoplastic polymers in the areas of fiber, coating, adhesive and biomedical technology [44].

1.4 Types of nanofillers

Nanofillers, materials with at least one dimension in the nanometer range (<100 nm), can be categorized based on their dimensions, one dimensional filler: nanotubes and nanowires; two dimensional filler: nanoclay and graphene; and three dimensional filler: spherical and cubical nanoparticles. Nowadays, there are many different types of nanofillers (synthetic and natural) that can be incorporated into a polymer matrix to adjust its chemical and physical properties for emerging applications.

1.4.1 Nanoclay

Clays are naturally found as aluminosilicate platelets, which are naturally formed as stacks from a few to thousands of layers. They can be divided into four groups based on different crystalline structure: kaolinite, montmorillonite/smectite, illite and chlorite groups [45]. Montmorillonites are the most widely investigated and used to prepare nanocomposites. This is attributed to their high aspect ratio, unique intercalation/exfoliation properties and high Young's modulus (178-265 GPa) [46,47]. As shown in Figure 1.5, the structure of montmorillonites is one

alumina octahedral layer sandwiched by two silica tetrahedral layers. This three-layer structure is defined as a tactoid with a thickness ~1nm, which is the basic component for clay [48]. The gap between two tactoid layer is called the gallery or interlayer, where the cations exist to counterbalance the negative charge produced by the isomorphic substitution of atoms from the crystal. These cations usually are hydrated K^+, Na^+, which lead the clay to be hydrophilic and incompatible with hydrophobic polymer matrices [49]. In order to make a nanoclay polymer composite, the layered silicates are modified, by replacing the inorganic exchange cations in the gallery to alkyl-ammonium, phosphonium surfactant. These longer cations not only increase the gaps between tactoids but facilitate interactions with a polymer [50].

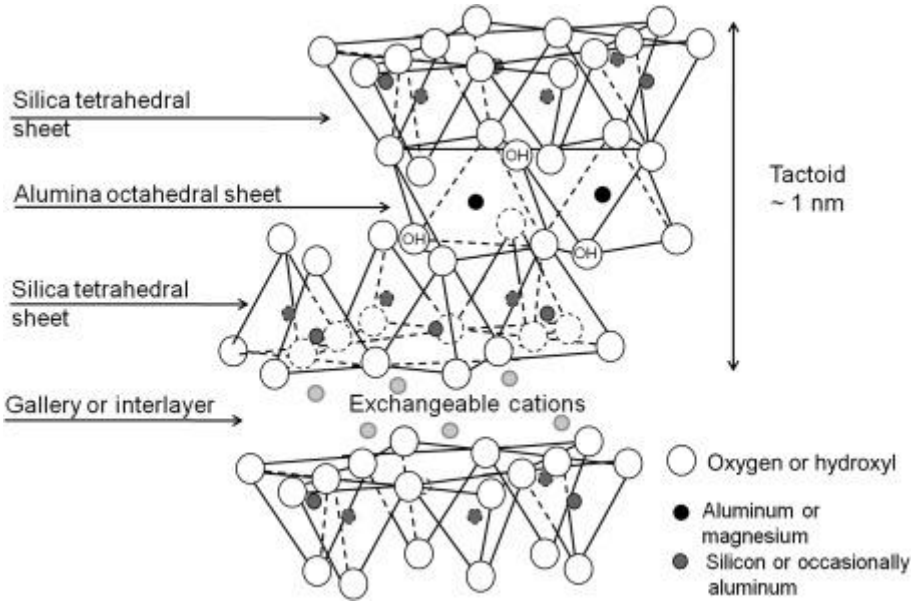

Figure 1.5. Structure of layered silicate [51]

Clay-polymer composites could be divided into three types as shown in Figure 1.6, the immiscible composites, intercalated composites and miscible exfoliated composites [52]. In most conditions, the exfoliated type shows the best reinforcement effect since a very high surface area

is exposed. But the state of nanoclay in the polymer matrix depends on the method of preparation for polymer composite. The most widely used ways to modify the clays are cation exchange, silane grafting and adsorption of polar polymers [53]. The cation exchange is controlled by the crystal size, pH and the type of exchangeable ions. The functionalized clay with more active sites can interact with the polymer matrix, and in some conditions, initiate the polymerization of monomers to improve the strength of the clay-polymer interface. For some commonly used polymers, like polyolefins, they do not have any polar groups which could react with aluminosilicate surface of the clay, a maleic anhydride polymer can be added into the system as the compatibilizer to enhance the mechanical properties of the clay-polymer composite [54,55].

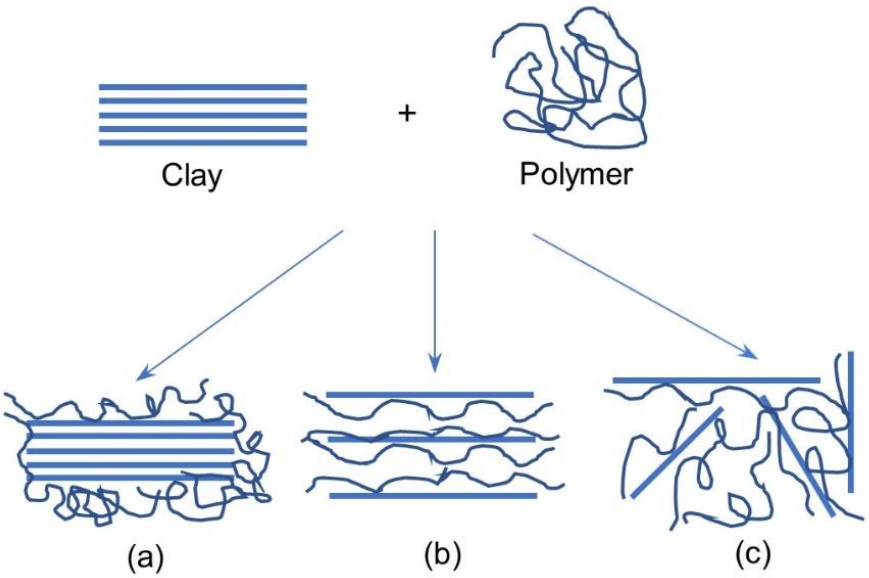

Figure 1.6. Schematic representation of different types of composite: (a) Phase separated; (b) Intercalated; (c) Exfoliated [51]

1.4.2 Carbon Based Nanofiller

Graphene sheets, one atom thick two-dimensional layers of sp^2-bonded carbon, have become a very interesting 2D material since their first isolation in 2004 [7]. This novel material possesses of a range of unusual properties, such as large theoretical surface area (2630 $m^2 g^{-1}$) [5,6], high

basal plane mechanical properties (~1 TPa elastic modulus and ~130 GPa ultimate strength) [57], outstanding thermal conductivity (~5000W m^{-1} K^{-1}) [58] and carrier mobility at room temperature (~10000 cm^2 V^{-1} s^{-1}) [59]. Graphene is also the building block for other carbon allotropes. As shown in Figure 1.7, it can be wrapped up to form a 0D particle, fullerenes; rolled into 1D nanotubes and stacked multiple layers to form the graphite. In 1985, fullerene was discovered as third allotrope form of carbon [60], soon after that, multi-wall/single-wall carbon nanotubes were reported by Iijima [61]. In addition to above mentioned three kinds of carbon based fillers and their derivatives, carbon black and carbon fiber are also widely researched as reinforcing fillers for improving the performance of polymer composite [62-65].

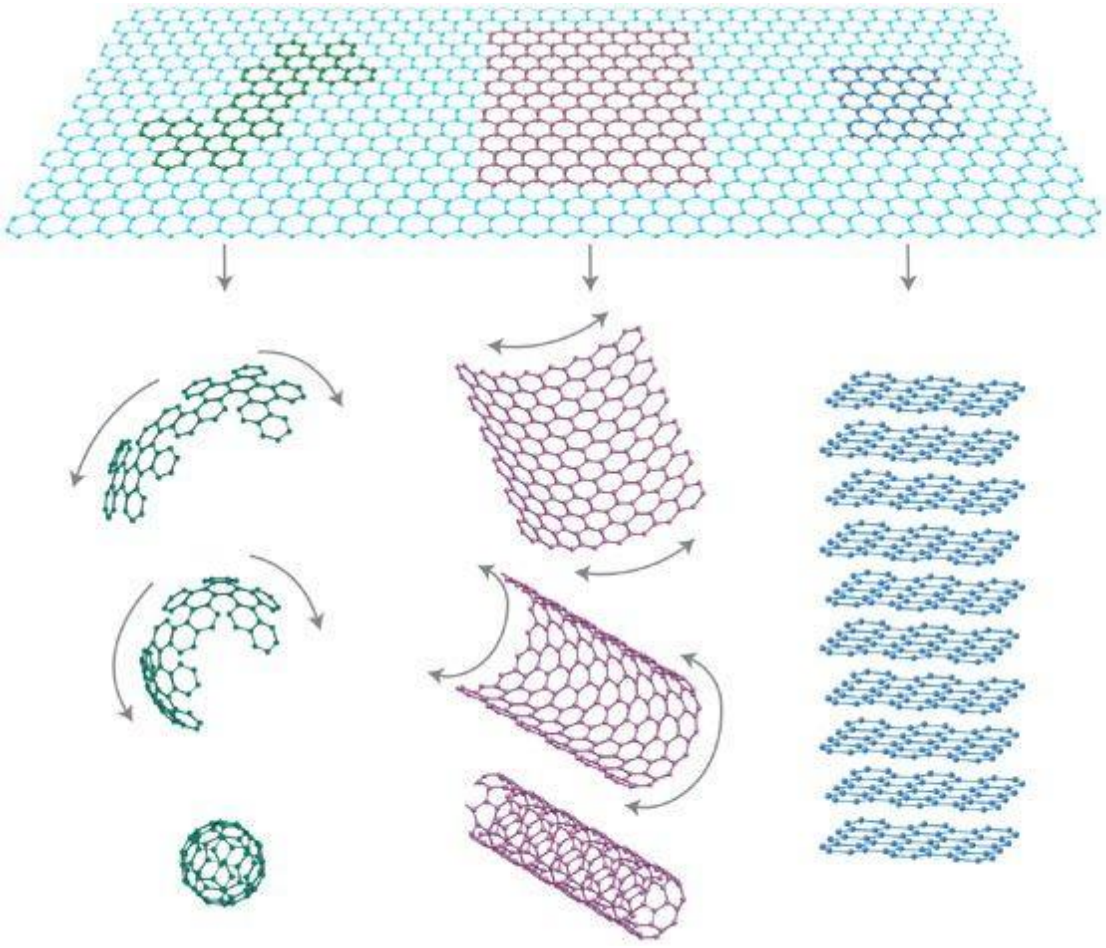

Figure 1.7. Illustration of graphene as building block to assemble into other carbon allotrope [66]

Carbon nanotubes have attracted attentions because of their unique structures and properties. High Young's modulus in the longitudinal direction, electrical conductivity varies from insulating to metallic based on the diameter and chirality of the tubes and their special hollow structures. Reports show that nanotubes possess extraordinary mechanical properties: tensile modulus ~1 TPa, tensile strength range from 50 to 150 GPa and a failure strain in excess of 5% [67,68]. Ebbesen et al. proved that conductivity of carbon nanotubes varied widely from tube to tube and they reported electrical conductivity of individual multi-wall carbon nanotube ranged from 10^7-10^8 S m^{-1} [69]. Berber et al. investigated the thermal conductivity of isolated nanotubes, the value was over 6000 W m^{-1} K^{-1}, which is comparable to graphene nanolayer [70]. Currently, most widely used methods to produce the carbon nanotubes are arc discharge method [61], laser ablation method [71] and chemical vapor deposition method [72]. But the cost for producing the carbon nanotubes remains high and increasing the manufacturing output is a continuing goal. While graphene with its extraordinary properties is considered as optimal filler for polymer matrix, at the same time, it is also faced with issues of large scale production for high quality sheets. Some general ways to produce the graphene: (1) mechanical exfoliation, it is operated as using the scotch tape to delaminate or peel off the layers of graphene from pyrographic graphite, but this method gives a small yield that is not sufficient for making polymer nanocomposite [7]; (2) chemical exfoliation, under this method, the graphite is reacted with mineral acids and strong oxidants, which imposes different oxygen based functional groups on the surface of graphene sheets, followed by ultrasonication process to create graphene oxide-single or multi layers of graphene with functional groups on its surface [73,74]. The graphene oxide, as an important derivate intermediate, is widely used as alternative filler for polymer composite. Because of its rich functional groups on surface, which could increase the affinity with polymer matrix and

further pave the way for surface designing based on its active sites on basal plane [75]. Graphene oxide must be chemically reduced by heat shock or a chemical reducing agent to restore the graphene structure, but one drawback of this method is formation of defects which disrupting and modifying the graphene surface and its electronic properties. (3) chemical vapor deposition, this method is a popular way to produce large scale, single or few layers of graphene. Ni and Co are mostly used as template, as they have high carbon solubility. Under high temperature, the carbon source diffuses onto the template surface where it reforms into graphene and can be subsequently peeled away from the template surface after cooling. During this process, the quality of graphene product is controlled by the cooling rate, reaction temperature, types of template and catalyst, concentration of carbon feeding source and residence time [76,77]. In Figure 1.8, the conventional synthesis methods of graphene and their applications are summarized.

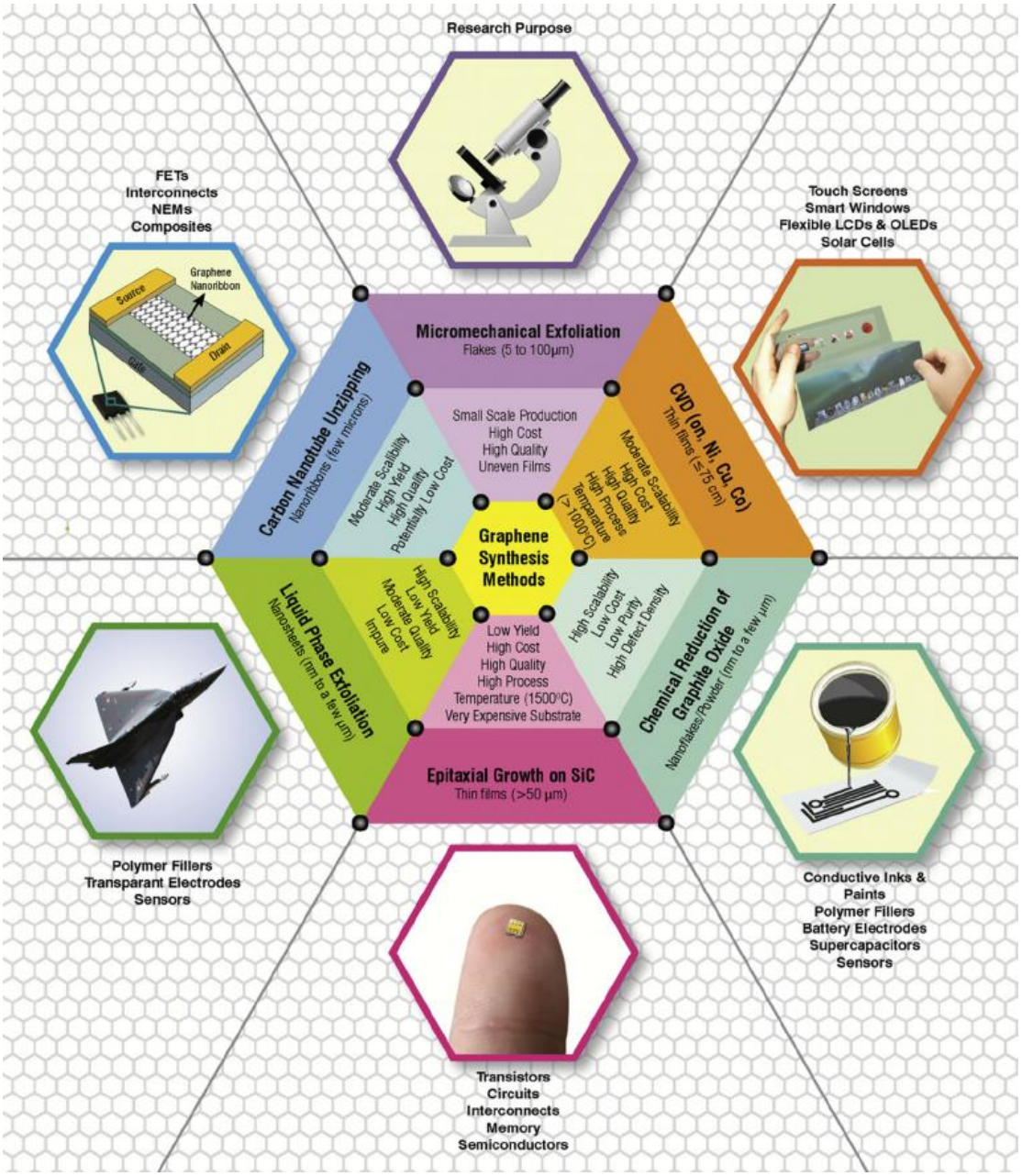

Figure 1.8. Schematic depicting various conventional synthesis methods of graphene and their applications [78]

Graphene nanoplatelets (GnP) are a stack of a few layers of graphene with thickness in the range of 5-15 nm and diameters from sub-micron to ~50 microns as shown in Figure 1.9.

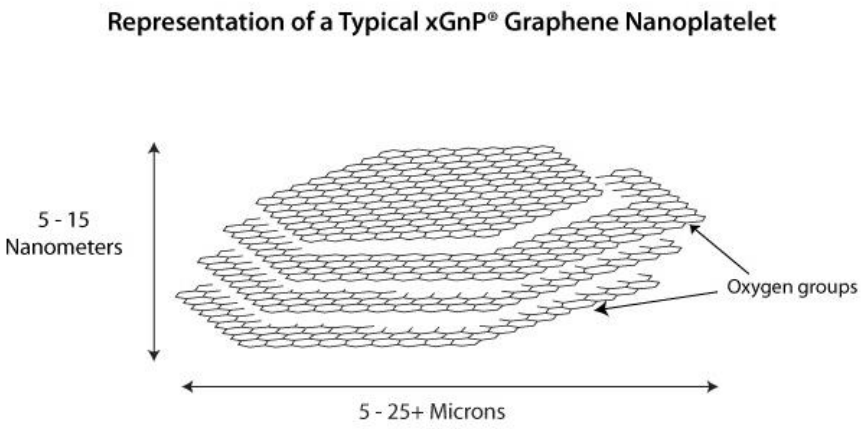

Figure 1.9. The structure of graphene nanoplatelets (GnP)

This is material is available commercially and produced in an industrial scale by thermal exfoliation of graphite intercalated compounds through microwave processing followed by pulverization [79]. Figure 1.10 represents the scanning electron microscopy images of each stage of GnP production. This material is now widely used as a nano-filler for polymer composites, based on its low cost, good mechanical, thermal and electrical properties. However, similar to graphene nanosheet, this material also possesses a relative clean surface, with fewer than 5% of non-carbon functional groups on the edges, which means in order to improve the interfacial properties between GnPs and polymer matrix, the modification or functionalization on its surface is necessary. As mentioned above, besides using the traditional covalent or non-covalent methods, graphene oxide, is considered as an ideal coupling agent for large loading GnP-polymer composite. The graphene oxide not only improves the dispersion of GnPs in the polar solvents but also offering bonding sites which react with polymer chains. This idea is explained in more detail in chapter 3, about using graphene oxide or amine functionalized graphene oxide to improve the mechanical properties of GnP-epoxy composite.

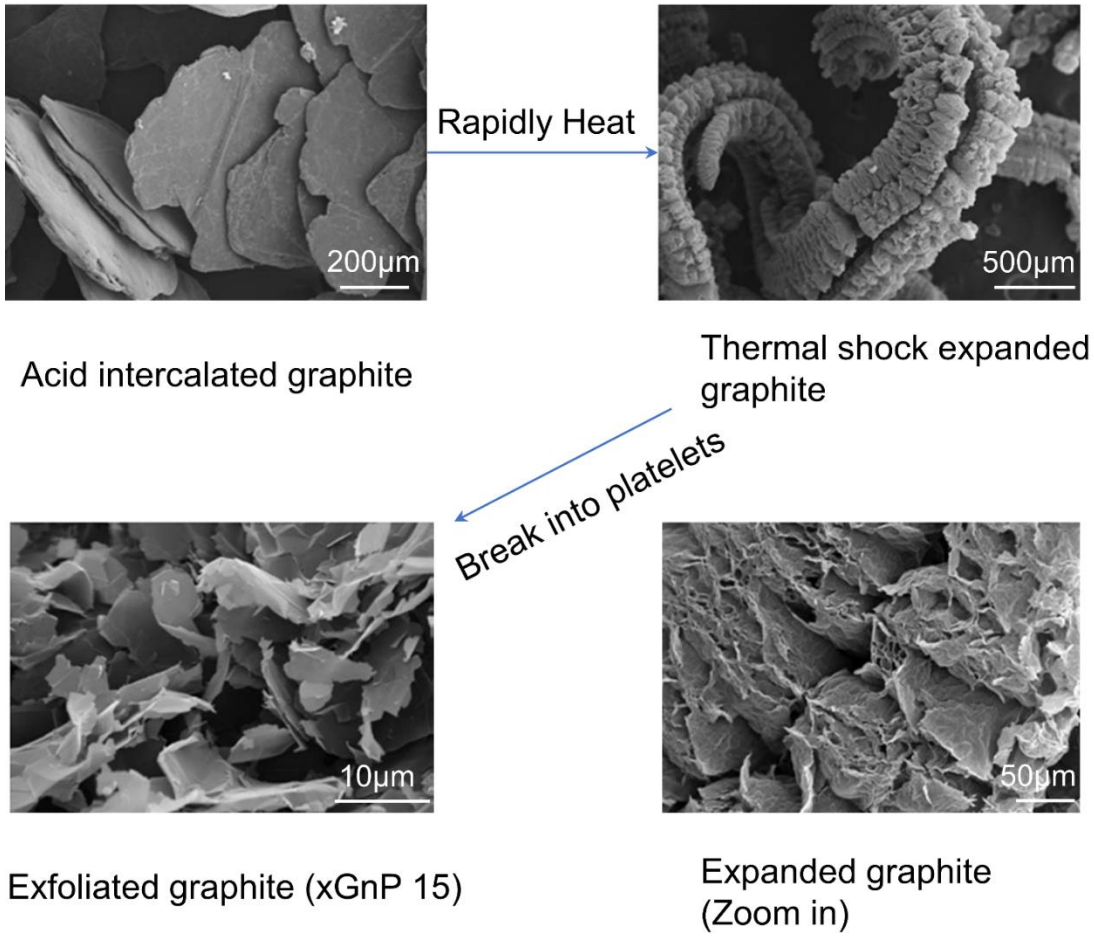

Figure 1.10. Synthesis process of graphene nanoplatelets [79]

1.5 Nanocomposite processing methods

A key to optimizing the properties of a nanocomposite, it is necessary to disperse nanofillers uniformly into the polymer matrix with optimized interfacial properties. Till now, various methods are applied to optimize the dispersion and interaction, among of them, the widely used and commercially available ones are solution mixing, melting processing and in situ polymerization.

Solution mixing is the most straightforward method for preparing polymer nanocomposite. Nanofillers and polymer are dispersed into a volatile solvent for uniformly mixing by ultrasonication, shear mixing or magnetic stirring. The solvent is evaporated in a controlled condition after a good dispersion is achieved. The solvent compatibility of polymer and filler is the critical factor. Acetone, dimethylformamide, tetrahydrofuran, N-methyl-2-pyrrolidone etc. are some commonly used solvents for preparing polymer composites [80,81]. However, re-stacking, aggregation or folding may occur during the process, which reduces the efficiency of the reinforcing effect. Thus, surface functionalization or the addition of a coupling agent are adopted to modify fillers for better dispersion and interaction.

For the melt processing, no solvent is needed, and fillers mix with polymer in the melted state. Extrusion and injection are widely used based on this method, during the process, shear force is generated to break apart aggregates of nanofillers. The dispersion state of fillers depends the residence time, extruder design and rotating speed and operating temperature [82]. Compared to solution mixing method, since solvent is not required, there is no need to worry about solvent selection or recovery of the solvent from evaporating process. However, there are also some limitations for this method, first one is that the mixing elements must be designed for dispersion of nanoparticles in a thermoplastic; second, the viscosity increases along with higher loading of fillers, which increases mixing time and hinders the uniformly dispersion; and third, there is a higher probability of reduction in particle size.

In the in situ polymerization method, fillers are usually dispersed within the liquid monomers, then polymerization is initiated by increasing temperature, adding an initiator or mixing two monomers. One of the advantages of this method is that it allows grafting polymer chains onto the surface of fillers. Besides, this technique is useful for some polymers which are

not soluble in most common solvent or thermally unstable. A variety of polymer composites have been prepared by this approach [83-85].

Besides the above mentioned methods, two other methods that can be used based on the application are the electro-spinning method and the layer-by-layer method. For electro-spinning, a high voltage power supply, a spinneret, and a collector are required. The spinneret is connected to a syringe where polymer composite solution or melt is stored. With the help of syringe pump, the solution can be fed through the spinneret with a constant and adjustable rate. When a voltage is applied, the pendent drop of polymer composite at the end of spinneret will be charged over the time. Two types of electrostatic force applied at this time: the electrostatic repulsive force and Coulombic force produced by external electric field. Once the electrostatic force overcomes the surface tension of polymer composite, the liquid jet is ejected from the nozzle and a stress is generated as a result of the stretching and whipping action, resulting in forming a long polymer composite fiber. Parameters which affects the final properties of polymer fiber are solution properties (viscosity, conductivity, surface tension), system properties (applied voltage, distance between spinneret and collector), environmental conditions (humidity, air velocity) [86]. For the layer-by-layer method, opposite ionic charges of polymer and nanofiller are used to sequentially produce a multilayer composite. A substrate is dipped into a solution with a cationic polymer, dried and dipped into a solution with an anionic nanoparticle. This process is repeated by several times until desired thickness is obtained. The thickness of the film relies on the concentration of polymer in the solution, molecular weight of polymer, ionic strength, pH and temperature. This method is not limited to electrostatic interaction only, subsequently, hydrogen bonding, charge-transfer interactions, coordination bonding and covalent bonding are applied to develop layer-by-layer composites [87-89].

1.6 Properties and Applications of nanocomposites

Any one or multiple nanoparticles ca be introduced into the polymer matrix for adjusting, modifying their properties, based on the main objectives and research experience. This section focusses on mechanical, thermal conductivity and gas barrier properties.

1.6.1 Mechanical Property

Mechanical properties are the important factors used to qualify ability of polymer composites for different applications. Some widely used criterions are tensile/flexural strength, modulus, impact strength, toughness. Standard sample preparation process and testing details have been established by American Society for Testing Methods (ASTM). Carbon based nanofillers are considered as the optimal reinforcing materials based on their extraordinary mechanical properties, and their high aspect ratio offers more active sites for further functionalization with different organic/inorganic molecules, which could adjust the mechanical properties of nanocomposites with different desirable attributes. At same time, different mathematical models are developed for estimating the properties of composite. Three widely used ones are shown below: rule of mixtures, Halpin-Tsai and Kerner-Lewis model [90-92]. The rule of mixture is straightforward, shown in equation (1):

$$E = E_f V_f + E_m V_m \quad (1)$$

Where, E_f, E_m, V_f, V_m are the modulus and volume faction of the filler and matrix. This equation is based on the assumption of iso-strain, that is $\varepsilon=\varepsilon_f=\varepsilon_m$. This model does not take the interaction between filler and matrix, or the geometric factor of different fillers into consideration, which lead to a rough estimation. The Halpin-Tsai model is developed that gives

quite satisfactory approximation of more complicated micromechanics results, shown in following equations:

$$\frac{E}{Em} = \frac{\left(1+\zeta\eta V_f\right)}{1-\eta V_f} \tag{2}$$

$$\eta = \frac{\frac{E_f}{E_m}-1}{\frac{E_f}{E_m}+\zeta} \tag{3}$$

Here, E_f, E_m, V_f are the modulus and volume faction of the filler and matrix, in general ζ=2s/t, where s is the length of the filler and t is the thickness. The volume fraction V_f should be below 0.7 otherwise, another empirical term is needed to put into for higher filler loading. Kerner-Lewis model shows similar format of the equation but changing the parameter ζ to A and A is calculated based on equation (4):

$$A = \frac{7-5\nu_m}{8-10\nu_m} \tag{4}$$

ν_m is the Poisson's ratio for the matrix, once again adjustment must be made for high volume factions of filler close to the maximum packing volume fraction.

Apart from mathematical proof, many experimental results have been used to verify the reinforcing effect of different nanofillers. Qi et al [93]. prepared thermotropic liquid crystalline epoxy(TLCP) grafted graphene oxide and incorporating this filler into epoxy matrix through solution mixing and casting method. With 1wt% loading, the impact and tensile strength improved to 51.4 kJ m^{-2}, 79.0 MPa, compared to neat epoxy 26.3 kJ m^{-2} and 55.4 MPa. The flexural modulus also increased from 1840 to 2275 MPa. Kanagaraj et al [94]. used multi-wall carbon nanotube, with diameter of 60-100 nm, length of 5-15 μm, to greatly improve the

toughness, Young's modulus which are 842.5 J and 1.3 GPa compared to 634.5 J , 1.1 GPa of neat polymer. One conclusion is that simply using one, pure carbon material as the filler to improve the mechanical property of composite cannot satisfy all growing requirements under different areas. Surface treatment/ functionalization applied onto carbon materials, such as oxidization, covalent/ non-covalent grafting molecules and taking advantage of the synergistic effect between different carbon allotropes have been investigated. This research focuses on investigating the addition of graphene oxide, with its highly oxidized basal plane offering the possibility of better interaction with the polymer matrix, which theoretically improves load transfer efficiency, and at the same time, having good interaction with the graphene nanoplatelet. As pointed out by Kim et al [15,16], graphene oxide works as a coupling agent for dispersing other carbon materials into polar solvents and maintaining a stable suspension for several weeks. In this research this property was important, and the GO was used as the coupling agent for improving the interaction between GnP/epoxy system. Further functionalization of the graphene oxide with different kinds of diamines was investigated, with a small amount of graphene oxide (ratio between graphene oxide and GnP set as 1:10, 1:50 by weight), the tensile modulus of final composite increased by over 50% with only 0.86wt% loading of GnP filler. The details are discussed in the following chapter.

1.6.2 Thermal conductivity

The thermal conductivity of graphene is due to the ease with which phonons can travel along the graphene basal plane. Figure 1.11 (a) depicts heat conduction in crystalline materials, which is also applicable to graphene. When the phonon contacts with outer crystal lattice, the phonon conducts from the outer atomic layers through the material by vibrations. Since the atoms are

densely stacked, the vibration quickly travels to the neighboring atoms. For graphene, because of strong covalent bonds, the vibration moves quickly in the basal plane which make graphene is highly thermally conductive. Different from crystalline materials, the heat transfer in polymers is not like the wave, as shown in Figure 1.11 (b), when the polymer contacts with heat source, heat also transfers to the outer atoms through vibration, however, this also leads to disordered vibration and rotation of atoms, which reduce the thermal conductivity [95]. When adding the conductive fillers into polymer matrix, a large number of interfaces are created, which causes phonon scattering and interfacial thermal resistance. Only when the loading excesses a specific amount—percolation threshold, the fillers could connect to each other and form the conductive path.

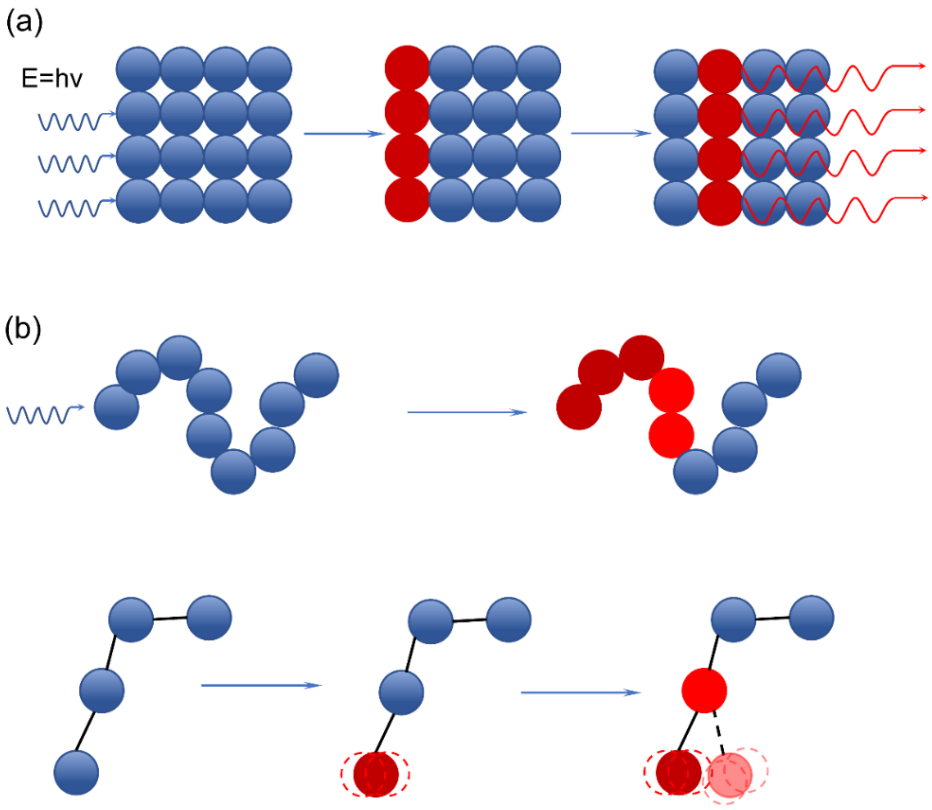

Figure 1.11. Schematic of thermal-conductive mechanisms: (a) crystalline materials, (b) polymer [95]

Mu et al [96]. prepared expanded graphite/silicone composite using solution-casting and melt-processing. They reported that thermal conductivity increased along with graphite content, the thermal conductivity obtained 0.32 W m^{-1} K^{-1} at 9phr, while for melt-mixing, it reached 0.24 W m^{-1} K^{-1}. Kostaginanakopoulou et al [97]. compared reinforcing effect between GnP and multi-wall carbon nanotubes(MWCNT) on epoxy composite. Through adding 3wt% filler into epoxy, thermal conductivity reached 0.36 W m^{-1} K^{-1} and 0.41 W m^{-1} K^{-1} for MWCNT and GnP respectively. When the loading was increased to 15wt%, the GnP-Epoxy had a conductivity of 0.80 W m^{-1} K^{-1}, which increased by a factor of 300% compared to neat epoxy. Further, researchers investigate the synergistic between different dimensions of carbon materials, like using CNT and GnP to build up 3D structure, then making the polymer composite based on this. And surface treatment is applied on the fillers to improve interfacial interaction, which also leads to less phonons scattering. In our research, the GnP-thermoplastic polyurethane (TPU) composite was prepared through extrusion, the effect of parameters such as extrusion speed, roller temperature, distance between roller and die on thermal conductivity of composite was investigated.

1.6.3 Gas barrier property

For a neat polymer, the crystallinity of the polymer greatly affects the barrier properties. Permeation of gas molecules require sufficient free volume for diffusing molecules to move through the polymer. The addition of 2D platelet fillers creates a tortuous pathway for a gas molecule, as shown in Figure 1.12. Both Neilson and Bharadwaj proposed a model to calculate gas permeability of polymer composite [98,99]. The interfacial strength also plays an important factor here, as a gap may form between fillers and matrix if the interaction is weak, and this gap

will be a path for gas molecules and thus causes less improvements. Various researchers have investigated using clay, graphene, graphene oxide or their functionalized derivatives to improve the gas barrier properties of different polymer matrix [100-102].

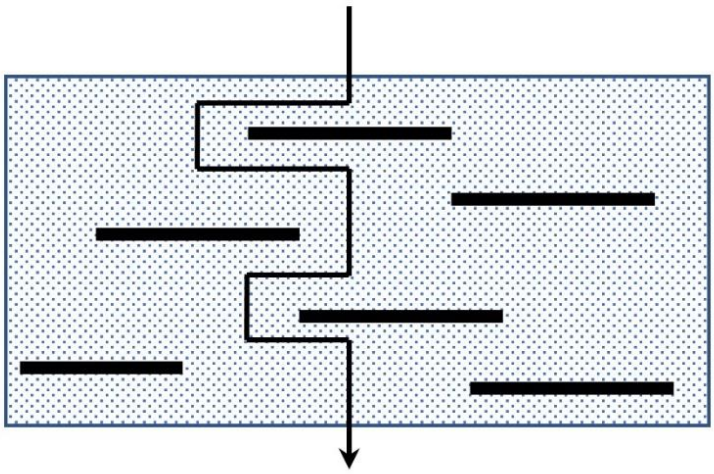

Figure 1.12. Zigzag diffusion path of a gas through platelets filler polymer composite [103]

As more different kinds of fillers are discovered or synthesized, and surface functionalized are further developed, multiple nanocomposite compositions are possible which broadens their applications. Based on improved mechanical properties, numerous automotive and general/industrial applications seeking the opportunities to use polymer composite to replace metal parts, such as vehicle structure or parts- engine covers, belts, door handles. For the platelets structure of filler in improving the gas barrier property, the polymer composite could be used in the fuel tank, fuel lines or containers. Adjustments in thermal/ electrical conductivity, pave the path for the polymer composite to be used as capacitors, sensors, fuel cell, solar cell. Surface functionalization and nanotechnology skills give the possibilities of polymer composite to be further used in biomedical applications, such as drug delivery, gene delivery and cancer

therapy [104,105]. With continues developing in science and technology, polymer nanocomposite have the potential to change our daily life in near future.

1.7 Dissertation Outline

This dissertation is divided into three main research chapters that provide a systematic review on using GnP, and its derivatives, graphene oxide, to improve the properties of different polymer matrix, and explore multiple applications. Chapter 2 discusses improvements of GnP on mechanical properties, gas barrier performance and thermal conductivity for a polyurethane matrix and compare the effect of distribution/ alignment of GnP on reinforcing results. Chapter 3 reviews using graphene oxide(GO)/f-GO as coupling agent to improve the interfacial properties between GnP and Epoxy. Chapter 4 looks at the use of GnP-Epoxy based system as an electrical actuator.

REFERENCES

REFERENCES

[1] Jordan J, Jacob KI, Tannenbaum R, Sharaf MA, Jasiuk I. Experimental trends in polymer nanocomposites—a review. Materials science and engineering: A. 2005 Feb 25;393(1-2):1-1.

[2] Kuilla T, Bhadra S, Yao D, Kim NH, Bose S, Lee JH. Recent advances in graphene based polymer composites. Progress in polymer science. 2010 Nov 1;35(11):1350-75.

[3] Roy R, Roy RA, Roy DM. Alternative perspectives on "quasi-crystallinity": non-uniformity and nanocomposites. Materials Letters. 1986 Aug 1;4(8-9):323-8.

[4] Kojima Y, Usuki A, Kawasumi M, Okada A, Fukushima Y, Kurauchi T, Kamigaito O. Mechanical properties of nylon 6-clay hybrid. Journal of Materials Research. 1993 May;8(5):1185-9.

[5] Usuki A, Hasegawa N, Kato M, Kobayashi S. Polymer-clay nanocomposites. InInorganic polymeric nanocomposites and membranes 2005 (pp. 135-195). Springer, Berlin, Heidelberg.

[6] Krishnamoorti R, Vaia RA. Polymer nanocomposites. Journal of Polymer Science Part B: Polymer Physics. 2007 Dec 15;45(24):3252-6.

[7] Novoselov K.S.; Geim A.K.; Morozov S.V.; Jiang D.; Zhang Y.; Dubonos S.V.; Grigorieva I.V; Firsov A.A. Electric field effect in atomically thin carbon films. science. 2004 Oct 22;306(5696): 666-9.

[8] Chen K, Tian Q, Tian C, Yan G, Cao F, Liang S, Wang X. Mechanical reinforcement in thermoplastic polyurethane nanocomposite incorporated with polydopamine functionalized graphene nanoplatelet. Industrial & Engineering Chemistry Research. 2017 Oct 5;56(41):11827-38.

[9] Tong Y, Bohm S, Song M. The capability of graphene on improving the electrical conductivity and anti-corrosion properties of Polyurethane coatings. Applied Surface Science. 2017 Dec 1;424:72-81.

[10] Kim H, Miura Y, Macosko CW. Graphene/polyurethane nanocomposites for improved gas barrier and electrical conductivity. Chemistry of Materials. 2010 May 17;22(11):3441-50.

[11] Li A, Zhang C, Zhang YF. RGO/TPU composite with a segregated structure as thermal interface material. Composites Part A: Applied Science and Manufacturing. 2017 Oct 1;101:108-14.

[12] Naebe M, Wang J, Amini A, Khayyam H, Hameed N, Li LH, Chen Y, Fox B. Mechanical property and structure of covalent functionalised graphene/epoxy nanocomposites. Scientific reports. 2014 Mar 14;4:4375.

[13] Rafiee MA, Rafiee J, Srivastava I, Wang Z, Song H, Yu ZZ, Koratkar N. Fracture and fatigue in graphene nanocomposites. small. 2010 Jan 18;6(2):179-83.

[14] Ahmadi-Moghadam B, Sharafimasooleh M, Shadlou S, Taheri F. Effect of functionalization of graphene nanoplatelets on the mechanical response of graphene/epoxy composites. Materials & Design (1980-2015). 2015 Feb 5;66:142-9.

[15] Kim J, Cote LJ, Kim F, Yuan W, Shull KR, Huang J. Graphene oxide sheets at interfaces. Journal of the American Chemical Society. 2010 May 19;132(23):8180-6.

[16] Cote LJ, Kim J, Tung VC, Luo J, Kim F, Huang J. Graphene oxide as surfactant sheets. Pure and Applied Chemistry. 2010 Dec 1;83(1):95-110.

[17] May C, editor. Epoxy resins: chemistry and technology. CRC press; 1987 Dec 23.

[18] Pham HQ, Marks MJ. Epoxy resins. Ullmann's Encyclopedia of Industrial Chemistry. 2000 Jun 15.

[19] Dušek K. Network formation in curing of epoxy resins. InEpoxy Resins and Composites III 1986 (pp. 1-59). Springer, Berlin, Heidelberg.

[20] Smith IT. The mechanism of the crosslinking of epoxide resins by amines. Polymer. 1961 Jan 1;2:95-108.

[21] Karkanas PI, Partridge IK. Cure modeling and monitoring of epoxy/amine resin systems. I. Cure kinetics modeling. Journal of applied polymer science. 2000 Aug 15;77(7):1419-31.

[22] Liu H, Uhlherr A, Varley RJ, Bannister MK. Influence of substituents on the kinetics of epoxy/aromatic diamine resin systems. Journal of Polymer Science Part A: Polymer Chemistry. 2004 Jul 1;42(13):3143-56.

[23] Mijovic J, Fishbain A, Wijaya J. Mechanistic modeling of epoxy-amine kinetics. 1. Model compound study. Macromolecules. 1992 Mar;25(2):979-85.

[24] Flammersheim HJ. Typical sources of error in the kinetic analysis of models with pre-equilibria: DSC investigations of epoxide-amine curing reactions. Thermochimica acta. 1997 Aug 1;296(1-2):155-9.

[25] Ansong O. Anomalous but useful behavior of epoxy adhesive system. International Journal of Adhesion and Adhesives. 2011 Oct 1;31(7):620-8.

[26] Kamon T, Furukawa H. Curing mechanisms and mechanical properties of cured epoxy resins. InEpoxy Resins and composites IV 1986 (pp. 173-202). Springer, Berlin, Heidelberg.

[27] Domun N, Hadavinia H, Zhang T, Sainsbury T, Liaghat GH, Vahid S. Improving the fracture toughness and the strength of epoxy using nanomaterials–a review of the current status. Nanoscale. 2015;7(23):10294-329.

[28] Ladani RB, Wu S, Kinloch AJ, Ghorbani K, Zhang J, Mouritz AP, Wang CH. Improving the toughness and electrical conductivity of epoxy nanocomposites by using aligned carbon nanofibres. Composites Science and Technology. 2015 Sep 29;117:146-58.

[29] Wang X, Jin J, Song M. An investigation of the mechanism of graphene toughening epoxy. Carbon. 2013 Dec 1;65:324-33.

[30] Bortz DR, Heras EG, Martin-Gullon I. Impressive fatigue life and fracture toughness improvements in graphene oxide/epoxy composites. Macromolecules. 2011 Dec 2;45(1):238-45.

[31] Chandrasekaran S, Sato N, Tölle F, Mülhaupt R, Fiedler B, Schulte K. Fracture toughness and failure mechanism of graphene based epoxy composites. Composites Science and Technology. 2014 Jun 16;97:90-9.

[32] Zhang H, Tang LC, Zhang Z, Friedrich K, Sprenger S. Fracture behaviours of in situ silica nanoparticle-filled epoxy at different temperatures. Polymer. 2008 Aug 11;49(17):3816-25.

[33] Razeghi M, Pircheraghi G. TPU/graphene nanocomposite: Effect of graphene functionality on morphology of separated hard domains in thermoplastic polyurethane. Polymer. 2018 Jun 11.

[34] Crawford DM, Bass RG, Haas TW. Strain effects on thermal transitions and mechanical properties of thermoplastic polyurethane elastomers. Thermochimica Acta. 1998 Dec 7;323(1-2):53-63.

[35] Solouki Bonab V, Manas-Zloczower I. Revisiting thermoplastic polyurethane, from composition to morphology and properties. Journal of Polymer Science Part B: Polymer Physics. 2017 Oct 15;55(20):1553-64.

[36] Gogoi R, Alam MS, Niyogi UK. Effect of soft segment chain length on tailoring the properties of isocyanate terminated polyurethane prepolymer, a base material for polyurethane bandage. International Journal of Research in Engineering and Technology. 2013;2(10):395-8.

[37] Krol P. Synthesis methods, chemical structures and phase structures of linear polyurethanes. Properties and applications of linear polyurethanes in polyurethane elastomers, copolymers and ionomers. Progress in materials science. 2007 Aug 1;52(6):915-1015.

[38] Ilavsky M, Dusek K. Structure and elasticity of polyurethane networks. 5. Effect of diluent in the formation of model networks of poly (oxypropylene) triol and 4, 4-methylenebis (phenyl isocyanate). Macromolecules. 1986 Aug;19(8):2139-46.

[39] Versteegen RM, Sijbesma RP, Meijer EW. Synthesis and characterization of segmented copoly (ether urea) s with uniform hard segments. Macromolecules. 2005 Apr 19;38(8):3176-84.

[40] Hernandez R, Weksler J, Padsalgikar A, Choi T, Angelo E, Lin JS, Xu LC, Siedlecki CA, Runt J. A comparison of phase organization of model segmented polyurethanes with different intersegment compatibilities. Macromolecules. 2008 Nov 19;41(24):9767-76.

[41] Prisacariu C, Scortanu E. Influence of the type of chain extender and urethane group content on the mechanical properties of polyurethane elastomers with flexible hard segments. High Performance Polymers. 2011 Jun;23(4):308-13.

[42] Lamba NK. Polyurethanes in biomedical applications. Routledge; 2017 Oct 19.

[43] Mi HY, Jing X, Peng J, Turng LS, Peng XF. Influence and prediction of processing parameters on the properties of microcellular injection molded thermoplastic polyurethane based on an orthogonal array test. Journal of Cellular Plastics. 2013 Sep;49(5):439-58.

[44] Woods G. The ICI polyurethanes book. 1990 Nov.

[45] Uddin F. Clays, nanoclays, and montmorillonite minerals. Metallurgical and Materials Transactions A. 2008 Dec 1;39(12):2804-14.

[46] Chen B, Evans JR. Elastic moduli of clay platelets. Scripta materialia. 2006 May 1;54(9):1581-5.

[47] Suter JL, Coveney PV, Greenwell HC, Thyveetil MA. Large-scale molecular dynamics study of montmorillonite clay: emergence of undulatory fluctuations and determination of material properties. The Journal of Physical Chemistry C. 2007 Jun 14;111(23):8248-59.

[48] Pavlidou S, Papaspyrides CD. A review on polymer–layered silicate nanocomposites. Progress in polymer science. 2008 Dec 1;33(12):1119-98.

[49] Ishida H, Campbell S, Blackwell J. General approach to nanocomposite preparation. Chemistry of Materials. 2000 May 15;12(5):1260-7.

[50] LeBaron PC, Wang Z, Pinnavaia TJ. Polymer-layered silicate nanocomposites: an overview. Applied clay science. 1999 Sep 1;15(1-2):11-29.

[51] Peponi L, Puglia D, Torre L, Valentini L, Kenny JM. Processing of nanostructured polymers and advanced polymeric based nanocomposites. Materials Science and Engineering: R: Reports. 2014 Nov 1;85:1-46.

[52] Chen B, Evans JR, Greenwell HC, Boulet P, Coveney PV, Bowden AA, Whiting A. A critical appraisal of polymer–clay nanocomposites. Chemical Society Reviews. 2008;37(3):568-94.

[53] Faucheu J, Gauthier C, Chazeau L, Cavaillé JY, Mellon V, Lami EB. Miniemulsion polymerization for synthesis of structured clay/polymer nanocomposites: short review and recent advances. Polymer. 2010 Jan 6;51(1):6-17.

[54] Kim DH, Fasulo PD, Rodgers WR, Paul DR. Structure and properties of polypropylene-based nanocomposites: Effect of PP-g-MA to organoclay ratio. Polymer. 2007 Aug 24;48(18):5308-23.

[55] Hotta S, Paul DR. Nanocomposites formed from linear low density polyethylene and organoclays. Polymer. 2004 Oct 13;45(22):7639-54.

[56] Stoller MD, Park S, Zhu Y, An J, Ruoff RS. Graphene-based ultracapacitors. Nano letters. 2008 Sep 13;8(10):3498-502.

[57] Lee C.; Wei X.; Kysar J.W.; Hone J. Measurement of the elastic properties and intrinsic strength of monolayer graphene. science. 2008 Jul 18;321(5887):385-8.

[58] Balandin A.A.; Ghosh S.; Bao W.; Calizo I.; Teweldebrhan D.; Miao F.; Lau C.N. Superior thermal conductivity of single-layer graphene. Nano letters. 2008 Feb 20;8(3):902-7.

[59] Huang X, Qi X, Boey F, Zhang H. Graphene-based composites. Chemical Society Reviews. 2012;41(2):666-86.

[60] Kroto HW, Heath JR, O'Brien SC, Curl RF, Smalley RE. C60: Buckminsterfullerene. Nature. 1985 Nov;318(6042):162.

[61] Iijima S. Helical microtubules of graphitic carbon. nature. 1991 Nov;354(6348):56.

[62] Donnet JB, editor. Carbon black: science and technology. CRC Press; 1993 May 13.

[63] Huang JC. Carbon black filled conducting polymers and polymer blends. Advances in Polymer Technology: Journal of the Polymer Processing Institute. 2002 Dec;21(4):299-313.

[64] Tang LG, Kardos JL. A review of methods for improving the interfacial adhesion between carbon fiber and polymer matrix. Polymer composites. 1997 Feb;18(1):100-13.

[65] Zhang Z, Hsu CT. Shear strengthening of reinforced concrete beams using carbon-fiber-reinforced polymer laminates. Journal of composites for construction. 2005 Apr;9(2):158-69.

[66] Geim AK, Novoselov KS. The rise of graphene. Nature materials. 2007 March; 6:183-191.

[67] Wong EW, Sheehan PE, Lieber CM. Nanobeam mechanics: elasticity, strength, and toughness of nanorods and nanotubes. science. 1997 Sep 26;277(5334):1971-5.

[68] Yu MF, Lourie O, Dyer MJ, Moloni K, Kelly TF, Ruoff RS. Strength and breaking mechanism of multiwalled carbon nanotubes under tensile load. Science. 2000 Jan 28;287(5453):637-40.

[69] Ebbesen TW, Lezec HJ, Hiura H, Bennett JW, Ghaemi HF, Thio T. Electrical conductivity of individual carbon nanotubes. Nature. 1996 Jul;382(6586):54.

[70] Berber S, Kwon YK, Tománek D. Unusually high thermal conductivity of carbon nanotubes. Physical review letters. 2000 May 15;84(20):4613.

[71] Guo T, Nikolaev P, Thess A, Colbert DT, Smalley RE. Catalytic growth of single-walled manotubes by laser vaporization. Chemical physics letters. 1995 Sep 8;243(1-2):49-54.

[72] Dai H. Carbon nanotubes: opportunities and challenges. Surface Science. 2002 Mar 10;500(1-3):218-41.

[73] Stankovich S, Dikin DA, Piner RD, Kohlhaas KA, Kleinhammes A, Jia Y, Wu Y, Nguyen ST, Ruoff RS. Synthesis of graphene-based nanosheets via chemical reduction of exfoliated graphite oxide. carbon. 2007 Jun 1;45(7):1558-65.

[74] Hummers Jr WS, Offeman RE. Preparation of graphitic oxide. Journal of the american chemical society. 1958 Mar;80(6):1339.

[75] Lerf A, He H, Forster M, Klinowski J. Structure of graphite oxide revisited. The Journal of Physical Chemistry B. 1998 Jun 4;102(23):4477-82.

[76] Somani PR, Somani SP, Umeno M. Planer nano-graphenes from camphor by CVD. Chemical Physics Letters. 2006 Oct 19;430(1-3):56-9.

[77] Li X, Cai W, An J, Kim S, Nah J, Yang D, Piner R, Velamakanni A, Jung I, Tutuc E, Banerjee SK. Large-area synthesis of high-quality and uniform graphene films on copper foils. science. 2009 Jun 5;324(5932):1312-4.

[78] Mittal G, Dhand V, Rhee KY, Park SJ, Lee WR. A review on carbon nanotubes and graphene as fillers in reinforced polymer nanocomposites. Journal of Industrial and Engineering Chemistry. 2015 Jan 25;21:11-25.

[79] Kim S, Do I, Drzal LT. Thermal stability and dynamic mechanical behavior of exfoliated graphite nanoplatelets-LLDPE nanocomposites. Polymer composites. 2010 May;31(5):755-61.

[80] Du F, Fischer JE, Winey KI. Coagulation method for preparing single-walled carbon nanotube/poly (methyl methacrylate) composites and their modulus, electrical conductivity, and thermal stability. Journal of Polymer Science Part B: Polymer Physics. 2003 Dec 15;41(24):3333-8.

[81] Wang F, Drzal LT, Qin Y, Huang Z. Mechanical properties and thermal conductivity of graphene nanoplatelet/epoxy composites. Journal of materials science. 2015 Feb 1;50(3):1082-93.

[82] Dennis H, Hunter DL, Chang D, Kim S, White JL, Cho JW, Paul DR. Effect of melt processing conditions on the extent of exfoliation in organoclay-based nanocomposites. Polymer. 2001 Nov 1;42(23):9513-22.

[83] Xiao X, Xie T, Cheng YT. Self-healable graphene polymer composites. Journal of Materials Chemistry. 2010;20(17):3508-14.

[84] Yu A, Ramesh P, Itkis ME, Bekyarova E, Haddon RC. Graphite nanoplatelet− epoxy composite thermal interface materials. The Journal of Physical Chemistry C. 2007 May 31;111(21):7565-9.

[85] Zhang K, Zhang LL, Zhao XS, Wu J. Graphene/polyaniline nanofiber composites as supercapacitor electrodes. Chemistry of Materials. 2010 Jan 27;22(4):1392-401.

[86] Li D, Xia Y. Electrospinning of nanofibers: reinventing the wheel? Advanced materials. 2004 Jul 19;16(14):1151-70.

[87] Such GK, Johnston AP, Caruso F. Engineered hydrogen-bonded polymer multilayers: from assembly to biomedical applications. Chemical Society Reviews. 2010 Dec 15;40(1):19-29.

[88] Shimazaki Y, Mitsuishi M, Ito S, Yamamoto M. Preparation of the layer-by-layer deposited ultrathin film based on the charge-transfer interaction. Langmuir. 1997 Mar 19;13(6):1385-7.

[89] Kohli P, Blanchard GJ. Applying polymer chemistry to interfaces: layer-by-layer and spontaneous growth of covalently bound multilayers. Langmuir. 2000 May 16;16(10):4655-61.

[90] Alger M. Polymer science dictionary. Springer Science & Business Media; 1996 Dec 31.

[91] Affdl JH, Kardos JL. The Halpin-Tsai equations: a review. Polymer Engineering & Science. 1976 May;16(5):344-52.

[92] Nielsen LE. Generalized equation for the elastic moduli of composite materials. Journal of Applied Physics. 1970 Oct;41(11):4626-7.

[93] Qi B, Lu SR, Xiao XE, Pan LL, Tan FZ, Yu JH. Enhanced thermal and mechanical properties of epoxy composites by mixing thermotropic liquid crystalline epoxy grafted graphene oxide. Express Polymer Letters. 2014 Jul 1;8(7).

[94] Kanagaraj S, Varanda FR, Zhil'tsova TV, Oliveira MS, Simões JA. Mechanical properties of high density polyethylene/carbon nanotube composites. Composites Science and Technology. 2007 Dec 1;67(15-16):3071-7.

[95] Li A, Zhang C, Zhang YF. Thermal conductivity of graphene-polymer composites: Mechanisms, properties, and applications. Polymers. 2017 Sep;9(9):437.

[96] Mu Q, Feng S. Thermal conductivity of graphite/silicone rubber prepared by solution intercalation. Thermochimica Acta. 2007 Oct 15;462(1-2):70-5.

[97] Kostagiannakopoulou C, Fiamegkou E, Sotiriadis G, Kostopoulos V. Thermal conductivity of carbon nanoreinforced epoxy composites. Journal of Nanomaterials. 2016.

[98] Nielsen LE. Models for the permeability of filled polymer systems. Journal of Macromolecular Science—Chemistry. 1967 Aug 1;1(5):929-42.

[99] Bharadwaj RK. Modeling the barrier properties of polymer-layered silicate nanocomposites. Macromolecules. 2001 Dec 18;34(26):9189-92.

[100] Yano K, Usuki A, Okada A, Kurauchi T, Kamigaito O. Synthesis and properties of polyimide–clay hybrid. Journal of Polymer Science Part A: Polymer Chemistry. 1993 Sep;31(10):2493-8.

[101] Wu J, Huang G, Li H, Wu S, Liu Y, Zheng J. Enhanced mechanical and gas barrier properties of rubber nanocomposites with surface functionalized graphene oxide at low content. Polymer. 2013 Mar 22;54(7):1930-7.

[102] Compton OC, Kim S, Pierre C, Torkelson JM, Nguyen ST. Crumpled graphene nanosheets as highly effective barrier property enhancers. Advanced materials. 2010 Nov 9;22(42):4759-63.

[103] Azeez AA, Rhee KY, Park SJ, Hui D. Epoxy clay nanocomposites–processing, properties and applications: A review. Composites Part B: Engineering. 2013 Feb 1;45(1):308-20.

[104] Das TK, Prusty S. Graphene-based polymer composites and their applications. Polymer-Plastics Technology and Engineering. 2013 Mar 16;52(4):319-31.

[105] Anandhan S, Bandyopadhyay S. Polymer nanocomposites: from synthesis to applications. Nanocomposites and polymers with analytical methods. 2011 Aug 9;1:1-28.

CHAPTER 2 – GRAPHENE NANOPLATELETS-THERMAL PLASTIC POLYURETHANE COMPOSITE FILMS FOR PACKAING APPLICATIONS

2.1 Introduction

Thermoplastic polyurethane (TPU) elastomers are linear block copolymers consisting of linear segmented blocks of hard and soft segments. TPUs are usually prepared through the reaction between three components, long chain diols (polyester or polyether based), diisocyanates (aromatic or aliphatic based) and small amounts of short chain diols (chain extender), forming a morphology of alternating rigid and flexible blocks [1]. Due to the different polarity and chemical structure of these two blocks, they form hard and soft phases [2]. The hard phase contains highly polar groups formed by the reaction between the diisocyanates and short chain diols; while the soft phase is formed through the reaction of polyols with diisocyanates. The properties of polyurethanes can be easily adjusted through varying the volume fraction or chain length of each phase [3-8] or by manufacturing parameters [9-10]. This leads the polyurethane to be a versatile synthetic soft material that has been widely used as fibers, coatings, adhesives [11] and in biomedical applications [12]. However, despite these advantages, low tensile strength and modulus, poor thermal and electrical conductivity, and low gas barrier performance limit its ability to fulfill many packaging application requirements.

Numerous studies revealed that the addition of layered materials into the TPU matrix improved its performance to meet the packaging requirements. Nanoclay was considered as one option and improvements for TPU composite were observed in thermal stability, mechanical properties and gas barrier properties [13-18]. However, another 2D material, graphene nanoparticles is a promising alternative which can simultaneously improve thermal conductivity, gas barrier performance, and mechanical properties. Graphene was first isolated in 2004 [19],

with its unique 2D structure and outstanding properties: high basal plane elastic modulus, around 1TPa and ultimate strength, around 130 GPa [20], outstanding thermal conductivity (~5000 W m^{-1} K^{-1}) [21], and large theoretical specific surface area (2630 m^2 g^{-1}) [22]. Research published over the last few years [23-26], showed that few-layer exfoliated graphene nanoplatelets (GnP) can be produced by flash thermal exfoliation of graphite intercalated compounds via a cost-effective process which can be utilized at industrial. This material and its derivatives are promising carbon based fillers for polymers. Chen et al. reported incorporating 0.5wt% GnP into TPU and found that the Young's modulus increased from 21.8 MPa to 30.2 MPa and tensile strength improved from 9.7 MPa to 24.5 MPa. Further, with polydopamine functionalization GnP (PDA-GnP), and under the same loading, the tensile strength reached 40.1 MPa [27]. Yadav et al. prepared 4-aminophenethyl alcohol and 3-methyl butyl nitrite functionalized GnP and found that with 2wt% of this functionalized GnP incorporated into polyurethane, the modulus improved from 12 MPa to 113 MPa and an enhancement of thermal stability of 30 $^{\circ}$C was measured [28]. Li et al. used a dip-coating method to produce a 1wt% loading of reduced graphene oxide coated polyurethane particles, and after compression molded obtained a composite, with a thermal conductivity of about 0.8 W m^{-1} K^{-1} [29].

In this work, the mechanically strengthened, thermally conductive composite TPU film was produced by a large scale extrusion process. Graphene nanoplatelets (GnP) were introduced into a thermoplastic polyurethane (TPU) through twin-screw extrusion. The effects of extrusion speed on dispersion and alignment of GnP fillers, composite thermal conductivity, gas barrier performance, and transient and dynamic mechanical properties of the composite films were evaluated.

2.2 Experimental section

2.2.1 Materials

The graphene nanoplatelets (GnP) used in the research were GnP-R10 supplied by XG Sciences, having an average diameter of 10μm and surface area of 30-60 $m^2 g^{-1}$ [30]. The TPU polymer used in the research was branched Elastollan 1185A10 [31] purchased from BASF and supplied in pellet form. The properties of these two materials are available on their official website.

2.2.2 Fabrication of GnP-TPU Composite Films

The TPU pellets were dried at 100 ˚C for 2 h in a vacuum oven before melt-blending with GnP. A Leistritz twin-screw extruder (MIC27/6L-48D), operating in the counter-rotation mode with a length/diameter of 48:1, was used for preparing GnP-TPU composite films. The twin screw rotating speed was fixed at 100 rpm. Loading speed for TPU/GnP was set as 0.23 kg h^{-1} and 0.68 kg h^{-1} based on the nominal 25wt%(14vol%) of filler in the final product, with filler content verified by the TGA. Figure 1 shows the schematic illustration of the film manufacturing process. The whole extrusion chamber consists of eleven zones and the die, with the length of each zone around 10.8 cm. TPU pellets were fed into the extruder at zone #1, and the side feeder for the GnP fillers was fixed at zone #5. The temperature settings for each zone are shown in Figure 2.1. Roller 1,2,3,5 were kept at the same speed defined as the ‘film extrusion speed’; rollers 4,6 were freely rotating. The thickness of composite film was controlled by the gap of the die and the film extrusion speed. Three film extrusion speeds (2FPM, 3FPM, 5FPM) were selected to produce films with thickness around 140 μm, 100 μm and 80 μm. The neat TPU, GnP-TPU-2FPM, 3FPM, and 5FPM are referred to as ‘Neat’, ‘2FPM’, ‘3FPM’ and ‘5FPM’.

Zone	#1	#2	#3	#4	#5	#6	#7	#8	#9	#10	#11	Die
T (°C)	170	170	180	190	200	190	180	170	170	170	170	175

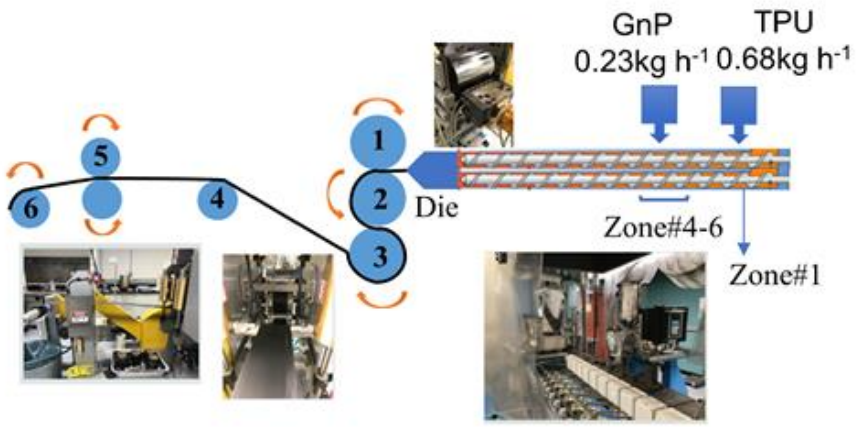

Figure 2.1. Schematic process for producing composite film and temperature setting for difference zones along the extrusion chamber

2.2.3 Characterizations of the GnP/TPU Composite Films

The thermal conductivity of the laminate films is related to their thermal diffusivity, density, and heat capacity by the following equation:

$$k = \alpha \rho C_p$$

where k is the thermal conductivity in W $m^{-1}K^{-1}$, α is the thermal diffusivity, m^2 s^{-1}, and C_p is the heat capacity J kg^{-1} K^{-1}. A Netzsh HyperFlash® system was used to measure the thermal diffusivity of the laminate films via the laser flash method. Four 1.3 x 1.3 cm squares were cut from each composite film. Both sides of the squares were coated with graphite to reduce light reflection. Five laser shots were performed on each specimen with a 25% filter, a pulse width ~170 µs and with applied voltage of 304 V. The Micromeritics AcccuPyc II 1340 was used to measure the film density through inert gas displacement and the average calculated from 10 measurements. A TA instruments Q2000 differential scanning calorimeter (DSC) was used to

measure heat capacity of the films. The temperature ramped from -10 °C to 50 °C at a rate of 10 °C min^{-1} for at least three replicates for each composite film composition.

The O_2 permeability was measured with a Mocon OX-TRAN 2/20 ML for a circular sample with area of 5 cm^2, tested at room temperature. The results were collected for at least ten cycles after equilibrium was reached. All the reported results were normalized to the thickness of the sample.

The transient and dynamic tensile properties were examined with a TA Instrument RSA III Solids Analyzer equipped with a force-convection oven. All the samples were cut into a rectangular shape ~60 mm in length and ~6.5 mm in width. The thickness varied with the film extrusion speed. For tensile testing, the sample was strained and retracted in two consecutives tensile cycles, with the speed 0.1 mm s^{-1} for 30 s. The initial gage length was fixed at 20 mm. Each specimen was replicated five times and the results were averaged. The frequency was swept from 0.5 to 50 rad s^{-1}, with a strain amplitude of 0.1%. The properties of GnP-TPU composite were measured at 25 °C and 50 °C. Three replicates of each composite were measured.

The Dynamical mechanical analysis (DMA) of the samples was conducted with a TA Instruments DMA Q800 in tension mode. The strain amplitude was set at 20 μm, at a frequency of 1 Hz. The samples were heated at 3 °C min^{-1} from -80 °C to 100 °C. Three replicates were tested for each sample.

The loss in weight with temperature was measured with a TA Instruments Thermogravimetric Analyzer TGA Q500 in high resolution mode. The temperature ramp was from 25 °C to 800 °C with 25 °C min^{-1}.

The distribution and alignment of GnP in the TPU matrix was investigated by ZEISS focused ion beam scanning electron microscope operated under 12 kV. The samples were cut

along extrusion/transverse direction, mounted into epoxy and followed by several polishing steps. Then the samples were coated with Tungsten before doing analysis.

2.3 Results and Discussion

2.3.1 Film Morphology

Scanning electron microscope (SEM) was used to investigate the dispersion and alignment of GnP in the TPU matrix. Figure 2.2 shows that, after mixing and extrusion, the GnP nanoparticles were randomly and uniformly dispersed in the TPU matrix. After going through the roller, the GnP nanoparticles started to align along the film extrusion direction. As the film extrusion speed increased, higher concentrations of small GnP formed concentrated along the center line of the extruded film. Likewise, it can be seen in the images of the 5 FPM sample that there are more gaps existing around the GnP as film extrusion speed increased.

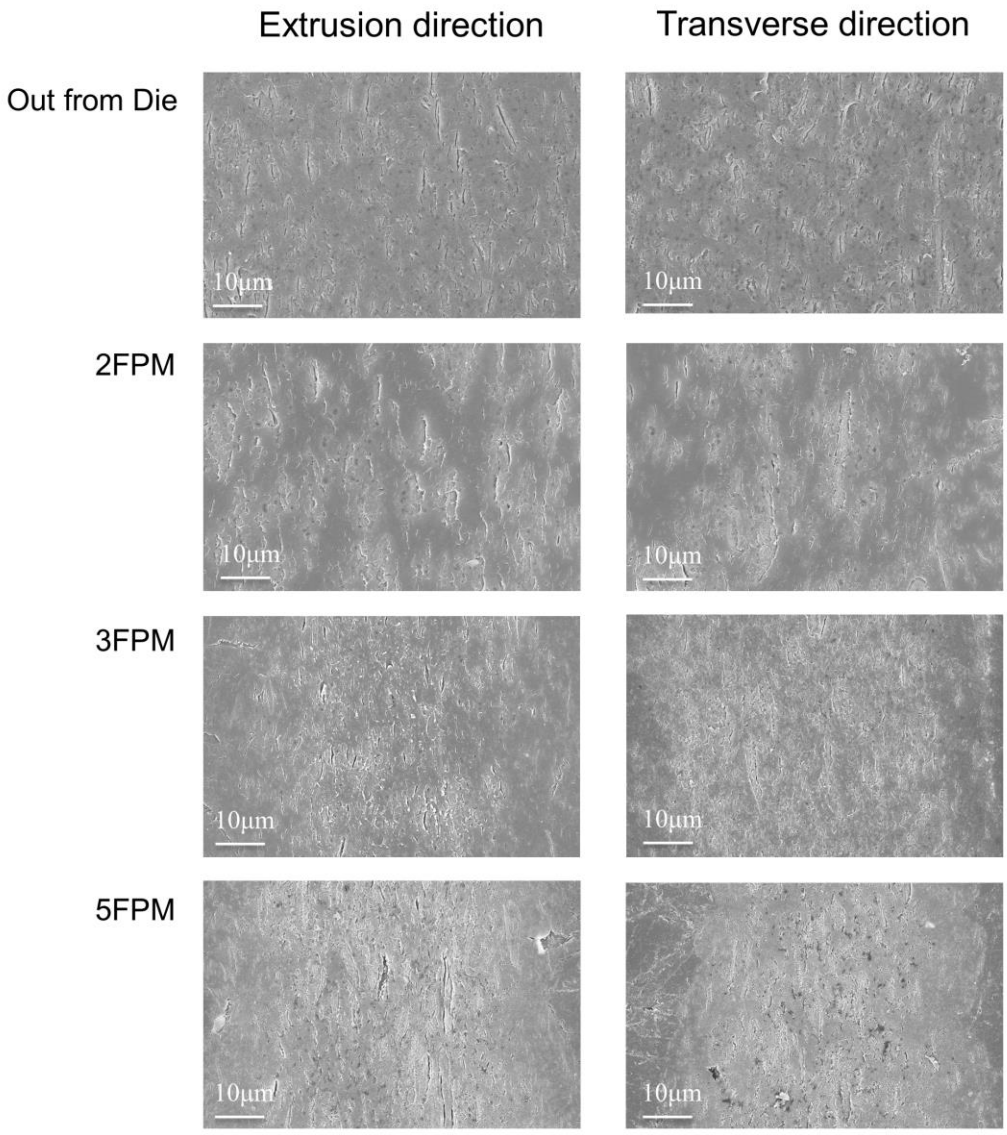

Figure 2.2. Cross-section for GnP/TPU composite under different film extrusion speeds

The higher magnification image of Figure 2.3 shows that all the samples show gaps between the fillers and matrix which was attributed to weak bonding between them. During the extrusion process, different viscosity and flexibility caused the fillers to separate from the matrix.

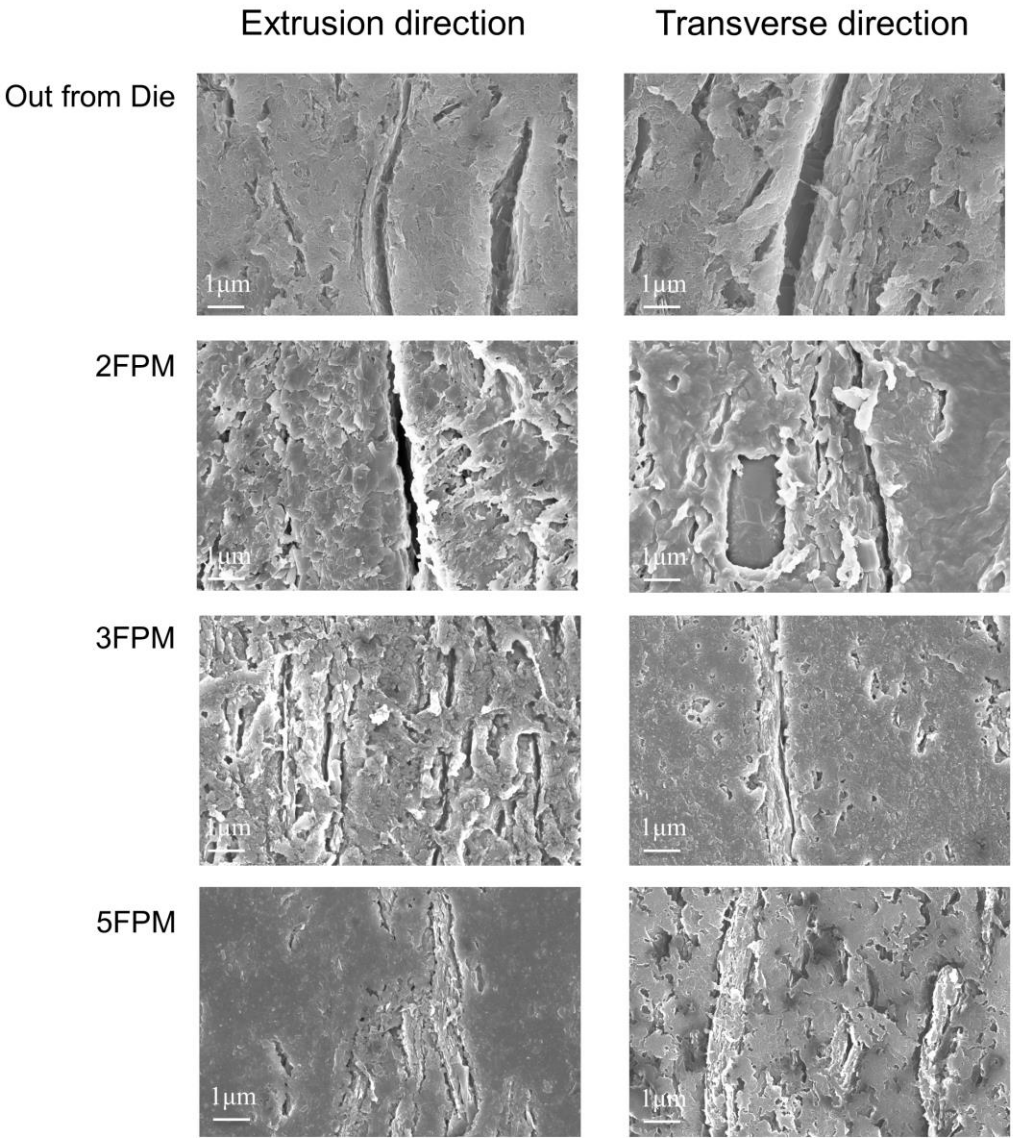

Figure 2.3. Cross-section for GnP/TPU composite under different film extrusion speeds (High magnification). Gaps between fillers and matrix can be clearly observed, and the gap density increases with higher roller speed.

2.3.2 Thermal Conductivity of the composite films

From Table 2.1, the GnP/TPU composite films increased their through-plane thermal conductivity up to 350% compared to the neat TPU. Other researchers have reported on using the GnP in epoxy matrix composites [32-34]. This thermoset system with less phonons scattering

could achieved conductivity of 3 W m^{-1} K^{-1} or higher with GnP loading of 20wt% or higher. In this research, a stretchable, thermally conductive film for packaging was produced. As GnP is a 2D material, the through plane thermal conductivity not only depends on dispersion but also the alignment of this filler and the contact between individual particles. The spacing between GnP particles increased with increasing stretching resulting in decreasing of the conductivity when film extrusion speed was increased. When the film extrusion speed increased, more GnP tended to be aligned in the x-y plane in the TPU matrix. However, this led to fewer vertical aligned nanoplatelets which could form a conductive path in the through-plane direction. GnP itself has a much higher in-plane thermal conductivity compared to through-plane at lower film extrusion speed, the higher through-plane thermal conductivity is the result of a combination of horizontal and vertical aligned nanoplatelets at lower speed. GnP is more randomly distributed along z-direction. Under high film extrusion speed conditions, this effect weakened, and fewer vertical aligned nanoplatelets were produced. These two possibilities led to the slightly drop in the through-plane thermal conductivity.

Table 2.1. Through-plane thermal conductivity of the GnP/TPU films

Sample	Conductivity W m^{-1} K^{-1}
Neat TPU	0.20±0.01
GnP/TPU-2FPM	0.90±0.19
GnP/TPU-3FPM	0.81±0.09
GnP/TPU-5FPM	0.77±0.04

2.3.3 Oxygen Permeability of the composite films

In Table 2.2, Compared to the neat TPU film, the through film direction oxygen permeability of the GnP/TPU composite film decreased. This was attributed to platelet structure and large aspect ratio of GnP, which created a tortuous diffusion path due to the impermeability

of nanoplatelets [35,36]. When film extrusion speed increased from 2FPM to 3FPM, the oxygen permeability decreased around 65%, but after the speed increased, the permeability did not drop further. From 2FPM to 3FPM, the higher speed produced a greater degree of GnP in-plane alignment in the x-y plane which resulted in creating a better barrier to restrict gas diffusion. But once the speed exceeded a specific level, the GnP particles were pulled further apart. Also considering the weak interaction across the GnP-TPU interface, separation between the GnP and TPU resulted in a path for gas molecules and this was responsible for the lack of improvement in barrier properties [36,37].

Based on these results, other modifications such as surface functionalization of GnP nanoplatelets to improve the interaction with the TPU matrix could further decrease the permeability. Also, a process using a layer-by-layer technique could also be beneficial to creating a high density stack of GnP layers.

Table 2.2. Through-plane Oxygen permeability for GnP/TPU composite film

Sample	Permeability m^3-m [m^{-2} day^{-1}]*10^{-7}
Neat TPU	2.15±0.236
GnP-TPU-2FPM	1.73±0.120
GnP-TPU-3FPM	0.58±0.038
GnP-TPU-5FPM	0.61±0.052

2.3.4 Tensile Properties of Composite Films

Two stress-strain cycles were analyzed for the composite films as shown in Figure 2.4. The failure strain for the GnP-TPU composite film could reach around 70%, but 15% strain was selected to investigate the Mullins effect [38] and mechanical properties of the composite films. In Figure 2.4, the neat TPU displays typical elastomer properties, but when incorporating GnP into the matrix, the hysteresis is enhanced. The second cycle hysteresis is much lower than the

first cycle, which is attributed to the debonding of the GnP from the TPU and reorientation of GnP that occurred primarily in the first cycle. The GnP-TPU composites shown a significant softening effect compared to the neat TPU. Mechanical results summarized in Figure 2.5 calculated from stress-strain cycles, at 25 °C, show that the 2 FPM sample increased in modulus ~ 950% and in strength ~ 470% in the extrusion direction. The properties in the transverse direction dropped ~38% in modulus and strength. When the film extrusion speed increased, the modulus and peak stress decreased both in extrusion and transverse directions. This was the result of the inverse relationship between film extrusion speed and dispersion property of GnP. But if the ratio between Peak II and Peak I (the tensile stress at 15% strain from second and first stress-strain cycle) are compared, for different film extrusion speed samples, they show similar values indicating that the viscoelastic properties of the composite films are not as sensitive to varying the film extrusion speed. The same trend exists as the temperature increases up to 50 °C. Compared to the neat TPU at the same temperature, the 5 FPM composite film still has a 700% and 350% higher modulus and peak stress. Compared to modulus I, peak I there was a ~35% and ~6% decrease in modulus II and peak II. This was also attributed to poor interaction between the GnP fillers and TPU matrix. Since only weak Van der Waals forces were present, this led to low adhesion between the fillers and matrix. During the extrusion mixing process, it was observed that the GnP fillers tended to form agglomerates with gaps formed between the agglomerates and matrix. After the first stress-strain cycle, these defects aggregated which further deteriorated the mechanical property of composite films. The permanent strain after each cycle markedly increased after GnP was introduced into the TPU. The GnP acted as a rigid element which hindered the motion of flexible polymer chains. Under different film extrusion speeds or higher

temperatures, this permanent strain does not show a large difference, as the filler's loading and adhesion between fillers and matrix would be the dominating factors [39].

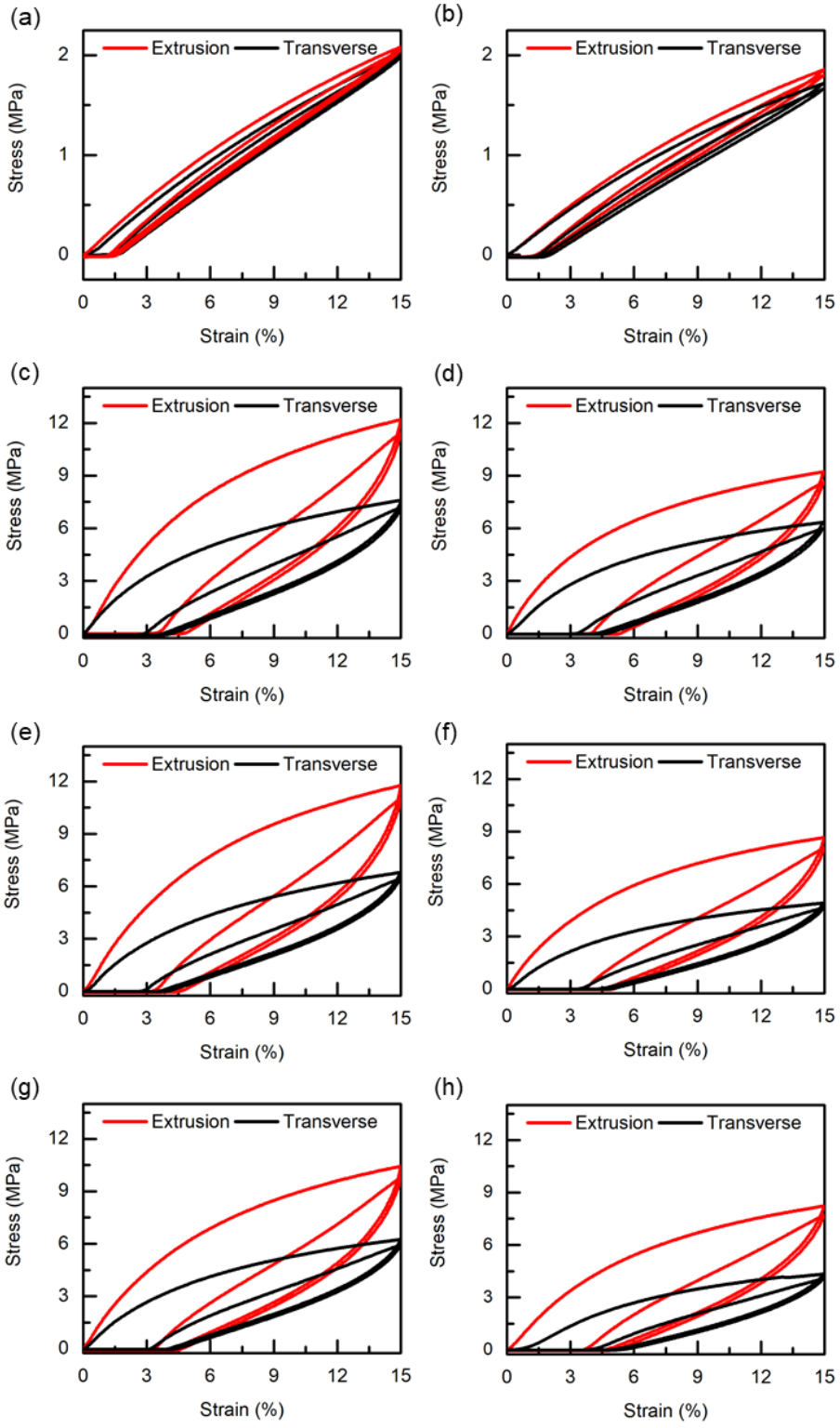

Figure 2.4. Two stress-strain cycles with strain amplitude of 15%. ((a): Neat TPU; (c): GnP-TPU-2FPM; (e): GnP-TPU-3FPM; (g): GnP-TPU-5FPM were samples tested under 25 °C, and (b): Neat TPU; (d): GnP-TPU-2FPM; (f): GnP-TPU-3FPM; (h): GnP-TPU-5FPM were samples tested under 50 °C

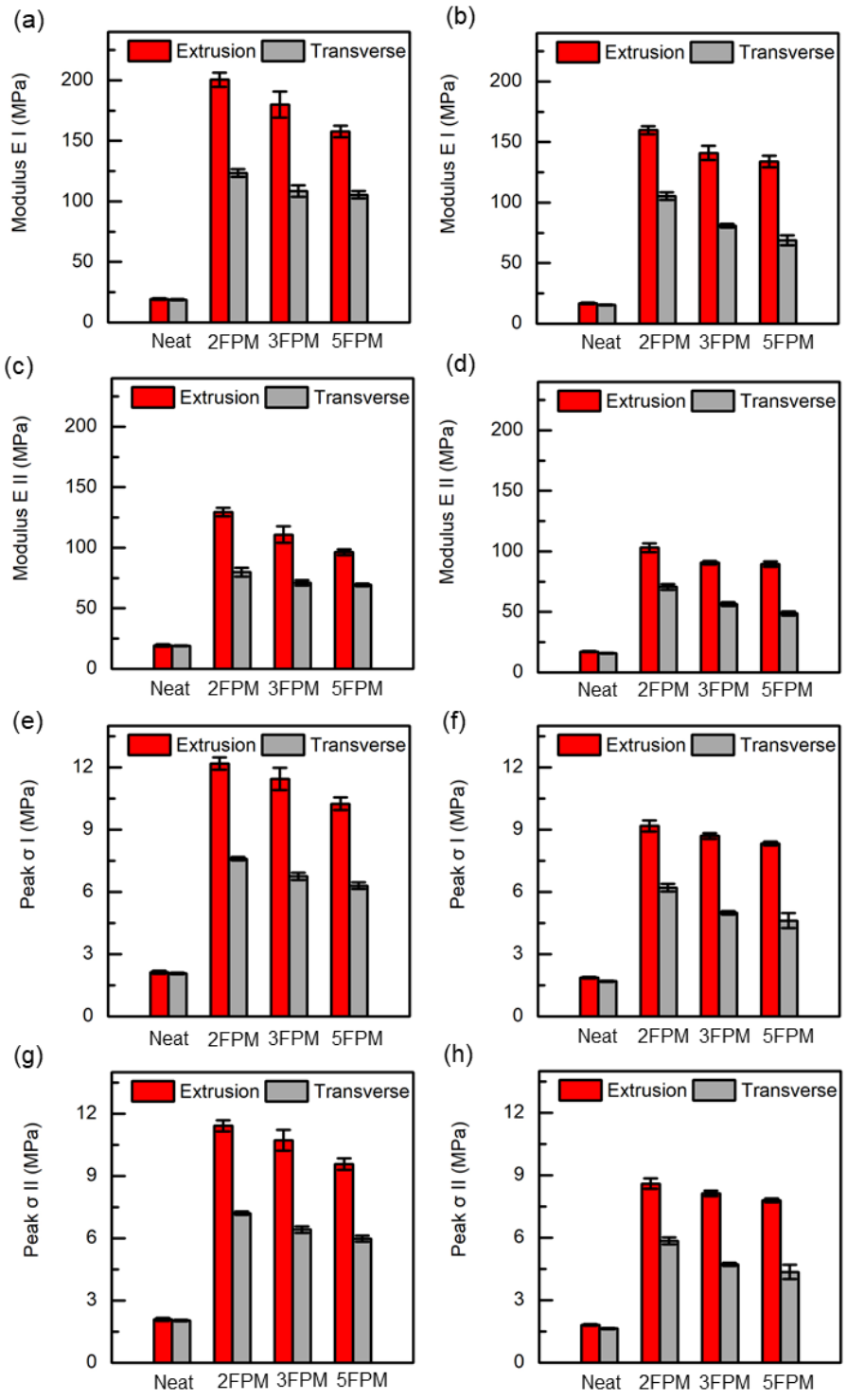

Figure 2.5. The tensile properties of composite film for each cycle under 25 ˚C and 50 ˚C (The Modulus I(II)/Peak I(II) recorded the modulus and peak stress (with 15% strain) calculated from first(second) stress-strain cycle. (a), (c), (e), (g) were samples tested under 25˚C and (b), (d), (f), (h) were samples tested under 50˚C)

Table 2.3. The strain in each cycle under 25°C

	Extrusion			Transverse		
25 °C	1st cycle end strain %	2nd cycle start strain %	2nd cycle end strain %	1st cycle end strain %	2nd cycle start strain %	2nd cycle end strain %
Neat-TPU	1.39±0.24	1.18±0.25	1.61±0.23	1.11±0.14	0.94±0.10	1.31±0.16
GnP-TPU-2FPM	4.25±0.22	2.95±0.41	4.57±0.21	3.63±0.32	2.72±0.18	4.02±0.35
GnP-TPU-3FPM	3.86±0.25	3.00±0.21	4.27±0.27	3.51±0.09	2.73±0.16	3.91±0.11
GnP-TPU-5FPM	3.80±0.19	3.00±0.19	4.24±0.15	3.73±0.17	2.87±0.16	4.12±0.25

Table 2.4. The strain in each cycle under 50°C

	Extrusion			Transverse		
50 °C	1st cycle end strain %	2nd cycle start strain %	2nd cycle end strain %	1st cycle end strain %	2nd cycle start strain %	2nd cycle end strain %
Neat-TPU	1.18±0.18	0.94±0.23	1.46±0.17	1.24±0.24	0.96±0.24	1.49±0.22
GnP-TPU-2FPM	4.79±0.15	3.74±0.15	5.20±0.15	3.90±0.11	3.04±0.06	4.35±0.13
GnP-TPU-3FPM	4.31±0.13	3.45±0.06	4.78±0.15	4.14±0.26	3.20±0.05	4.57±0.23
GnP-TPU-5FPM	4.59±0.07	3.62±0.10	4.99±0.12	4.29±0.20	3.18±0.08	4.72±0.36

A frequency sweep test was used to check the tendency of the TPU-GnP composite modulus to change after each cycle. Figure 2.6 and 2.7 summarize the storage modulus of the GnP-TPU composite films under different frequencies at 25 °C and 50 °C conditions. The data shows the same trends as the calculated Young's Modulus shown in Figure 2.5. At 25 °C, for the storage modulus before the first stretch-strain cycle, even the 5FPM sample still gave around 950% and 600% improvement in extrusion and transverse direction respectively compared to neat TPU. When the temperature was raised to 50 °C, the properties still were over 800% and 500% improvement. But as discussed above, after straining to 15%, the storage modulus E'II dropped 10~20% and 25~35% compared to E'I at 25 °C and 50 °C. The storage modulus also decreased

with increasing film extrusion speed. When the film extrusion speed increased, the GnP in the matrix tended to form larger agglomerates which accumulated in the center of the composite films, as shown in the SEM images. Similarly, the storage modulus in the extrusion direction was higher than the transverse direction. This can be explained by the film extrusion orientation effect and the dispersion and alignment effect. When the films went through the roller, there was a dragging force in the extrusion direction, tending to stretch and align the polymer chains and nano-fillers. This combined with the Poisson effect during the manufacturing process led to the mechanical difference in two directions. Second, the dispersion and alignment state of GnP in the two directions also affected the testing results.

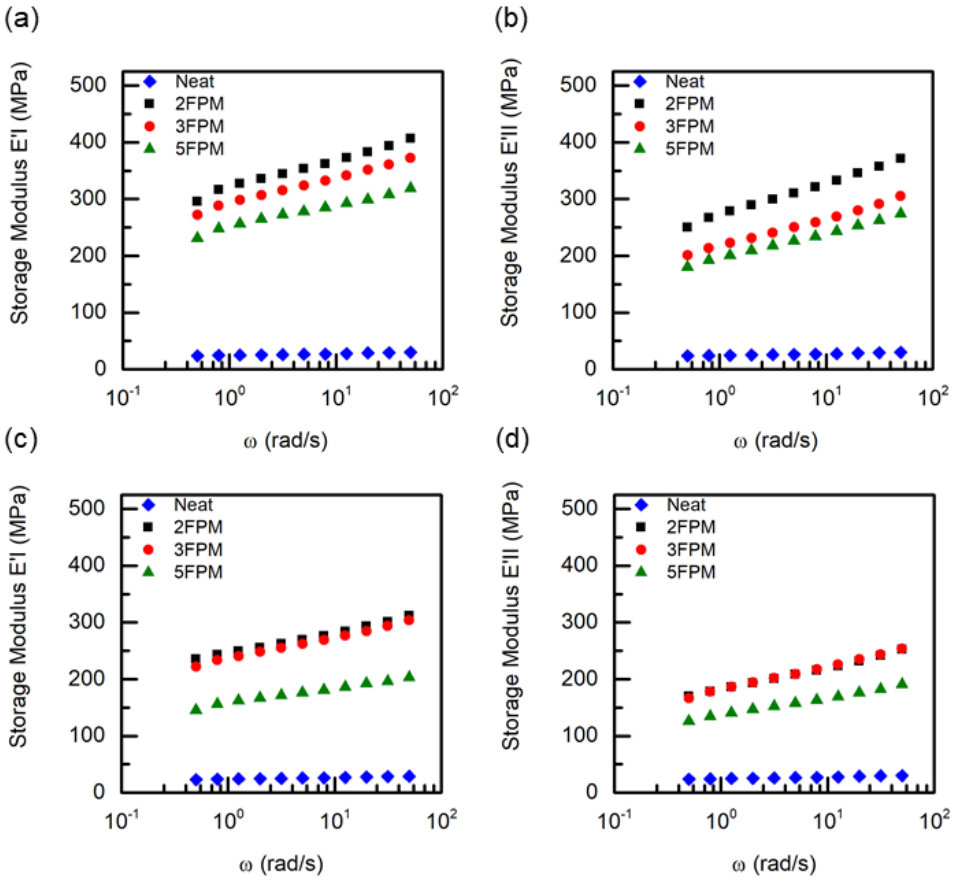

Figure 2.6. The storage modulus under 25 ˚C (E'I and E'II represented the modulus before and after first stress-strain cycle) (a), (b) were samples from the extrusion direction and (c), (d) were samples from the transverse direction

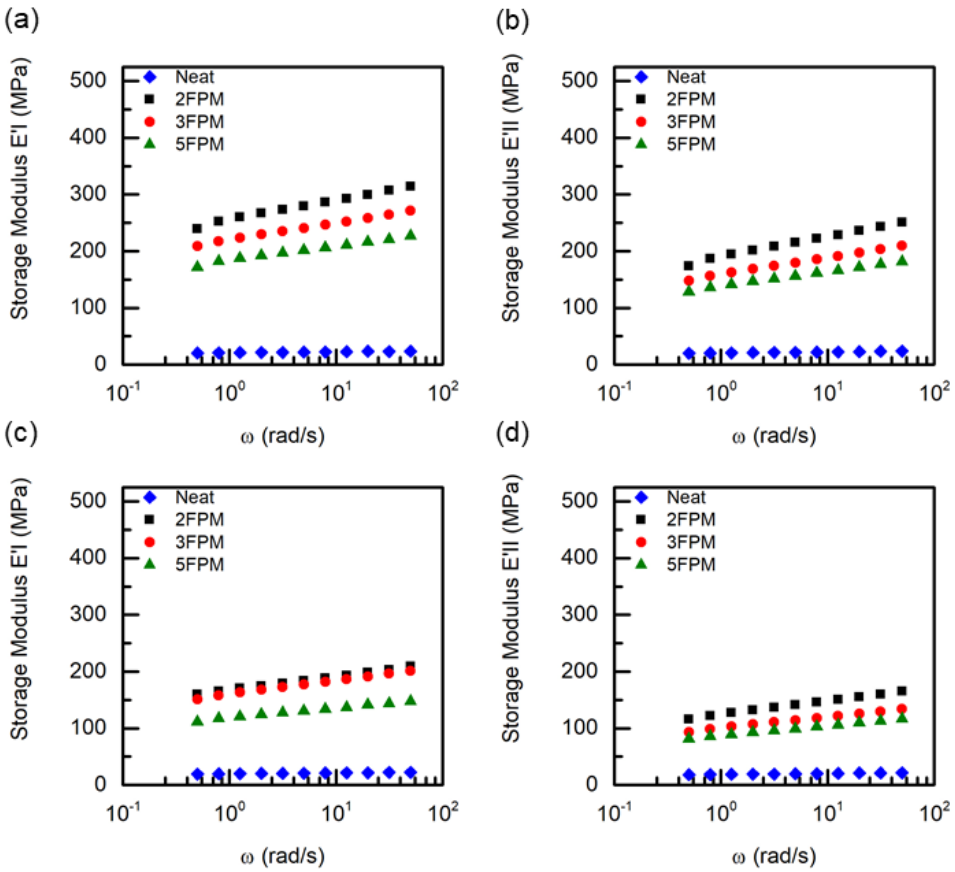

Figure 2.7. The storage modulus under 50 °C (E'I and E'II represent the modulus before and after the first stress-strain cycle) (a), (b) were samples from the extrusion direction and (c), (d) were samples from the transverse direction

The dissipated energy represented the area formed between the stretch-retract curves. The value in Figure 2.8 shows that it decreased along with increases in the film extrusion speed, by raising of the temperature or with more stretch-retract cycles. The energy came from two aspects: re-alignment of fillers in the matrix and peeling the polymer chains off the filler surface [40]. As the film extrusion speed went up, this gave better alignment of GnP in the TPU matrix, which caused less re-alignment in the stress-retract cycle. However, at the same time, more defects were created. When the speed went up, more detachments happened during the extrusion process, as the difference in the viscosity of fillers and matrix, combined with the weak

interaction between them. The result was that the TPU polymer separated from the GnP surface. Based on these two effects, composite samples with higher film extrusion speed showed the lower dissipated energy. When the temperature was increased, the modulus and strength of the TPU composite dropped, which meant that the restricting force, which blocked the GnP from moving in TPU matrix, was lowered. After the first stretch-retract cycle, part of polymer chains was pulled off from GnP surface, and this process was mostly irreversible. This phenomenon led to the second stretch-retract cycle requiring less dissipated energy. Compared to the extrusion direction, the dissipated energy for the transverse direction was much lower, because of the lower modulus in the transverse direction coupled with debonding during straining of the specimen. In the stretch-retract cycle for the transverse direction, a lower force was needed to re-align the nanoplatelets and less debonding happened during the process.

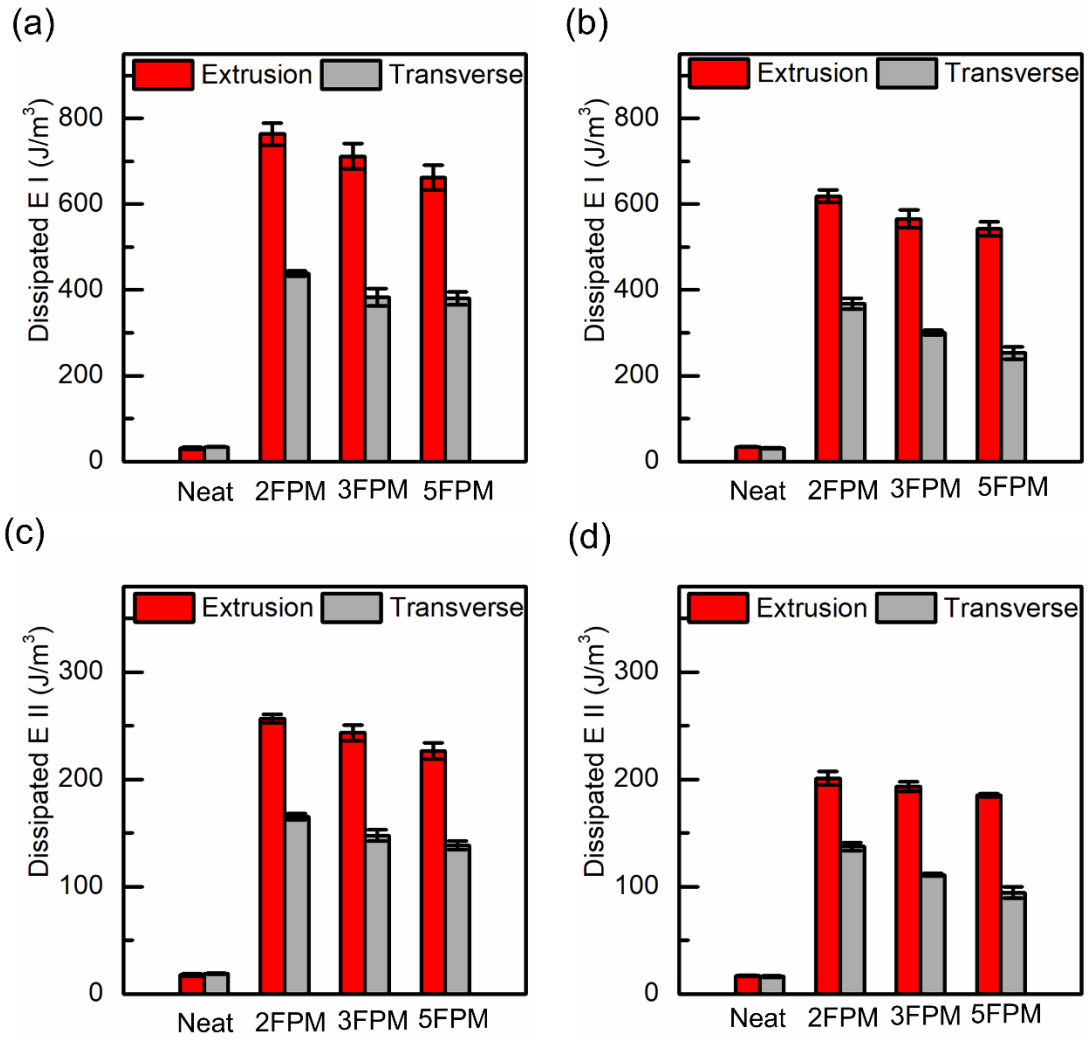

Figure 2.8. The dissipated energy of composite film for each cycle (The Dissipated E I(II) recorded the dissipated energy calculated from first(second) stress-strain cycle. (a), (c) were samples tested under 25 ˚C, and (b), (d)were samples tested under 50 ˚C)

2.3.5 The Dynamic Thermal Mechanical Properties of GnP/TPU Composite Films

The Dynamical thermal mechanical behavior of TPU and its composite are displayed in Figure 2.9. The storage modulus in the extrusion and transverse directions are shown in Figure 2.9 (a) and (b). Below T_g, there was a clear difference between neat TPU and GnP-TPU composites, as GnP has a strong influence on the elastic properties of the TPU matrix. When the film extrusion speed increased, the storage modulus started to drop. Two reasons led to this

result: first, when film extrusion speed increased, the concentration of GnP in a given area of matrix decreased; Second, as speed went up, the GnP in the TPU matrix tended to stack together forming the larger agglomerate and more defects created around these large aggregates. This phenomenon weakens the reinforcement effect from GnP. Even though the storage modulus increased substantially, Figure 2.9(c) and (d) show that the T_g only shifts around 4 $^{\circ}$C higher which agrees well with published work [41,42].

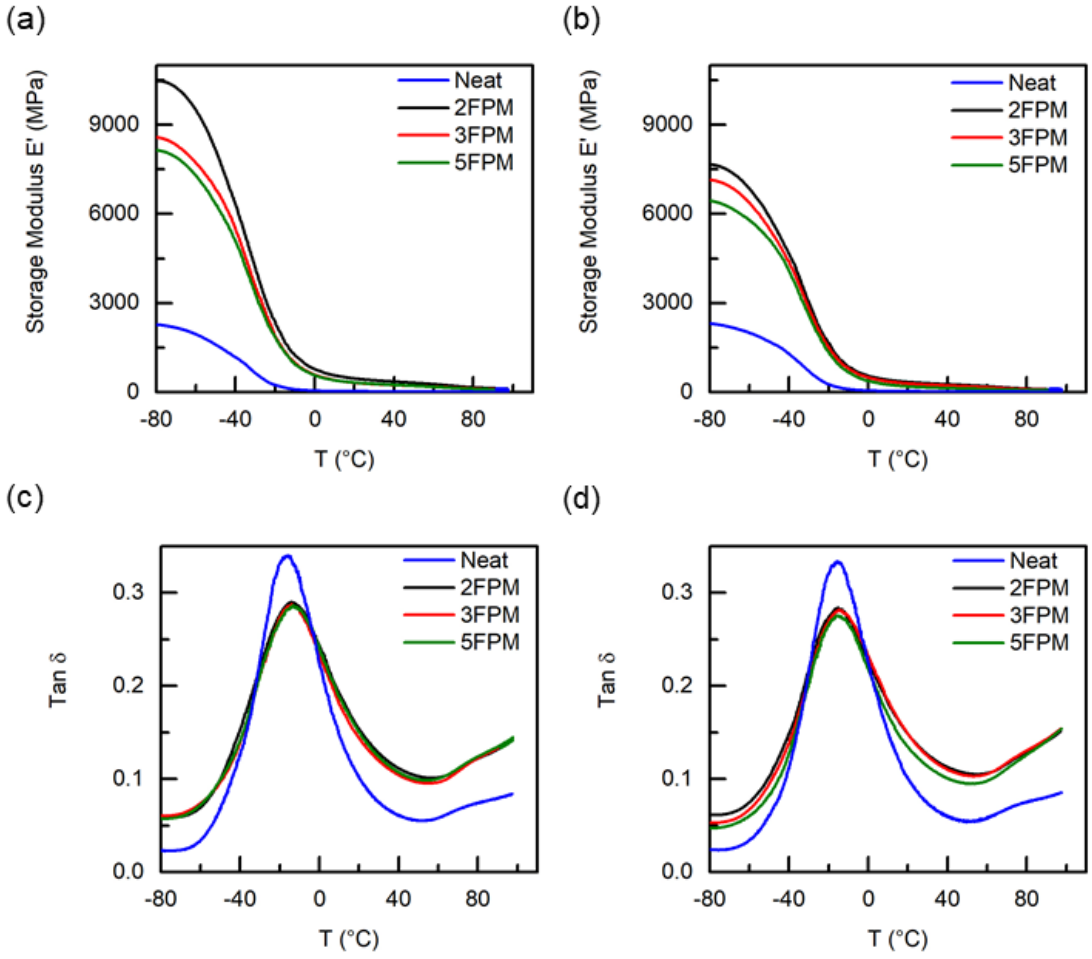

Figure 2.9. The dynamic properties of composite samples ((a), (c) were samples collected from the extrusion direction and (b), (d)were samples from the transverse direction)

2.3.6 The Thermal Stability of GnP/TPU Composite Film

TGA was used to verify the GnP content in the composite films. Figure 2.10 shows that under different extrusion speeds, the GnP in the final composite films all are around 25wt% (the actual weight percentage of GnP in the composite based on subtracting neat TPU curve from composite film curves). And, it shown that all the composite film gave a step-decrease compared to the straight-drop of neat epoxy, which proved that GnP could resist decomposition of TPU. The enhancement of thermal stability for the composite was due to the high aspect ratio of GnP which functionalized as a barrier and prevented the emission of gaseous molecules during the thermal degradation process. And the uniformly dispersed GnP disrupted the oxygen supply by forming the charred layers on the composite surface, therefore, also improved the thermal stability.

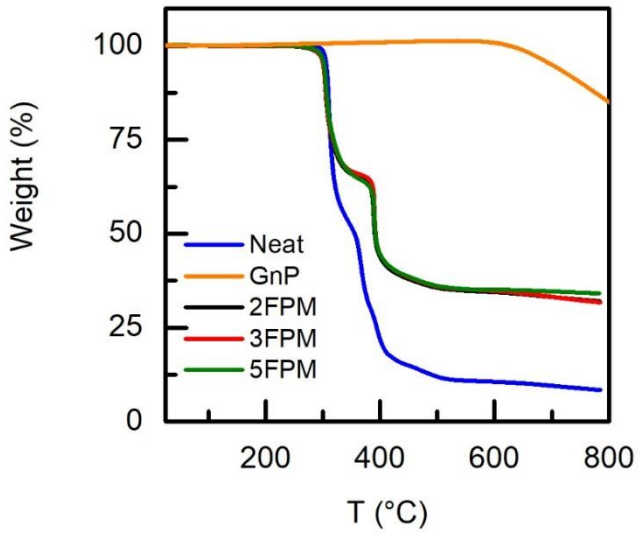

Figure 2.10. TGA curves for GnP-TPU composite film

2.4 Further modifications on composite paper

2.4.1 Press Forming Features into GnP/TPU Composite Film

As shown in Figure 2.11, a shaped material can be sealed between two GnP/TPU composite films by hot-pressing method which consisted of heating the composite film up to 180 °C, holding for 10min, then compression molding the GnP/TPU with an elastomeric platen to seal the edges of the composite films and encapsulate the materials inside. In addition, a composite pocket was prepared by hot pressing the composite films layered around a Teflon film. After cooling to room temperature, the Teflon sheet is removed, and an open pocket structure is formed, which could be used to package solids or liquids and can be sealed by hot compression of the package edges.

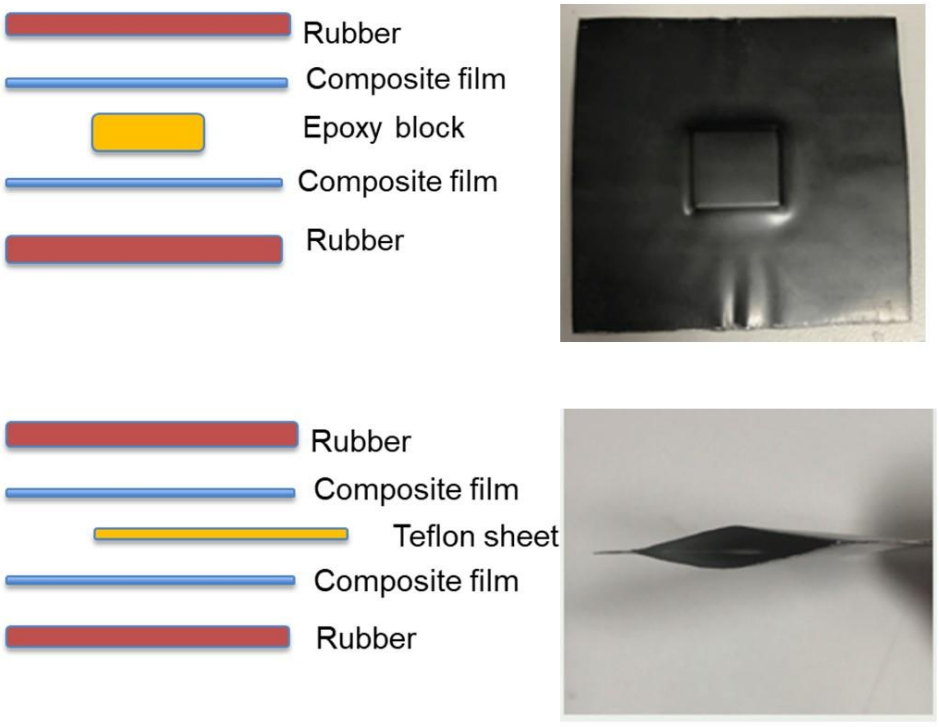

Figure 2.11. GnP-TPU composite film used for packaging application

Thermoforming can be used to create features into GnP-TPU composite film to facilitate multifunctional properties. In the construction described above, the thermal conductivity of the composite film was improved by 350%, however when the heat source in located inside the package and needs to be transferred from the interior to the surface, the introduction of surface features can enhance convective cooling. Surface features added to the GnP/TPU composite can be added to enhance turbulence of a gas or liquid passing over this surface as shown in Figure 2.12. The composite film was placed on a positive mold and covered with a soft rubber bladder. Heating the whole structure to above the softening point of the TPU combined with slow compression is an effective approach. The dimension/shape of the features, space between features, arrangement of features are parameters which can be adjusted to changing thermal convection requirements.

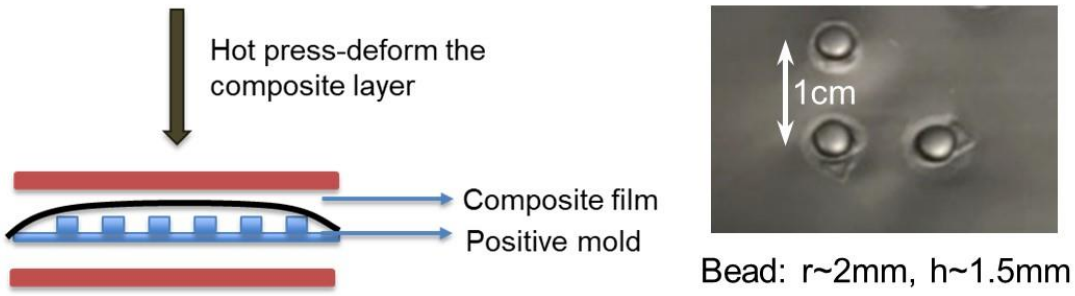

Figure 2.12. Press features onto GnP-TPU composite film

2.4.2 Compression Molding of the Surface Features into The GnP/TPU composite film

Based on the simulation results, surface features that enhance convective thermal conductivity were found to be effective at values over 3W m^{-1} K^{-1}. The GnP-TPU film for protection and gas barrier enhancement. The GnP paper was made based on a filtration method as shown in Figure 2.13, 2 g of GnP was dispersed into 400ml water with polyethylenimine

(PEI) (weight ratio PEI: GNP=1:2) as surfactant under 120 W, 5 min sonication. After filtration, the wet GnP paper on a designed mesh was compress with ~1500 lb load followed by drying the paper in hood overnight. This process produced the GnP paper with desired features having dimensions and spatial arrangement. This can also be accomplished through 3D printing, as shown in Figure 2.13 (c). Features with different sizes and spacing can be easily printed with a variety of polymeric systems. When the GnP paper with the desired features was created, it was covered with GnP-TPU composite film through a compression molding or spray coating process.

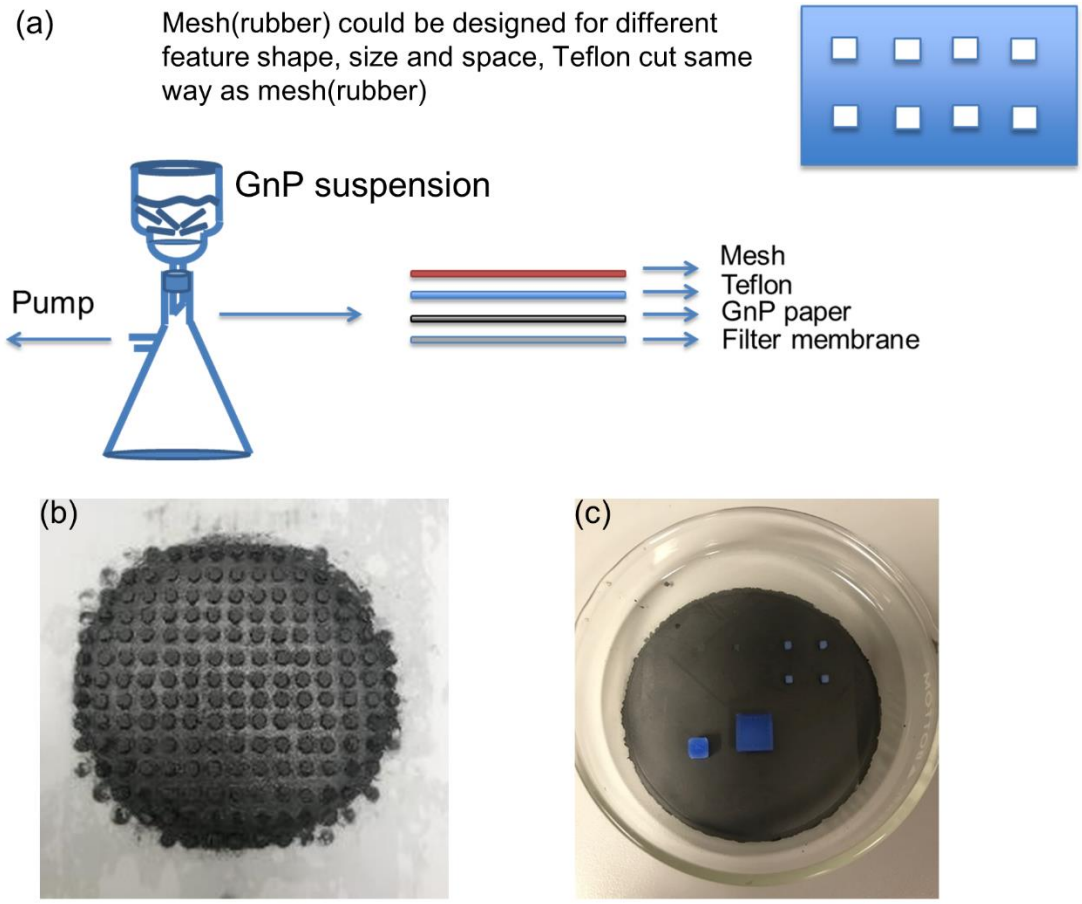

Figure 2.13. Press features onto GnP paper : (a) Schematic illustration for producing GnP paper and pressing features onto it; (b) GnP with features on surface (feature dimension: l, w: ~2 mm, h~1.5 mm); (c) 3D printing features onto GnP paper (features dimension: features dimension: from small to large: 2 x 2 mm, 5 x 5 mm, 10 x 110 mm, and all have same h ~ 1.5 mm)

Figure 2.14 shows the SEM images for the features created on the GnP surface through the press method. Figure 2.14 (a) and (b) represents the top view and 70º title view, the features after press, maintain the fine structure, which is beneficial for the thermal convection. Figure 2.14 (c) shows the sample which was mounted into epoxy and polished to investigate the cross-section morphology. It proves that the edge and transfer region of the features are in the designed shape.

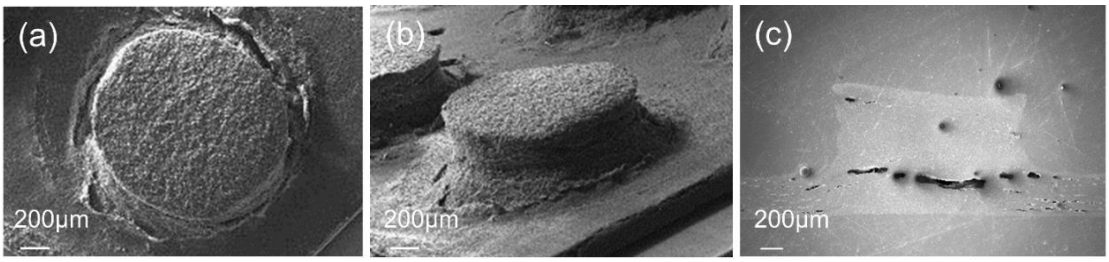

Figure 2.14. The SEM images for the features pressed onto GnP paper (a) Top view for the feature; (b) 70º title view for the feature; (c) cross-section for the feature.

2.5 Conclusion

Stretchable, formable, thermally conductive, electrically insulating GnP-TPU composite films were prepared through an extrusion process. The effect of GnP addition on the film thermal conductivity, oxygen permeability, static and dynamic mechanical properties and morphology of TPU composites was investigated. After incorporating 25wt% (14vol%) GnP into the TPU matrix, the thermal conductivity increased over 350% and oxygen permeability dropped by 75% compared to the neat TPU. The addition of GnP at increasing concertation increases the hysteresis phenomena and dissipated energy is altered, along with a 950% and 470% increase in tensile modulus and stress in the extrusion direction. For the transverse direction or at higher temperature, the mechanical properties decrease but are still much higher compared to neat TPU.

DMA results demonstrated that at -80 °C the storage modulus of the composite films at least improved ~260% and ~180% in the extrusion and transverse directions and exhibited an enhancement over the entire temperature range. The T_g for the composite films only increased by about 4 °C. This was attributed to the weak interaction between the GnP surface and the TPU matrix. These results indicate that the addition of GnP can increase a multitude of properties of the TPU, and that the surface modification of the GnP to improve its interaction with the TPU has the potential for achieving further improvements. Features were created onto the surface of the composite film improved the thermal convection performance. The effect of surface features with different dimensions, shapes and arrangement of features was demonstrated. on thermal convection results would be analyzed in the future research.

REFERENCES

REFERENCES

[1] Razeghi M, Pircheraghi G. TPU/graphene nanocomposite: Effect of graphene functionality on morphology of separated hard domains in thermoplastic polyurethane. Polymer. 2018 Jun 11.

[2] Petrović ZS, Ferguson J. Polyurethane elastomers. Progress in Polymer Science. 1991 Oct 1;16(5):695-836.

[3] Lee BS, Chun BC, Chung YC, Sul KI, Cho JW. Structure and thermomechanical properties of polyurethane block copolymers with shape memory effect. Macromolecules. 2001 Aug 28;34(18):6431-7.

[4] Crawford DM, Bass RG, Haas TW. Strain effects on thermal transitions and mechanical properties of thermoplastic polyurethane elastomers. Thermochimica Acta. 1998 Dec 7;323(1-2):53-63.

[5] Gogoi R, Alam MS, Niyogi UK. Effect of soft segment chain length on tailoring the properties of isocyanate terminated polyurethane prepolymer, a base material for polyurethane bandage. International Journal of Research in Engineering and Technology. 2013;2(10):395-8.

[6] Kojio K, Furukawa M, Nonaka Y, Nakamura S. Control of mechanical properties of thermoplastic polyurethane elastomers by restriction of crystallization of soft segment. Materials. 2010 Dec 1;3(12):5097-110.

[7] Silver JH, Myers CW, Lim F, Cooper SL. Effect of polyol molecular weight on the physical properties and haemocompatibility of polyurethanes containing polyethylene oxide macroglycols. Biomaterials. 1994 Jan 1;15(9):695-704.

[8] Solouki Bonab V, Manas-Zloczower I. Revisiting thermoplastic polyurethane, from composition to morphology and properties. Journal of Polymer Science Part B: Polymer Physics. 2017 Oct 15;55(20):1553-64.

[9] Mi HY, Jing X, Peng J, Turng LS, Peng XF. Influence and prediction of processing parameters on the properties of microcellular injection molded thermoplastic polyurethane based on an orthogonal array test. Journal of Cellular Plastics. 2013 Sep;49(5):439-58.

[10] Yilgör I, Yilgör E, Wilkes GL. Critical parameters in designing segmented polyurethanes and their effect on morphology and properties: A comprehensive review. Polymer. 2015 Feb 10;58:A1-36.

[11] Woods G. The ICI polyurethanes book. 1990 Nov.

[12] Lamba NK. Polyurethanes in biomedical applications. Routledge; 2017 Oct 19.

[13] Sheng D, Tan J, Liu X, Wang P, Yang Y. Effect of organoclay with various organic modifiers on the morphological, mechanical, and gas barrier properties of thermoplastic polyurethane/organoclay nanocomposites. Journal of materials science. 2011 Oct 1;46(20):6508.

[14] Shamini G, Yusoh K. Gas Permeability Properties of Thermoplastic Polyurethane Modified Clay Nanocomposites. International Journal of Chemical Engineering and Applications. 2014 Feb 1;5(1):64.

[15] Pandey S, Jana KK, Aswal VK, Rana D, Maiti P. Effect of nanoparticle on the mechanical and gas barrier properties of thermoplastic polyurethane. Applied Clay Science. 2017 Sep 15;146:468-74.

[16] Pizzatto L, Lizot A, Fiorio R, Amorim CL, Machado G, Giovanela M, Zattera AJ, Crespo JS. Synthesis and characterization of thermoplastic polyurethane/nanoclay composites. Materials Science and Engineering: C. 2009 Mar 1;29(2):474-8.

[17] Pattanayak A, Jana SC. High-strength and low-stiffness composites of nanoclay-filled thermoplastic polyurethanes. Polymer Engineering & Science. 2005 Nov;45(11):1532-9.

[18] Barick AK, Tripathy DK. Preparation and characterization of thermoplastic polyurethane/organoclay nanocomposites by melt intercalation technique: effect of nanoclay on morphology, mechanical, thermal, and rheological properties. Journal of applied polymer science. 2010 Jul 15;117(2):639-54.

[19] Novoselov KS, Geim AK, Morozov SV, Jiang DA, Zhang Y, Dubonos SV, Grigorieva IV, Firsov AA. Electric field effect in atomically thin carbon films. science. 2004 Oct 22;306(5696):666-9.

[20] Lee C, Wei X, Kysar JW, Hone J. Measurement of the elastic properties and intrinsic strength of monolayer graphene. science. 2008 Jul 18;321(5887):385-8.

[21] Balandin AA, Ghosh S, Bao W, Calizo I, Teweldebrhan D, Miao F, Lau CN. Superior thermal conductivity of single-layer graphene. Nano letters. 2008 Feb 20;8(3):902-7.

[22] Stoller MD, Park S, Zhu Y, An J, Ruoff RS. Graphene-based ultracapacitors. Nano letters. 2008 Sep 13;8(10):3498-502.

[23] Fukushima H, Drzal L, Rook B, Rich M. Thermal conductivity of exfoliated graphite nanocomposites. Journal of thermal analysis and calorimetry. 2006 Jul 1;85(1):235-8.

[24] Kalaitzidou K. Exfoliated graphite nanoplatelets as reinforcement for multifunctional polypropylene nanocomposites. Michigan State University; 2006.

[25] Fukushima H. Graphite nanoreinforcements in polymer nanocomposites. Michigan State University; 2003.

[26] Wu H, Rook B, Drzal L T. Dispersion optimization of exfoliated graphene nanoplatelet in polyetherimide nanocomposites: Extrusion, precoating, and solid state ball milling. Polymer Composites, 2013, 34(3): 426-432.

[27] Chen K, Tian Q, Tian C, Yan G, Cao F, Liang S, Wang X. Mechanical reinforcement in thermoplastic polyurethane nanocomposite incorporated with polydopamine functionalized graphene nanoplatelet. Industrial & Engineering Chemistry Research. 2017 Oct 5;56(41):11827-38.

[28] Yadav SK, Cho JW. Functionalized graphene nanoplatelets for enhanced mechanical and thermal properties of polyurethane nanocomposites. Applied surface science. 2013 Feb 1;266:360-7.

[29] Li A, Zhang C, Zhang YF. RGO/TPU composite with a segregated structure as thermal interface material. Composites Part A: Applied Science and Manufacturing. 2017 Oct 1;101:108-14.

[30] XG Science https://xgsciences. com/

[31] BASF Corporation http://www. polyurethanes. basf. us/

[32] Debelak B, Lafdi K. Use of exfoliated graphite filler to enhance polymer physical properties. Carbon. 2007 Aug 1;45(9):1727-34.

[33] Yu A, Ramesh P, Sun X, Bekyarova E, Itkis ME, Haddon RC. Enhanced thermal conductivity in a hybrid graphite nanoplatelet–carbon nanotube filler for epoxy composites. Advanced Materials. 2008 Dec 17;20(24):4740-4.

[34] Yu A, Ramesh P, Itkis ME, Bekyarova E, Haddon RC. Graphite nanoplatelet− epoxy composite thermal interface materials. The Journal of Physical Chemistry C. 2007 May 31;111(21):7565-9.

[35] Nielsen LE. Models for the permeability of filled polymer systems. Journal of Macromolecular Science—Chemistry. 1967 Aug 1;1(5):929-42.

[36] Kalaitzidou K, Fukushima H, Drzal LT. Multifunctional polypropylene composites produced by incorporation of exfoliated graphite nanoplatelets. Carbon. 2007 Jun 1;45(7):1446-52.

[37] Gavgani JN, Adelnia H, Gudarzi MM. Intumescent flame retardant polyurethane/reduced graphene oxide composites with improved mechanical, thermal, and barrier properties. Journal of materials science. 2014 Jan 1;49(1):243-54.

[38] Mullins L. Softening of rubber by deformation. Rubber chemistry and technology. 1969 Mar;42(1):339-62.

[39] Lozano-Pérez C, Cauich-Rodríguez JV, Avilés F. Influence of rigid segment and carbon nanotube concentration on the cyclic piezoresistive and hysteretic behavior of multiwall carbon nanotube/segmented polyurethane composites. Composites Science and Technology. 2016 May 18;128:25-32.

[40] Tang J, Xu G, Sun Y, Pei Y, Fang D. Dissipative properties and chain evolution of highly strained nanocomposite hydrogel. Journal of Applied Physics. 2014 Dec 28;116(24):244901.

[41] Cai D, Yusoh K, Song M. The mechanical properties and morphology of a graphite oxide nanoplatelet/polyurethane composite. Nanotechnology. 2009 Feb 3;20(8):085712.

[42] Pokharel P, Pant B, Pokhrel K, Pant HR, Lim JG, Kim HY, Choi S. Effects of functional groups on the graphene sheet for improving the thermomechanical properties of polyurethane nanocomposites. Composites Part B: Engineering. 2015 Sep 1;78:192-201.

CHAPTER 3 - IMPROVING THE MECHANICAL PROPERTIES OF GRAPHENE NANOPLATELET/EPOXY COMPOSITES USING FUNCTIONALIZED GRAPHENE AS COUPLING AGENT

3.1 Introduction

Graphene sheets, one atom thick two-dimensional layers of sp^2-bonded carbon, have become a celebrated material since its first isolated in 2004 [1]. This novel material possesses of a range of unusual properties, such as large theoretical surface area (2630 $m^2 g^{-1}$) [2], high basal plane mechanical properties (~1 TPa elastic modulus and ~130 GPa ultimate strength) [3], outstanding thermal conductivity (~5000 W $m^{-1} K^{-1}$) [4] and carrier mobility at room temperature (~10000 $cm^2 V^{-1} s^{-1}$) [5,6]. Graphene can be prepared by various methods including micromechanical cleavage, chemical vapor deposition, exfoliation of graphite intercalation compounds and chemical oxidation-reduction methods [7-12]. One possible route to harnessing its extraordinary properties for applications would be to incorporate graphene sheets into a composite material. Chandrasekaran et al. [13] prepared a graphene/epoxy composite using a three-roll mill technique and saw the electrical conductivity increase by 500% at a loading of 0.3wt% graphene. The thermal conductivity increased by 6% for a 1wt% addition and was doubled to 14% for a 2wt% graphene loading at 30 ˚C. Wan et al. [14] synthesized Triton treated graphene and incorporated it into an epoxy matrix, achieving ~57% and ~7% enhancement in tensile strength and modulus. Qin et al. [15] applied graphene coated carbon fiber as filler for epoxy based composite, the results showed a 52%, 7% and 19% increase in 90° flexural strength, 0° flexural strength and interlaminar shear strength compared to non-coated carbon fiber/epoxy composite. Jia et al. [16] designed cellular-structured graphene foam/epoxy composites. The 3D interconnected graphene network behaved as fast channels for charge carriers, increasing electrical conductivity of the composites, 3 S cm^{-1}, with 0.2wt% graphene.

The manufacture of such composites requires not only graphene to be produced at a sufficient scale but also to be homogeneously distributed in the matrix and with optimized interfacial properties. Currently, chemical oxidation and reduction is the most effective, low-cost way to produce graphene at a large scale. In this process, graphene oxide (GO) stands out as the key derivatized intermediate product. GO is an oxidized graphene sheet having its basal plane decorated with epoxide and hydroxyl groups and carbonyl, carboxyl groups located at the edges [11, 17]. These oxygen functional groups make GO sheets highly hydrophilic and a stable aqueous dispersion can be obtained [18,19]. The functional groups improve the affinity between the graphene basal plane and the polymer matrix. Additional functionalization applied on the GO surface can optimize the interfacial properties with the polymer matrix to enhance the load transfer efficiency and reinforcing effect. Li et al. [20] incorporated 0.2wt% amino-functionalized GO (APTS-GO) into epoxy resin, the composite yielded a 32% increase in Young's modulus and 16% increase in tensile strength. Wan et al. [21] prepared diglycidyl ether of bisphenol-A functionalized GO(DGEBA-f-GO). For epoxy composite with 0.25wt% DGEBA-f-GO, the tensile modulus and strength improved ~13% and ~75%. And the quasi-static fracture toughness (K_{IC}) was enhanced ~26% and ~41% at 0.25wt% loading of GO and DGEBA-f-GO, respectively. Bortz et al. [22] reported enhancements of 28-111% in mode I fracture toughness and up to 1580% in uniaxial tensile fatigue life through the addition of small amounts ($\leq$ 1wt%) of graphene oxide to an epoxy system.

GO has been thought to behave as a surfactant due to its unique chemical structure consisting of hydrophobic and hydrophilic moieties at different proportion [23,24]. Hydrophobicity is attributed to the un-oxidized aromatic domain while the oxygen-functional groups interact with other constituents through a combination of hydrogen bond and electrostatic

forces. This enhances the possibility for GO to act as a novel dispersant to stabilize different carbon materials [25-28].

Epoxy resin, one of most widely used thermoset polymers, is known for its good mechanical and thermal properties, electrical insulation, high adhesive strength and chemical and corrosion resistance [29-31]. However, researchers are still trying to improve its toughness, strength, resistance to crack propagation in order to satisfy the increasing demands in high-performance applications. To address this issue, incorporating nano-fillers has been considered as an efficient approach to improve the performance of epoxy resins [32-35].

In this research, GO was used as coupling agent for dispersing graphene nanoplatelets (GnPs) into an epoxy matrix. Because of π-π interaction, the basal plane of GO attached onto the GnP surface, while the oxygen functional group bonded with epoxy resin. Different chain length diamines (p-phenylenediamine(PPDA) and Jeffamine D2000) were applied to modify the GO-GnP couple in order to further improving the interfacial properties. The tensile properties were recorded and combined with fracture surface morphology to evaluate the effect of using GO/fGO as the coupling agent in improving the properties of the GnP-Epoxy composites.

3.2. Experimental section

3.2.1 Materials

The graphene nanoplatelets (GnP) used in the research was GnP-R10 supplied by XG Sciences, with an average diameter of 10μm and surface area of 30-60 $m^2 g^{-1}$ [36]. The concentrated phosphoric acid was supplied by Columbus Chemical Industries, Inc. The concentrated sulfuric acid and hydrochloric acid were obtained from Macron Fine Chemicals.

30% hydrogen peroxide was purchased from Fisher Chemical. Potassium permanganate and p-phenylenediamine (PPDA) were supplied by Sigma-Aldrich. Jeffamine D2000/D400 were received from Huntsman Corporation. Diglycidyl ether of bisphenol-A(DGEBA), with an equivalent weight (EEW) of 185-195, was used as the epoxy resin and was from Hexion. All the chemicals were used as received.

3.2.2 Preparation of graphene oxide (GO)

GO was prepared from GnP-R10 based on improved Hummers' method [37]. A 9:1 mixture of concentrated H_2SO_4/ H_3PO_4 (360 ml/40 ml) was added into a flask, containing 3 g GnP-R10 powder. Then slowly introduced 18 g $KMnO_4$ into the solution. The reaction was then heated to 50 $^{\circ}$C and stirred for 12 h. The reaction was then cooled to room temperature and poured into the 2 L beaker with around 300 ml water. The beaker was surrounded by the dry ice to control the temperature. Slowly adding 30% H_2O_2 into the solution until bubble generation ceased, and the color of the solution changed to golden yellow. Centrifugation (4000 rpm) was applied to remove extra acid and wash the residual solid for 5 times with 10% HCl. Dialysis was used to further purify the GO product for around 4 weeks after which the GO uniformly dispersed in the water phase.

3.2.3 Preparation of GO-GnP/ f-(GO-GnP) couple

GnPs were dispersed into the GO suspension, with adjusted volume to be 100 ml and the mixture was sonicated under 90 W for 30 min. Total weight of GnP and GO together was fixed at 0.5 g or 1 g, varying weight ratios, 1:10 and 1:50 between GO and GnP were investigated.

After sonication, GnP and GO interacted with each other through π-π bond, and uniformly dispersed in the water phase, which was defined as 'GO-GnP couple'.

For functionalization of this GO-GnP couple (f-(GO-GnP)), two diamines were used here, p-phenylenediamine (PPDA) and Jeffamine D2000. Excess amount of these diamines (weight ratio between PPDA/Jeffamine D2000: GO was 5:1 and 100:1) were added into above prepared GO-GnP suspension. The reaction was conducted under 80 °C and stirred for 30 min [38]. The products were washed with water and ethanol to remove unreacted diamines.

Either GO-GnP or f-(GO-GnP) couple was further dried in the oil bath ~75 °C to remove solvent, producing the GO-GnP or f-(GO-GnP) slurry.

3.2.4 GO-GnP/f-(GO-GnP) composite preparation

GO-GnP or f-(GO-GnP) slurry was re-dispersed into 100 ml dimethylformamide (DMF) with tip sonication under 150 W for 30 min, then the epoxy resin was added into the suspension and further sonicated for 30 min at 100 W. The mixture was then heated in the oil bath at ~80 °C for 24 h to remove the DMF. Then the mixture passed through a three-roll mill with 20 μm gap for 5 passes. The stoichiometric amount of curing agent (Jeffamine D400) was added and stirred to achieve the uniform suspension. The suspension was degassed for ~10min under 80 °C and poured into silicone molds, cured at 75 °C for 2 h and 125 °C for 2.5 h. The composites with two different loadings of fillers(0.43wt%, 0.86wt%) were investigated in this research.

3.2.5 Characterizations of the composites

Raman spectroscopy was carried out using LabRAM ARAMIS (HORIBA JOBIN YVON, Inc) in the range of 1200-1800 cm^{-1}. The excitation laser wavelength was 532 nm. X-ray

diffraction (XRD) of GO and GnP were analyzed with D2 PHASER (BRUKER Corporation) at a scan rate of 0.02 $^{\circ}$ s^{-1} in between 2θ range of 5°-35°. The wavelength of X-ray beam, λ=1.54 Å (Cu-Kα radiation). The thermogravimetric analysis (TGA) was performed with TA instrument Q500 under high resolution mode, temperature ramp from 25 $^{\circ}$C to 800 $^{\circ}$C with rate of 25 $^{\circ}$C min^{-1}, resolution of 4 in the N_2 condition. The atomic force microscopy (AFM) was carried out using Asylum Research Cyber (OXFORD instrument) with contact mode, the scan rate was 1Hz and scan area was 20 μm x 20 μm. The silicon tip coated with Ti/Ir was applied for the measurements. Fourier transform infrared (FTIR) measurements were performed with FT/IR-4600 (Jascon, Inc), scanning from 400 cm^{-1} to 4000 cm^{-1}, with resolution of 4 cm^{-1} and scan number of 128. The surface composition of GO and fGO were characterized through X-ray photoelectron spectroscopy (XPS) using a PHI 5400 ESCA system. Tensile test was carried out with United Testing system, based on ASTM D638, each sample had five replicates. The standard dumbbell shaped specimens (165 mm x13 mm x 3.2 mm) were prepared through pouring and casting in silicon mode. Crosshead speed was fixed at 5 mm/min with 1000 lb load cell. The morphology of the fractured composite was investigated with a ZEISS focused ion beam scanning electron microscope operated under 20 kV and 2 kV.

3.3 Results and Discussion

3.3.1 Analysis for produced GO

Figure 3.1 summarizes the basic properties of graphene oxide (GO) synthesized through the improved Hummers' method. Figure 3.1 (a) shows the Raman results for GnP and GO. GnP is a stack of several layers of graphene which displays a prominent G peak at ~1560 cm^{-1},

corresponding to the first order scattering of E_{2g} mode [11,39]. For the GO sample, the G peak is broadened and shifted to ~1595 cm^{-1} [40], and a high intensity D peak appears at ~1360 cm^{-1}, indicating the distortion of bonds and destruction of symmetry were possible because of reduction in the size of in-plane sp^2 domains caused by oxidation process [21,41,42]. The intensity ratio of D peak and G peak of GO increased to ~0.95 and is characteristic of the extent of defects after the oxidation process. The XRD spectroscopy is shown in Figure 3.1 (b), The characteristic diffraction peak at ~26.5° of GnP was the 002 reflection peak, corresponding to an interlayer space of 0.34 nm [43-46]. For the GO sample, the sharp peak appeared at ~11.3°, reflecting the increased interlayer space of ~0.8 nm [47-50].

Figure 3.1 (c) summarizes the thermogravimetric analysis (TGA) for the GnP and GO samples under N_2 condition. A weight loss of ~7wt% of GO sample up to 100 °C could be attributed to evaporation of water molecules from the samples. A significant weight loss at about ~200 °C, was due to elimination of interlamellar water, followed by loss of oxygen functional groups from the GO platelets. The other steep drop of weight appeared at ~450 °C, because of bulk pyrolysis of carbon skeleton, which could also reflect from GnP curves [50-52]. AFM was used to evaluate the level of exfoliation of GO sample. Previous investigations identified the thickness of GO single layer at about 1nm, but this value varies depending on the amount of absorbed water between adjacent GO layers [53-55]. Shown in Figure 3.1 (d), the thickness of GO sheet varied from 1nm-2nm, which represented around single or double layers of GO were produced during the oxidation process.

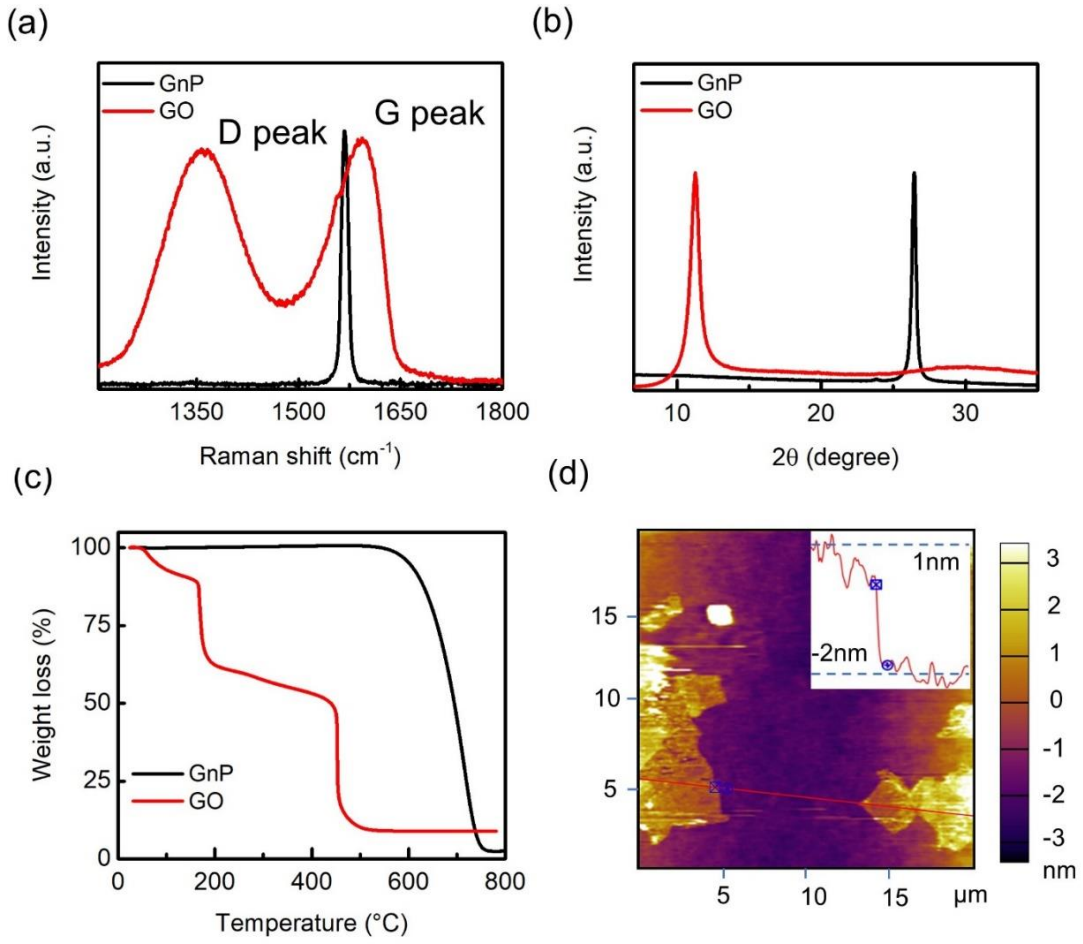

Figure 3.1. Analysis for GO product: (a) Raman spectroscopy; (b) XRD spectroscopy; (c) TGA; (d) AFM spectroscopy

3.3.2 Surface analysis for functionalized GO

The functionalization of GO with PPDA and Jeffamine D2000 was studied with XPS and FTIR spectroscopy. Figure 3.2 (b) represents the FTIR results. The broad peak at around 3400 cm^{-1} for GO or functionalized GO was identified as the vibration of O-H bond. While, the peaks at ~1735, ~1625 and ~1065 cm^{-1} belonged to C=O in carboxyl group, C=C in aromatic ring and C-O-C in epoxide group, respectively. After reaction with PPDA or Jeffamine D2000, the characteristic absorption intensity of -OH, -COOH decreased. For PPDA functionalized GO, the intensity of C-O-C also dropped, suggesting the ring opening reaction happened. For Jeffamine

D2000 functionalized GO, the intensity of C-O-C did not change much, which was attributed to the presence of this bond in the backbone structure of Jeffamine D2000. Furthermore, new peaks appearing at ~1500 cm^{-1} and ~2900 cm^{-1} were related to C-N and N-H bond, indicating that PPDA and Jeffamine D2000 bonded onto the GO surface. XPS was applied to analyze surface chemical composition and their changes for GO and different diamine functionalized GO. GO was composed of two typical peaks, the C1s and O1s peak, new peaks appeared at ~400 eV, after reaction with diamines was attributed to N1s peak(shown in Figure 3.2 (a)). The C/O ratio for GO sample was ~2.3 which was consistent with reported value around 2 [40,56]. Using PPDA or Jeffamine D2000 to treat the GO surface, this ratio increased to 5.7 and 3.4 because of incorporation of carbon atoms after functionalization by diamines. As oxygen atoms existed in the Jeffamine D2000 main chain, it gave a lower value compared to PPDA functionalized GO. Figure 3.2 (c) and (d) show the details for N1s peak for different diamines functionalized GO: three peaks presented presence of nitrogen in the forms of NH_2(~398.4 eV), N-C(O)(399.5 eV) and H^+_3N-C(401.2 eV). These peaks supported the reaction of diamine with GO through both ring opening and ammonium carboxylate formation [38,49,57,58].

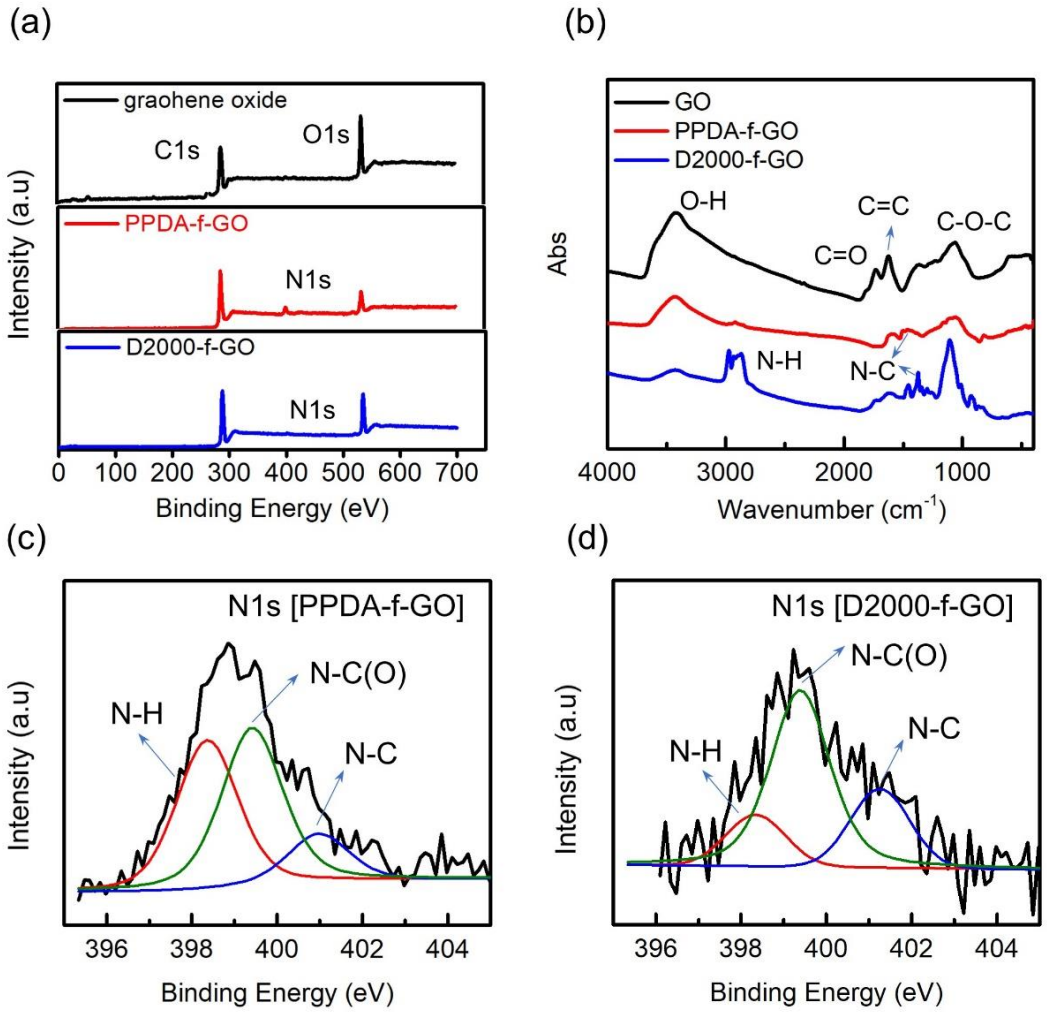

Figure 3.2. Surface analysis: (a) XPS element peak for different diamine treated GO; (b)FTIR for different diamine treated GO; (c) N1s peak for PPDA-f-GO; (d) N1s peak for D2000-f-GO

3.3.3 Mechanical properties for composites

In Figure 3.3, several experimental process factors were investigated in order to optimize the composite preparation procedures. In Figure 3.3(a) two GO drying states were analyzed, one is GO in slurry state with water, the other one was dried under 75 ˚C for 24 h, as completely removing all the water from GO, it would form the hard thick plates and was hard to re-disperse into other solvent unless using the high power sonication. Published research also mentioned that GO in the wet sate would relieve this negative effect [38]. Using the GO slurry to make the

epoxy composite under the same conditions showed better modulus enhancement compared to dried GO. Here the different between two states of GO was not remarkable and was attributable to two factors. One was the sonication condition in composite preparation, GO was re-dispersed into DMF under 150W sonication for 30min, this high power sonication helps GO hard platelets to exfoliate and be dispersed into the solvent; the second one was DMF was an ideal solvent for GO dispersion, even though it has high boiling point. Under other conditions, like using other solvent such as IPA, acetone, or lower sonication power, would lead to a relative larger drop if dried GO was used.

In Figure 3.3(b), the functionalization approach for making diamine functionalized GO-GnP was investigated. Two methods could be considered; one was preparing diamine functionalized GO and then mixing it with GnP to produce (PPDA-f-GO)-GnP and the other method sonicated GO and GnP in water together first and then using diamine to treat them together to achieve PPDA-f-(GO-GnP). Under 0.43wt% loading, using the second way to prepare the filler and make composite gave a ~17% improvement.

Figure 3.3(c) shows the effect of the 3 roll mill processing, which was used for improving the dispersion state of the filler. At higher loading, 0.86wt%, under same composition, PPDA-f-(GO:GnP 1:10), the composite made with 3 roll milling gave ~8% higher tensile modulus compared to one without it. Based on these testing results, the experimental procedures were set as above, using GO or GO-GnP slurry; mixing GO-GnP first to make GO-GnP couple, then functionalizing the couple with diamine and last add 3 roll mill before adding curing agent to make composite.

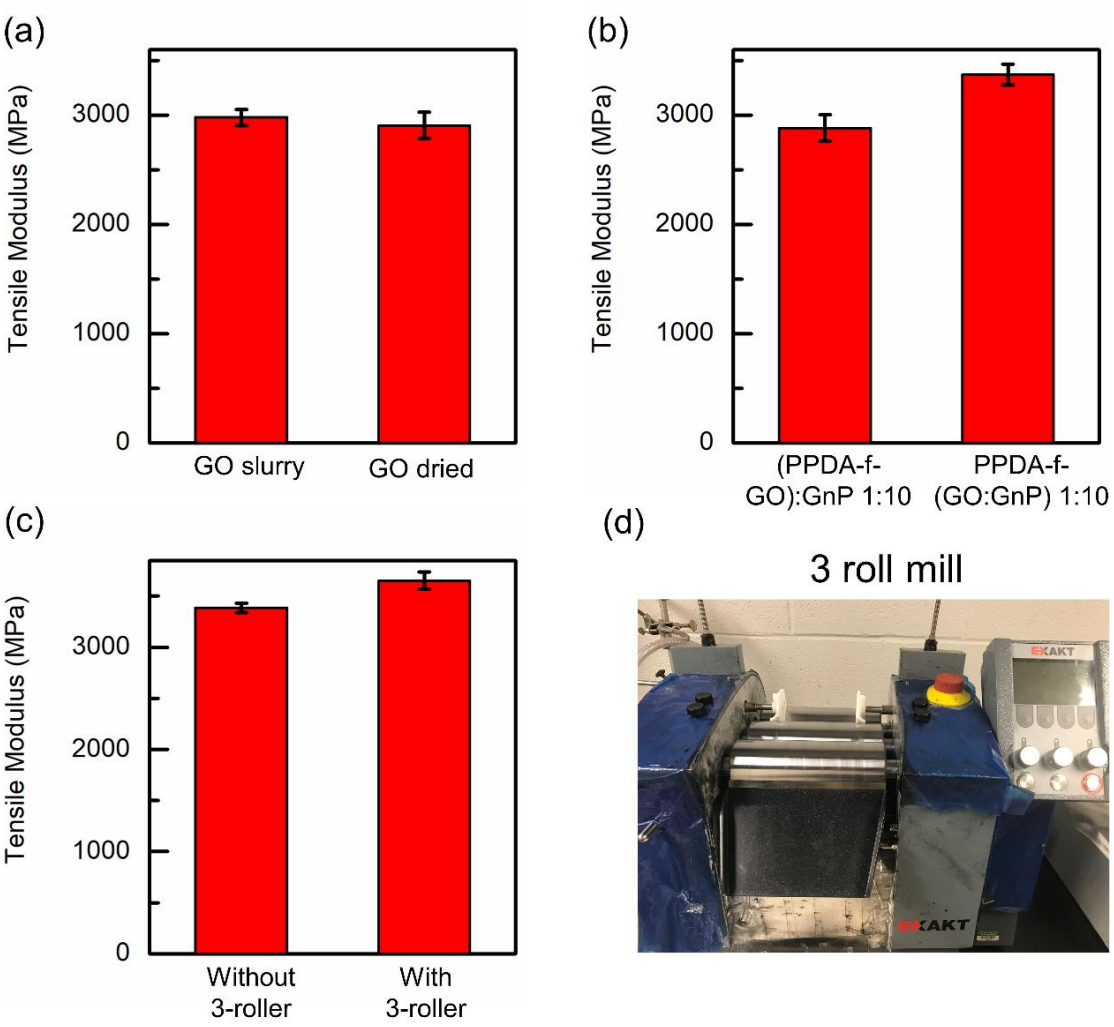

Figure 3.3. The effect of experimental preparation factors on properties of composite (a) 0.43wt% filler, GO under two different drying state: GO slurry or dried GO (75 °C, 12h, forming the hard plate); (b) 0.43wt% filler, either using PPDA functionalizing GO or GO-GnP couple; (c) 0.86wt% filler, PPDA functionalized GO-GnP couple(GO:GnP 1:10), with or without 3-roll mill; (d) The set-up for 3-roll mill

The tensile properties of the neat epoxy and its composites are summarized in Figure 3.4. Here, the GO and GnP synergistic effect and further treatment of the GO surface with different diamines was investigated. First, GO-GnP synergistic effect was analyzed. Compared to neat epoxy, simply using GO or GnP or GO-GnP couple gave enhancements in tensile modulus which varied from ~20% to 30%. While the tensile strength was maintained almost same as neat

epoxy, as the filler loading increased from 0.43wt% to 0.86wt%, simply using GO as the filler, the tensile strength and modulus dropped around 55% and 22%, respectively. This was attributed to two reasons: first, the higher GO loading led to poor dispersion in the epoxy matrix; second, some curing agent reacted with functional group on the GO surface, and in addition some epoxy monomer chains could attach onto the GO surface, which decreased their mobility to react with other curing agent and monomers to form crosslinks. The advantages of using GO-GnP couple as the filler became clearer at higher loading (0.86wt%) compared to lower loading (0.43wt%). At 0.86wt% filler loading, GO-GnP couple, with weight ratio between GO and GnP of 1:10, gave the highest improvements in tensile modulus ~30% compared to ~22% drop for GO sample and ~21% increased from GnP sample. Part of sp^2 structure of GnP was destroyed and formed the sp^3 structure in GO because oxygen based functional groups were bonded to the carbon atoms in the basal plane, which resulted in defects in the GO structure and lowered its mechanical properties. GO worked as a coupling agent, improving interfacial interaction between GnP and epoxy matrix. As reflected from results, the ratio between GnP and GO was important, the ideal condition was all the GnP platelets were coated with GO layer, and this existed as the reinforcing unit uniformly dispersed into the epoxy matrix. However, in reality, the percentage of GO bonded to GnP, the re-stacking happened between GO and GO, GnP and GnP or even GO-GnP couple with each other, and dispersion property of these units affected the expecting results.

GO, GO-GnP couple was functionalized with two diamines with molar mass ~108g mol^{-1} (PPDA) and 2000g mol^{-1} (Jeffamine D2000). At different filler contents, the highest improvements in tensile modulus all come from the PPDA-f-(GO-GnP) sample, but under different loadings from different GO/GnP combinations. The ~40% and ~60% enhancement in

tensile modulus were achieved from PPDA functionalized GO-GnP couple with weight ratio of 1:10 (0.43wt% filler loading) and 1:50 (0.86wt% filler loading) respectively. The diamines formed bonds between the GO surface and the epoxy matrix which increased the load transfer efficiency and interfacial strength producing further improvements compared to simply using the GO-GnP couple. Under the same GO-GnP combination, the PPDA functionalized sample compared to the Jeffamine D2000 functionalized ones, produced a greater improvement in tensile modulus especially under larger filler loading. This was attributed to these two diamines with different chain length and structures forming different interphase structures between filler and bulk polymer [41]. The grafting of PPDA chains onto the GO surface would primarily produce interphase structures, in which the mobility of the segments was constrained and thus led to limited load transfer at interphase. The Jeffamine D2000 chains on the GO surface could undergo significantly higher deformation based on the soft and flexible interphase due to longer linear molecular chain length. This was beneficial for improving the mobility of the fillers in the polymer matrix and energy dissipation during the deformation. One unexpected result was a significant drop for PPDA-f-GO sample under 0.86wt% loading, which showed a much lower tensile modulus. This was possibly due to the short chain length of PPDA, which was rigid and easier to form a structure with one diamine bonded to GO, and the other unbonded while for Jeffamine D2000, which was flexible and both diamine ends could bond to the GO surface. This produced PPDA-f-GO with more free primary amines on the GO surface which reacted with the epoxy leading to more linear chains and decreasing cross-link density.

The toughness of epoxy based composites calculated from tensile stress-strain curves is summarized in Figure 3.4 (e) and (f). The addition of GO increased the toughness of composite over 200% compared to neat epoxy. This was the result of the surface functional groups of the

GO interacting with the epoxy matrix. This led to deflection of the propagating crack and as a result, more energy was needed for crack growth. GO-GnP couple as the filler was not as good as GO in enhancing toughness. At 0.43wt% loading, a ~30-40% drop in toughness was measured and at 0.86wt% loading, the GO-GnP with mass ratio of 1:50 still produced a ~20% decrease. However, when the GO-GnP ratio was adjusted to 1:10 the toughness increased ~11% which was much better than using GnP alone which showed a ~42% drop. This was because at higher loading, GO acts as a surfactant and increases the dispersion and interfacial strength of GnP with the epoxy matrix. A possible explanation for why GO-GnP couple fillers gave lower enhancement in toughness compared to GO as filler may be due to the small size of GO-GnP filler which is not as effective in producing crack deflection within the matrix [59]. Another possibility could be attributed to different failure modes for layered fillers. Pinning/bi-furcation and crack deflection plus separation between layers were discussed by Chandrasekaran et al [60]. For the first mode, the crack was initially pinned to layered fillers, and bifurcated the particles, but continued to propagate in the 'shadow' of the particles. As a result, both cracks grew around the fillers, and later connected again, this led to the height level of one crack plane as not always same as that of adjacent one. The other mode, the separation between layered fillers where the crack penetrates through the layered fillers and separated them to continue growth. In comparing the GO and GO-GnP, the interaction between particles of GO is π-π plus hydrogen bonds because the GO surface is rich in oxygen functional groups, while the interaction between GO and GnP particles is π-π only which requires less energy to separate the fillers. After functionalization with the two different diamines, the interfacial strength increased. The Jeffamine D2000 treated GO gave higher toughness, as this diamine with longer chains,

improved matrix ductility and increased energy dissipation for crack deflection/growth [41]. This gave the lower tensile modulus compared to short chains diamine functionalized samples.

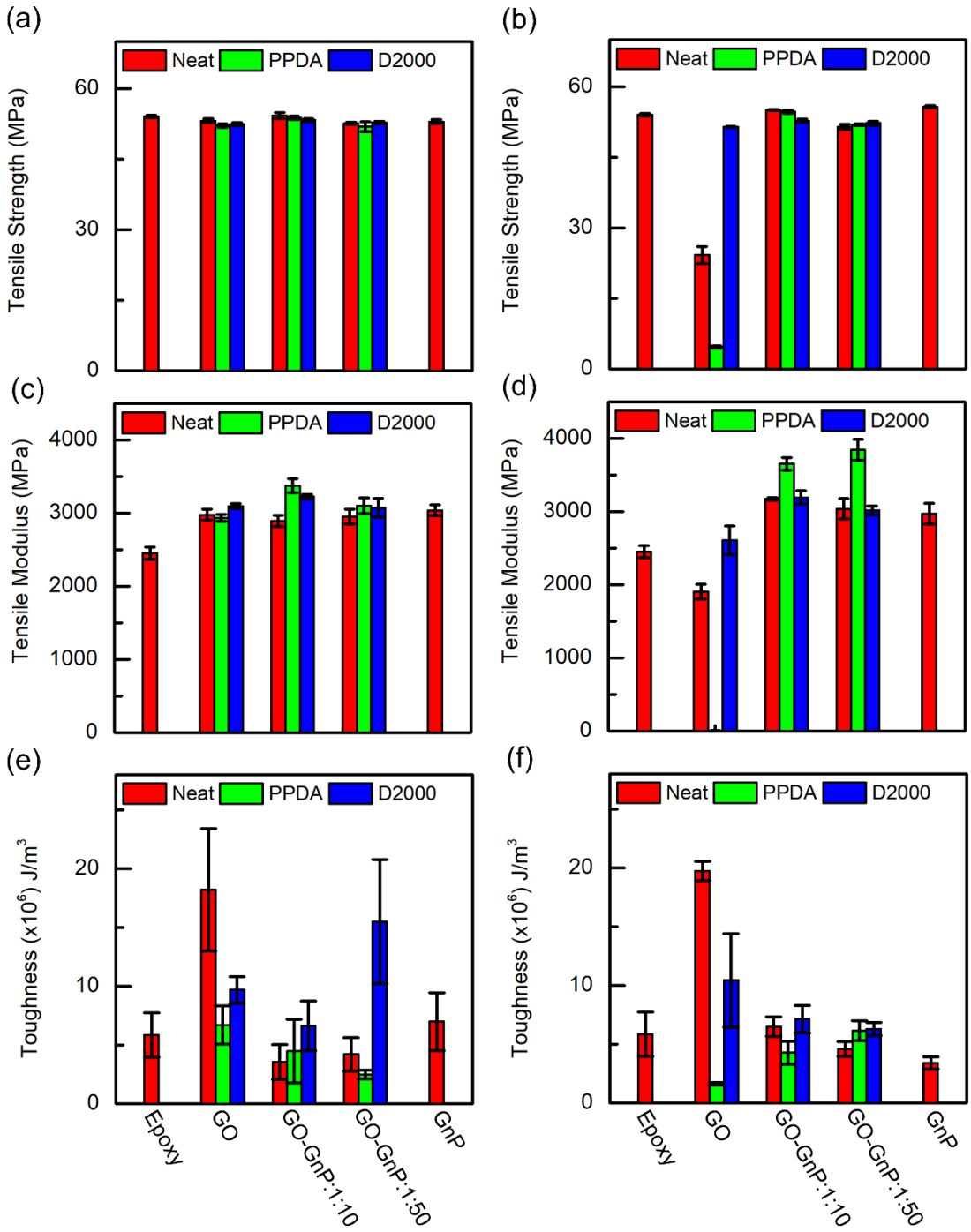

Figure 3.4. Tensile properties for epoxy composite: (a), (c), (e) are samples with 0.43wt% filler loading; (b), (d), (f) are samples with 0.86wt% filler loading

3.3.4 Analysis for fracture surface and interface

The fracture surface of the tensile specimens was observed to explore the interface between filler and epoxy matrix and dispersion state of different fillers. Figure 3.5&3.6 and 3.7&3.8 summarizes the facture morphology for all composites with 0.43wt% and 0.86wt% filler loading, respectively. The neat epoxy baseline has a clean and smooth fracture surface resulting from fast crack growth due to the brittle structure and poor resistance to crack growth. After incorporating GO, GnP, GO-GnP couple, or functionalized these nano-layered fillers into the matrix, a rough, coarse surface with multiplane features on the fracture surface is observed suggesting that the layered fillers have caused deflection of in the propagating crack fronts. This process led to off-plane loading that generated a new fracture surface and therefore increased the required energy for crack growth [22]. The facture surface roughness increased as the GO was replaced with GnP and with increased filler loading. Large agglomerates are not observed on the fracture surfaces indicating that dispersion of all the fillers after functionalization with different diamines is good. Crack pinning was detected in fracture surface. When the propagating crack reached the GnP particles, the crack front was deflected by bowing between particles but remained pinned at the particles. This is apparent from the appearance of the bowed lines that appear on the fracture surface. This phenomenon appears more intense with increased filler loading and filler functionalized with diamines.

Another failure mode was observed as shown in Figure 3.9. Here flow patterns are not observed which is typical for the fracture surface of epoxy. However, in this case this surface is composed of the surface of layered fillers. Compared to the GO and GnP sample, the diamine functionalized GO-GnP couple, showed better dispersion and interaction with matrix. The

functionalized GO-GnP filler maintained its layered structure that could fully make use of their high surface area and reinforcing effect compared to the GnP sample.

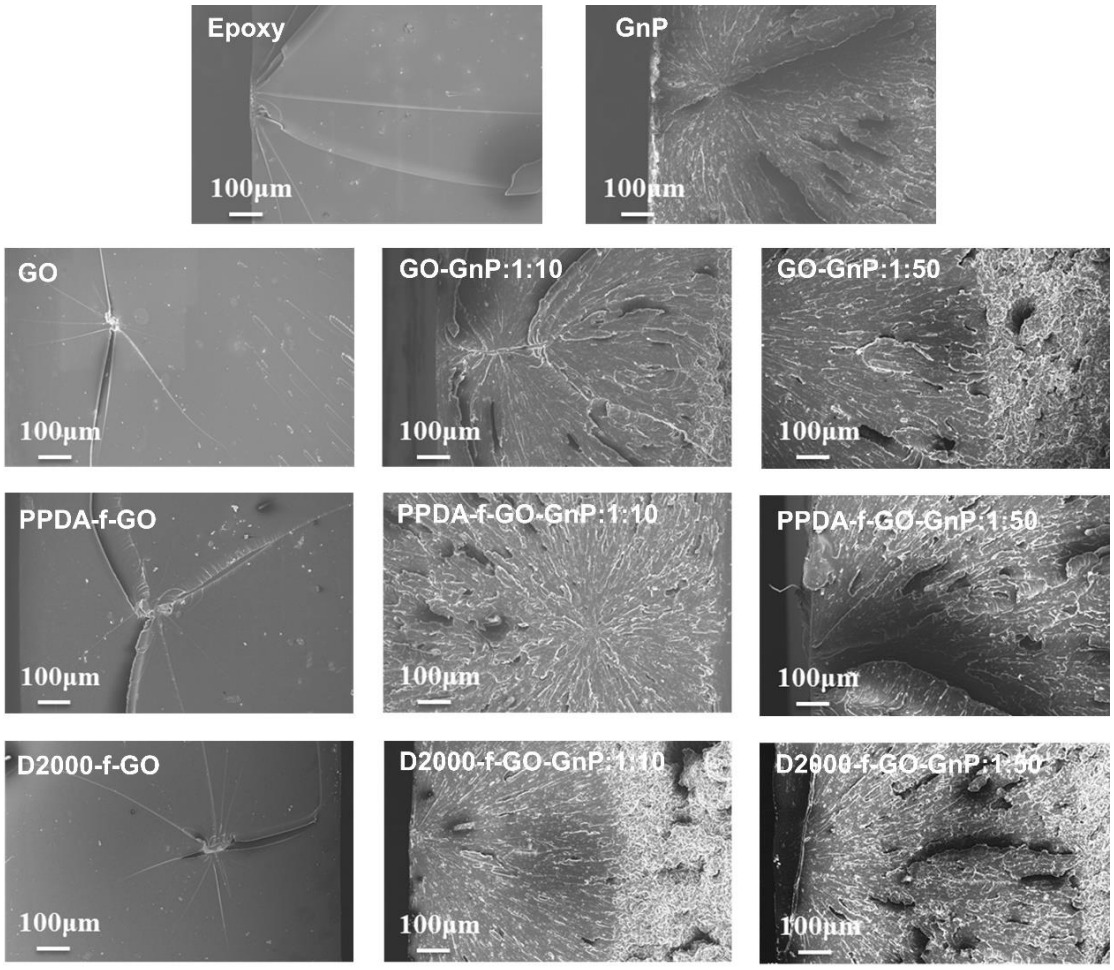

Figure 3.5. Fracture morphology for composite sample with 0.43wt% filler loading (including breaking center)

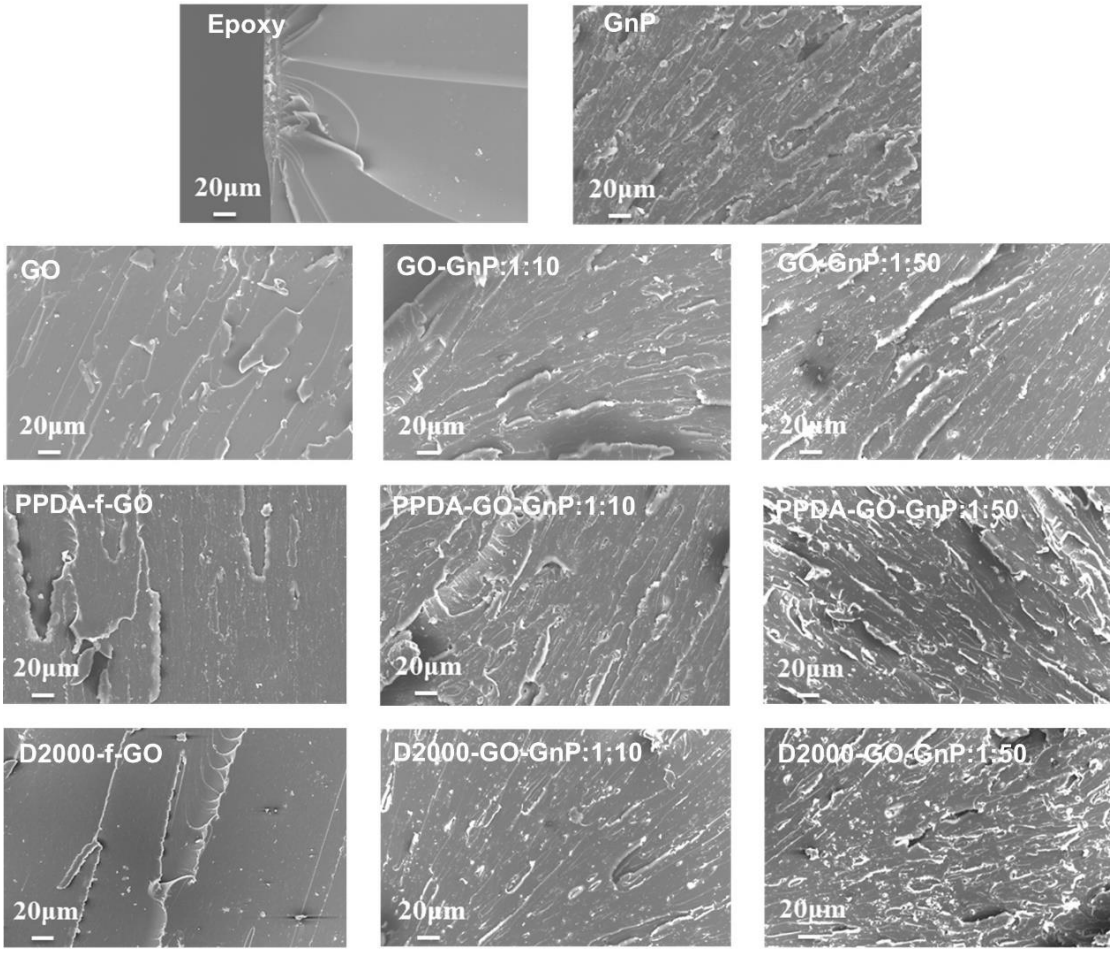

Figure 3.6. Fracture morphology for composite sample with 0.43wt% filler loading

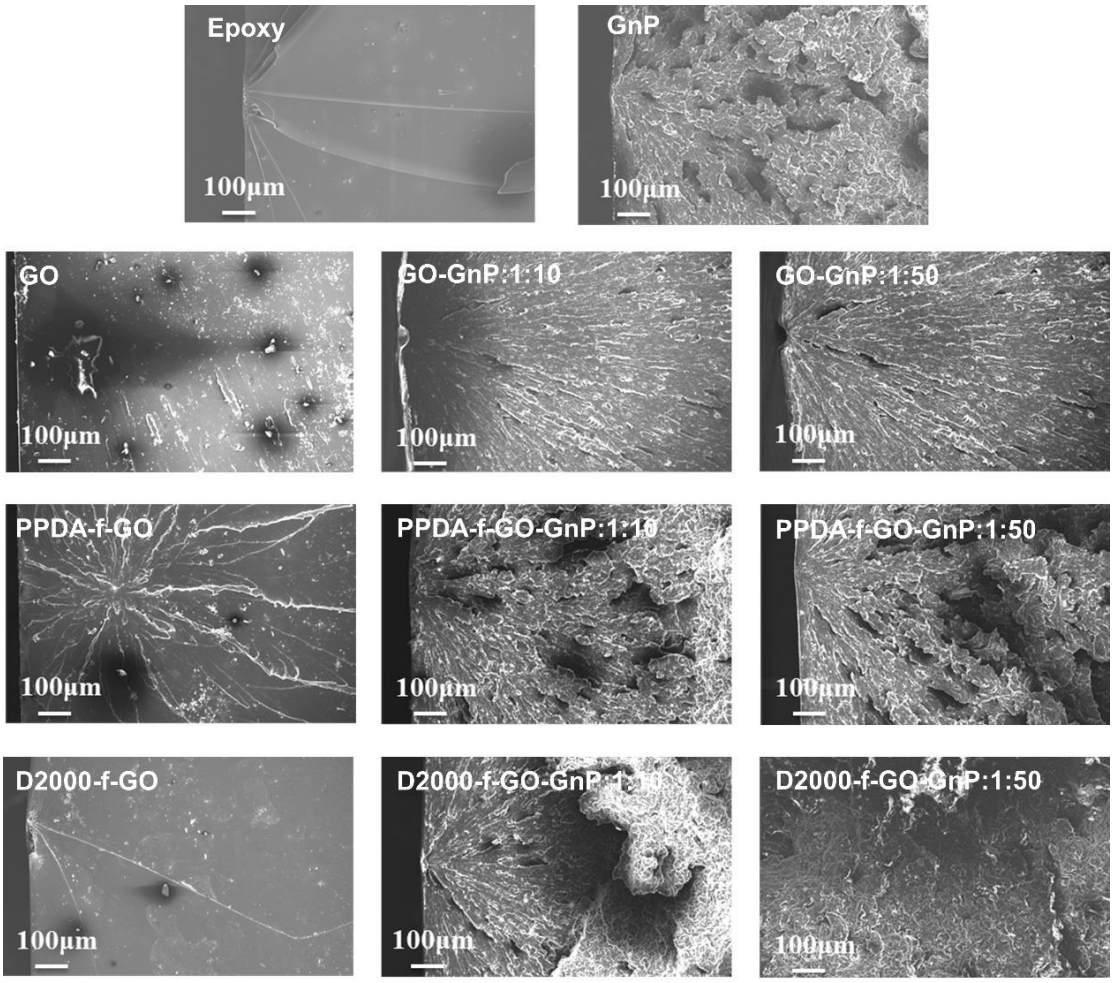

Figure 3.7. Fracture morphology for composite sample with 0.86wt% filler loading (including breaking center)

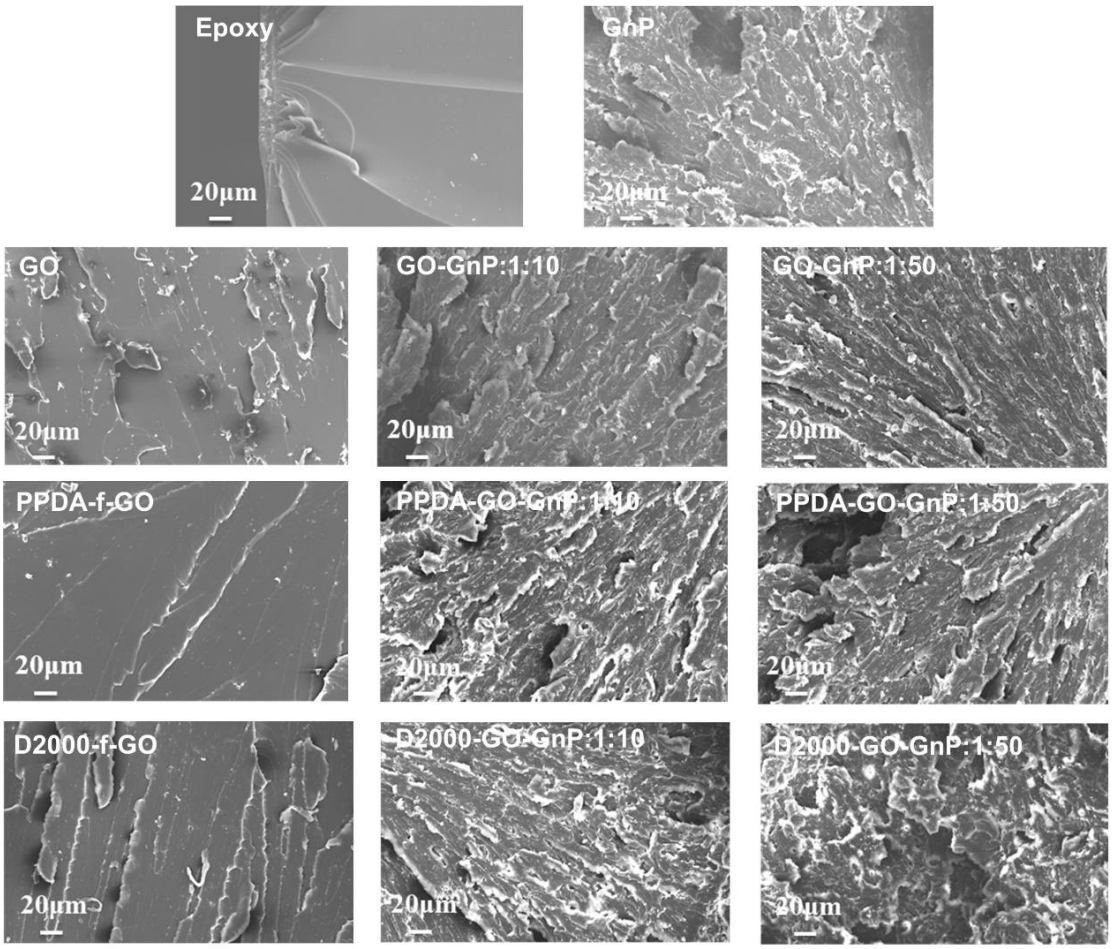

Figure 3.8. Fracture morphology for composite sample with 0.86wt% filler loading

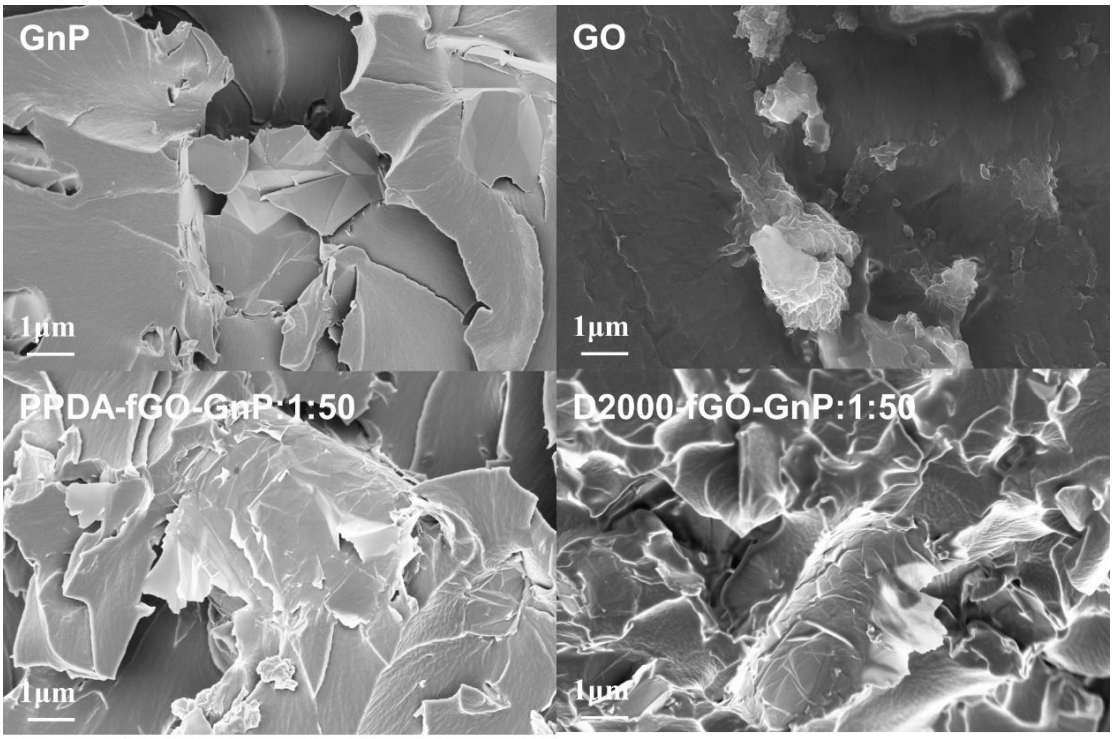

Figure 3.9. Interfacial properties for selected composite samples with 0.86wt% filler loading

3.4 Conclusion

GO was shown to be able to function as a surfactant assisting in the dispersion of other carbon materials into different solvents, because of both π-π interaction and its highly oxidized surface. As a result, it has been shown that GO can be used as a coupling agent to improve the interfacial properties between GnP and the epoxy matrix. In this paper, GO-GnP used as a reinforcing couple for an epoxy matrix was surface treated with two diamines with different chain length (PPDA and Jeffamine D2000). The enhancement for different weight ratios of GO to GnP, functionalization with different diamines, filler loadings of 0.43wt% and 0.86wt%, was investigated. The PPDA-f-(GO-GnP: 1:10) sample gave ~40% increase in the tensile modulus at 0.43wt%, while at 0.86wt%, the tensile modulus increased to ~60% for the PPDA-f-(GO-GnP: 1:50) sample. These results were far better than simply using GO or GnP by themselves as

fillers to the epoxy. The GnP has a 2D layered morphology heterogeneous surface with a large basal plane and edges with low functionalization. To improve its interaction with the epoxy matrix, GO because of its large content of surface functional groups, was added to the system as a coupling agent. The functionalized GO-GnP couple with a relatively small amount of GO, has shown enhanced interaction between the GnP and epoxy matrix, achieving better results compared to simply using GnP or GO. Further at higher loading, 0.86wt%, the functionalized GO-GnP couple produced up to a ~110% better performance in toughness compared with only using GnP as the filler. Thus, functionalized the GO-GnP couple has been shown as a possible method to increase both mechanical properties and toughness in an epoxy matrix.

REFERENCES

REFERENCES

[1] Novoselov KS, Geim AK, Morozov SV, Jiang D, Zhang Y, Dubonos SV, Grigorieva IV, Firsov AA. Electric field effect in atomically thin carbon films. science. 2004 Oct 22;306(5696):666-9.

[2] Stoller MD, Park S, Zhu Y, An J, Ruoff RS. Graphene-based ultracapacitors. Nano letters. 2008 Sep 13;8(10):3498-502.

[3] Lee C, Wei X, Kysar JW, Hone J. Measurement of the elastic properties and intrinsic strength of monolayer graphene. science. 2008 Jul 18;321(5887):385-8.

[4] Balandin AA, Ghosh S, Bao W, Calizo I, Teweldebrhan D, Miao F, Lau CN. Superior thermal conductivity of single-layer graphene. Nano letters. 2008 Feb 20;8(3):902-7.

[5] Huang X, Qi X, Boey F, Zhang H. Graphene-based composites. Chemical Society Reviews. 2012;41(2):666-86.

[6] Geim AK, Novoselov KS. The rise of graphene. Nature materials. 2007 March; 6:183-191.

[7] Galpaya D, Wang M, Liu M, Motta N, Waclawik ER, Yan C. Recent advances in fabrication and characterization of graphene-polymer nanocomposites. Graphene. 2012;1(2):30-49.

[8] Kim KS, Zhao Y, Jang H, Lee SY, Kim JM, Kim KS, Ahn JH, Kim P, Choi JY, Hong BH. Large-scale pattern growth of graphene films for stretchable transparent electrodes. nature. 2009 Feb;457(7230):706.

[9] Li X, Zhang G, Bai X, Sun X, Wang X, Wang E, Dai H. Highly conducting graphene sheets and Langmuir–Blodgett films. Nature nanotechnology. 2008 Sep;3(9):538.

[10] Berger C, Song Z, Li T, Li X, Ogbazghi AY, Feng R, Dai Z, Marchenkov AN, Conrad EH, First PN, De Heer WA. Ultrathin epitaxial graphite: 2D electron gas properties and a route toward graphene-based nanoelectronics. The Journal of Physical Chemistry B. 2004 Dec 30;108(52):19912-6.

[11] Stankovich S, Dikin DA, Piner RD, Kohlhaas KA, Kleinhammes A, Jia Y, Wu Y, Nguyen ST, Ruoff RS. Synthesis of graphene-based nanosheets via chemical reduction of exfoliated graphite oxide. carbon. 2007 Jun 1;45(7):1558-65.

[12] Hummers Jr WS, Offeman RE. Preparation of graphitic oxide. Journal of the american chemical society. 1958 Mar;80(6):1339.

[13] Chandrasekaran S, Seidel C, Schulte K. Preparation and characterization of graphite nano-platelet (GNP)/epoxy nano-composite: Mechanical, electrical and thermal properties. European Polymer Journal. 2013 Dec 1;49(12):3878-88.

[14] Wan YJ, Tang LC, Yan D, Zhao L, Li YB, Wu LB, Jiang JX, Lai GQ. Improved dispersion and interface in the graphene/epoxy composites via a facile surfactant-assisted process. Composites science and technology. 2013 Jun 18;82:60-8.

[15] Qin W, Vautard F, Drzal LT, Yu J. Mechanical and electrical properties of carbon fiber composites with incorporation of graphene nanoplatelets at the fiber–matrix interphase. Composites Part B: Engineering. 2015 Feb 1;69:335-41.

[16] Jia J, Sun X, Lin X, Shen X, Mai YW, Kim JK. Exceptional electrical conductivity and fracture resistance of 3D interconnected graphene foam/epoxy composites. Acs Nano. 2014 May 27;8(6):5774-83.

[17] Lerf A, He H, Forster M, Klinowski J. Structure of graphite oxide revisited. The Journal of Physical Chemistry B. 1998 Jun 4;102(23):4477-82.

[18] Konios D, Stylianakis MM, Stratakis E, Kymakis E. Dispersion behaviour of graphene oxide and reduced graphene oxide. Journal of colloid and interface science. 2014 Sep 15;430:108-12.

[19] Paredes JI, Villar-Rodil S, Martínez-Alonso A, Tascon JM. Graphene oxide dispersions in organic solvents. Langmuir. 2008 Aug 29;24(19):10560-4.

[20] Li Z, Wang R, Young RJ, Deng L, Yang F, Hao L, Jiao W, Liu W. Control of the functionality of graphene oxide for its application in epoxy nanocomposites. Polymer. 2013 Nov 1;54(23):6437-46.

[21] Wan YJ, Tang LC, Gong LX, Yan D, Li YB, Wu LB, Jiang JX, Lai GQ. Grafting of epoxy chains onto graphene oxide for epoxy composites with improved mechanical and thermal properties. Carbon. 2014 Apr 1;69:467-80.

[22] Bortz DR, Heras EG, Martin-Gullon I. Impressive fatigue life and fracture toughness improvements in graphene oxide/epoxy composites. Macromolecules. 2011 Dec 2;45(1):238-45.

[23] Kim J, Cote LJ, Kim F, Yuan W, Shull KR, Huang J. Graphene oxide sheets at interfaces. Journal of the American Chemical Society. 2010 May 19;132(23):8180-6.

[24] Cote LJ, Kim J, Tung VC, Luo J, Kim F, Huang J. Graphene oxide as surfactant sheets. Pure and Applied Chemistry. 2010 Dec 1;83(1):95-110.

[25] Mohd Zubir MN, Badarudin A, Kazi SN, Nay Ming H, Sadri R, Amiri A. Investigation on the use of graphene oxide as novel surfactant for stabilizing carbon based materials. Journal of Dispersion Science and Technology. 2016 Oct 2;37(10):1395-407.

[26] Kazi SN, Badarudin A, Zubir MN, Ming HN, Misran M, Sadeghinezhad E, Mehrali M, Syuhada NI. Investigation on the use of graphene oxide as novel surfactant to stabilize weakly charged graphene nanoplatelets. Nanoscale research letters. 2015 Dec 1;10(1):212.

[27] Zhang C, Ren L, Wang X, Liu T. Graphene oxide-assisted dispersion of pristine multiwalled carbon nanotubes in aqueous media. The Journal of Physical Chemistry C. 2010 Jun 15;114(26):11435-40.

[28] Qiu L, Yang X, Gou X, Yang W, Ma ZF, Wallace GG, Li D. Dispersing carbon nanotubes with graphene oxide in water and synergistic effects between graphene derivatives. Chemistry–A European Journal. 2010 Sep 17;16(35):10653-8.

[29] Ellis B, editor. Chemistry and technology of epoxy resins. London: Blackie Academic & Professional; 1993 Jan.

[30] May C, editor. Epoxy resins: chemistry and technology. CRC press; 1987 Dec 23.

[31] Lee H, Neville K. " Book Review-Handbook of Epoxy Resins". Industrial & Engineering Chemistry. 1967 Sep;59(9):16-7.

[32] Tang LC, Zhang H, Sprenger S, Ye L, Zhang Z. Fracture mechanisms of epoxy-based ternary composites filled with rigid-soft particles. Composites Science and Technology. 2012 Mar 8;72(5):558-65.

[33] Rafiee MA, Rafiee J, Wang Z, Song H, Yu ZZ, Koratkar N. Enhanced mechanical properties of nanocomposites at low graphene content. ACS nano. 2009 Dec 3;3(12):3884-90.

[34] Thostenson ET, Chou TW. Processing-structure-multi-functional property relationship in carbon nanotube/epoxy composites. Carbon. 2006 Nov 1;44(14):3022-9.

[35] Wang K, Chen L, Wu J, Toh ML, He C, Yee AF. Epoxy nanocomposites with highly exfoliated clay: mechanical properties and fracture mechanisms. Macromolecules. 2005 Feb 8;38(3):788-800.

[36] XG Science https://xgsciences.com

[37] Marcano DC, Kosynkin DV, Berlin JM, Sinitskii A, Sun Z, Slesarev A, Alemany LB, Lu W, Tour JM. Improved synthesis of graphene oxide. ACS nano. 2010 Jul 22;4(8):4806-14.

[38] Gudarzi MM, Sharif F. Enhancement of dispersion and bonding of graphene-polymer through wet transfer of functionalized graphene oxide. Express Polymer Letters. 2012 Dec 1;6(12).

[39] Wan YJ, Gong LX, Tang LC, Wu LB, Jiang JX. Mechanical properties of epoxy composites filled with silane-functionalized graphene oxide. Composites Part A: Applied Science and Manufacturing. 2014 Sep 1;64:79-89.

[40] Kudin KN, Ozbas B, Schniepp HC, Prud'Homme RK, Aksay IA, Car R. Raman spectra of graphite oxide and functionalized graphene sheets. Nano letters. 2008 Jan 9;8(1):36-41.

[41] Guan LZ, Wan YJ, Gong LX, Yan D, Tang LC, Wu LB, Jiang JX, Lai GQ. Toward effective and tunable interphases in graphene oxide/epoxy composites by grafting different chain lengths of polyetheramine onto graphene oxide. Journal of Materials Chemistry A. 2014;2(36):15058-69.

[42] Shen B, Zhai W, Tao M, Lu D, Zheng W. Chemical functionalization of graphene oxide toward the tailoring of the interface in polymer composites. Composites Science and Technology. 2013 Mar 22;77:87-94.

[43] Lipson HS, Stokes AR. The structure of graphite. Proceedings of the Royal Society of London. Series A. Mathematical and Physical Sciences. 1942 Sep 24;181(984):101-5.

[44] Yasmin A, Luo JJ, Daniel IM. Processing of expanded graphite reinforced polymer nanocomposites. Composites Science and Technology. 2006 Jul 1;66(9):1182-9.

[45] Ganguli S, Roy AK, Anderson DP. Improved thermal conductivity for chemically functionalized exfoliated graphite/epoxy composites. Carbon. 2008 Apr 1;46(5):806-17.

[46] Li Y, Tang L, Li J. Preparation and electrochemical performance for methanol oxidation of Pt/graphene nanocomposites. Electrochemistry Communications. 2009 Apr 1;11(4):846-9.

[47] Jeong HK, Lee YP, Lahaye RJ, Park MH, An KH, Kim IJ, Yang CW, Park CY, Ruoff RS, Lee YH. Evidence of graphitic AB stacking order of graphite oxides. Journal of the American Chemical Society. 2008 Jan 30;130(4):1362-6.

[48] McAllister MJ, Li JL, Adamson DH, Schniepp HC, Abdala AA, Liu J, Herrera-Alonso M, Milius DL, Car R, Prud'homme RK, Aksay IA. Single sheet functionalized graphene by oxidation and thermal expansion of graphite. Chemistry of materials. 2007 Sep 4;19(18):4396-404.

[49] Ma HL, Zhang HB, Hu QH, Li WJ, Jiang ZG, Yu ZZ, Dasari A. Functionalization and reduction of graphene oxide with p-phenylene diamine for electrically conductive and thermally stable polystyrene composites. ACS applied materials & interfaces. 2012 Mar 26;4(4):1948-53.

[50] Park S, An J, Potts JR, Velamakanni A, Murali S, Ruoff RS. Hydrazine-reduction of graphite-and graphene oxide. Carbon. 2011 Aug 1;49(9):3019-23.

[51] Moon IK, Lee J, Ruoff RS, Lee H. Reduced graphene oxide by chemical graphitization. Nature communications. 2010 Sep 21;1:73.

[52] Wojtoniszak M, Chen X, Kalenczuk RJ, Wajda A, Łapczuk J, Kurzewski M, Drozdzik M, Chu PK, Borowiak-Palen E. Synthesis, dispersion, and cytocompatibility of graphene oxide and reduced graphene oxide. Colloids and Surfaces B: Biointerfaces. 2012 Jan 1;89:79-85.

[53] Stankovich S, Piner RD, Nguyen ST, Ruoff RS. Synthesis and exfoliation of isocyanate-treated graphene oxide nanoplatelets. Carbon. 2006 Dec 1;44(15):3342-7.

[54] Chen W, Yan L, Bangal PR. Preparation of graphene by the rapid and mild thermal reduction of graphene oxide induced by microwaves. Carbon. 2010 Apr 1;48(4):1146-52.

[55] Mkhoyan KA, Contryman AW, Silcox J, Stewart DA, Eda G, Mattevi C, Miller S, Chhowalla M. Atomic and electronic structure of graphene-oxide. Nano letters. 2009 Feb 6;9(3):1058-63.

[56] Ganguly A, Sharma S, Papakonstantinou P, Hamilton J. Probing the thermal deoxygenation of graphene oxide using high-resolution in situ X-ray-based spectroscopies. The Journal of Physical Chemistry C. 2011 Aug 10;115(34):17009-19.

[57] Hussein A, Sarkar S, Oh D, Lee K, Kim B. Epoxy/p-phenylenediamine functionalized graphene oxide composites and evaluation of their fracture toughness and tensile properties. Journal of Applied Polymer Science. 2016 Sep 10;133(34).

[58] Ramezanzadeh B, Bahlakeh G, Moghadam MM, Miraftab R. Impact of size-controlled p-phenylenediamine (PPDA)-functionalized graphene oxide nanosheets on the GO-PPDA/Epoxy anti-corrosion, interfacial interactions and mechanical properties enhancement: Experimental and quantum mechanics investigations. Chemical Engineering Journal. 2018 Mar 1;335:737-55.

[59] Sharmila TB, Antony JV, Jayakrishnan MP, Beegum PS, Thachil ET. Mechanical, thermal and dielectric properties of hybrid composites of epoxy and reduced graphene oxide/iron oxide. Materials & Design. 2016 Jan 15;90:66-75.

[60] Chandrasekaran S, Sato N, Tölle F, Mülhaupt R, Fiedler B, Schulte K. Fracture toughness and failure mechanism of graphene based epoxy composites. Composites Science and Technology. 2014 Jun 16;97:90-9.

CHAPTER 4 - GRAPHENE NANOPLATELET COMPOSITE 'PAPER' AS AN ELECTROSTATIC ACTUATOR

The materials in this chapter was published in the Journal Nanotechnology in June 2018 under the title Graphene nanoplatelet composite 'paper' as an electrostatic actuator. (10.1088/1361-6528/aac5c4)

4.1 Introduction

An actuator is a device, which can move or control a mechanism or system. Traditional actuators utilize pneumatics, motors, hydraulics or electronic motors [1]. In order to reduce size, weight and energy, alternative technologies are being investigated for different applications. Micro-electro-mechanical-system (MEMS), one kind of electronic actuator, is capable of moving a suspended microstructure precisely and integrating with microelectronic circuits to perform linear or angular motions [2]. Among different mechanisms used in assembling the MEMS actuator, the thermal/bimetallic bimorph [3-6], piezoelectric [7-10], electrostatic [11-14] and electromagnetic [15-19] actuation have been widely discussed in recent publications and used in MEMS applications.

Electrostatic actuators have been employed as the prime movers in various MEMS since 1980s [20], and nowadays most electrostatic actuators are used as micro-actuators in the application as electro-mechanical switches and replays, valves, flow control actuators, micro-scale mechanical testing instruments and structures, optical switches [21,22]. The mechanism for electrostatic actuator is the Maxwell stress effect or columbic attraction between opposite charges on the electrode, the schematic illustration is shown in Figure 4.1.

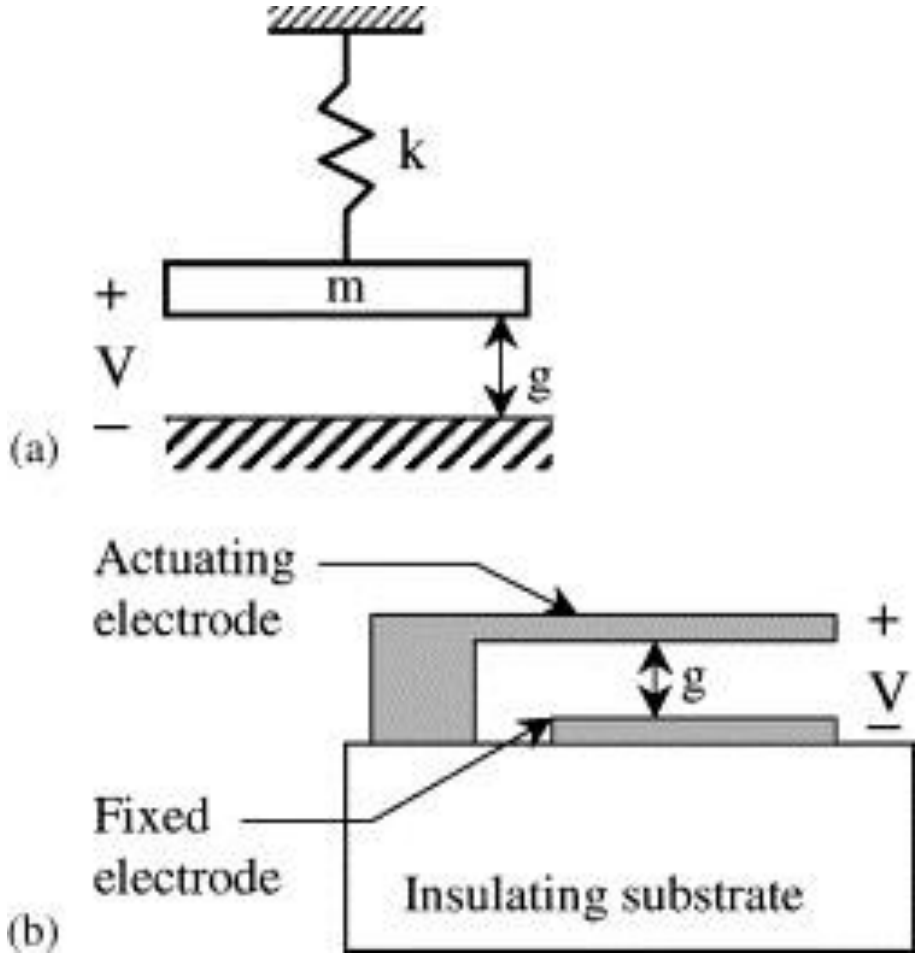

Figure 4.1. Electrostatic actuator: (a) Lump-parameter representation of an electrostatic actuator. (b) Schematic cross-section of a beam electrostatic actuator [21]

$$F_e = -\varepsilon_0 \varepsilon_r A V^2 / 2g^2 \tag{1}$$

where ε_0 is permittivity of the free space, ε_r is the relative permittivity, A is the area of electrode, V is the applied voltage and g is the gap between two electrodes. Based on this mechanism, various electrostatic actuator designs were put forward, such as parallel-plate, laterally comb drive and vertical comb drive actuators. The main benefits for using an electrostatic actuator are: the longer stroke; larger force with magnifying voltage or decreasing the gap; high power to weight ratio and low energy consumption [23]. However, the electrostatic attractive actuators have

a significant drawback in the 'pull-in effect' when the moveable electrode moves beyond one third of the initial gap. The stability between the mechanical force from the spring and the electrostatic force will diminish, limiting the actuation range of the electrostatic actuator. This could be explained based on the following equations:

The mechanical force(F_M) exerted by the spring on the movable plate can be calculated by

$$F_M = k\delta = k(g_0 - g) \tag{2}$$

here k is the stiffness of the spring, g_0 is the initial length of the spring and δ is the displacement of the actuator. The movable plate reaches the equilibrium when the electrostatic force equals to mechanical force F_e=F_M:

$$\frac{\varepsilon A V^2}{2g^2} = k(g_0 - g) \tag{3}$$

Therefore, the actuating voltage could be achieved:

$$V = \sqrt{\frac{2kg^2(g_0 - g)}{\varepsilon A}} \tag{4}$$

If the gap is reduced to two-thirds of the initial size, the stability will lose due to the pull-in effect, which limits the actuating distance. From equation(4), this pull-in voltage could be calculated:

$$V = \sqrt{\frac{8kg_0^3}{27\varepsilon A}} \tag{5}$$

Based on equation (2), it shows that, expression for mechanical force F_M is first order (straight line), while the expression for the electrostatic force F_e is a second order, the solution for equation is g, that is the space between two parallel plates, and if the curves are plotted in one figure, the solution is the crossing point of these two curves. When the voltage increases, the second-order curve will move up, where it will finally reach a position where the two curves

have one crossing point. That is the critical point, also defined as pull-in effect point. Above this point, there is no crossing-point between two curves, which means no solution for equation (3). Under this condition, the system loses its stability and the pull-in effect happens.

In our work, the electro-repulsive force is applied to two moveable electrodes each of which carries the same charge. The mechanism for electro-attractive actuators is applicable here but the 'pull-in effect' is no longer a factor which limits the actuation range.

The electrode material selection is another aspect of actuator design. Processing considerations once made silicon a popular choice for the actuator material, but recent developments in micromachining techniques now enable the integration of a number of different metals, alloys, ceramics, and polymers into MEMS [24]. As shown in Figure 4.2, Strikar et al [21]. have shown a materials chart for selecting different materials when assembling electrostatic actuators. For Figure 4.2 (a) it shows that the materials capable of a higher actuating speed also require a high modulus and large voltage. The materials lie on or close to the trend line which represents the ideal candidates for actuators. The other three figures show the balance among fracture strength, Young's modulus, actuating speed and electrical resistance. These charts compare different material performance for materials that could be used as electrodes. Polymers among all the other different materials, have a lower modulus, higher fracture strength, wide range electrical resistance, and are close to the trend line in Figure 4.2 (a). Furthermore, polymers possess versatility and flexibility in that they can be combined with different fillers to change their properties to broaden potential applications.

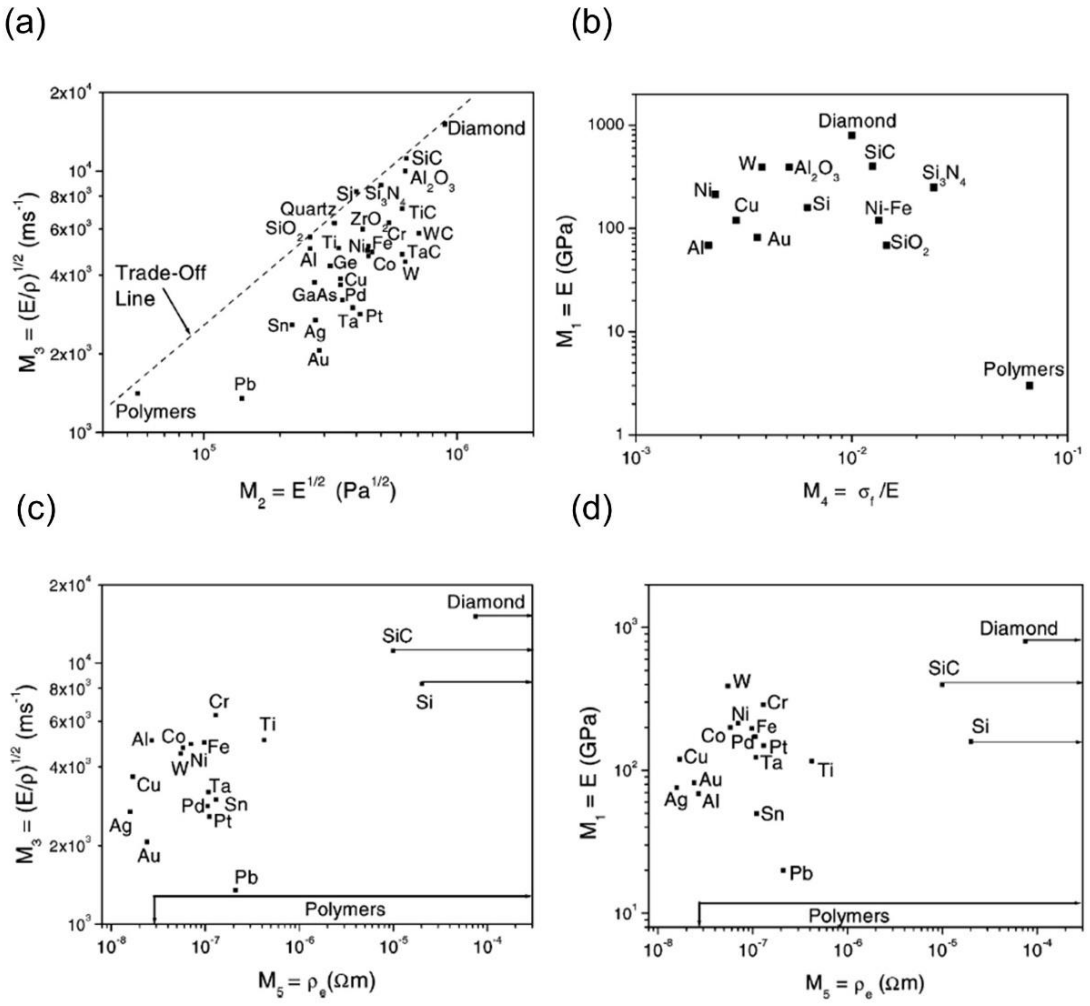

Figure 4.2. Materials selection chart for microfabricated electrostatic actuator: (a) Wave speed $\sqrt{(E/\rho)}$ plotted against the square root of Young's modulus; (b) Young's modulus (E) plotted against the ratio of the facture strength(σ_f) to the Young's modulus; (c) Wave speed $\sqrt{E/\rho}$ plotted against the electrical resistivity; (d) Young's modulus (E) plotted against electrical resistivity [21]

Graphene, first discovered in 2004[25], is a single layer of sp^2 carbon, which has outstanding properties and is widely used in various areas. It has excellent mechanical properties (~1 TPa Young's modulus and ~130 GPa in-plane strength [26]), thermal conductivity (~5000 W m^{-1} K^{-1} [27]), and electrical conductivity (up to 6000 S cm^{-1} [28]). Graphene nanoplatelets (GnP) are a stack of a few layers of graphene produced by exfoliating acid-intercalated natural graphite using

thermal shock methods [29]. Different nanoplatelet sizes of GnP can be easily produced with thicknesses of a few nanometers and diameter of each platelet from sub-micron to 25 μm. These GnP materials have excellent electrical, thermal and mechanical properties and can be easily assembled into continuous phases (graphene paper) capable of being used as the electrode materials.

Based on extraordinary properties of graphene and its derivatives, they are widely used to assemble the actuators capable of responding to different stimuli. Park et al. [30] used a filtration method to produce multi wall carbon nanotube(MWCNT)-graphene oxide(GO) bilayer material capable of responding to changes in humidity. Under 12% humidity, the bilayer paper rolled up with MWCNT side facing outward. As the humidity continually increased to 55% - 60%, the paper gradually unrolled, and became flat. When humidity increased to over 60%, the paper began to curl in the opposite direction. Liang et al. [31] prepared a sulfonated-graphene/ TPU composite film, with 1wt% loading, the nanocomposite actuator exhibited repeatable infrared-triggered actuation which could amazingly contract and lift a 21.6 g weight 3.1 cm with 0.21 N of force under exposure to infrared light. The energy density for this actuator was estimated to be over 0.33 J g^{-1}.

In the present work, GnP of approximately 10 microns in diameter are dispersed in water and fabricated into thin 'paper' electrodes by vacuum filtration. The nanoplatelets are easily assembled into the macro-scale paper structure and insulated with a thin epoxy layer. This material was used as the movable arm for the actuator. The performance of the actuator was measured by recording the distance between the movable arms and represented by the potential energy change from initial position to the actuated position. The GnP based electrodes possess outstanding electrical and mechanical properties and further increases in the relative permittivity and surface area of the GnP

based composite paper were explored to improve the performance of the electro-repulsive actuators. Even though a high voltage is required, compared to traditional micro-size electrostatic actuators, the actuating separate distance and output work are significantly improved.

4.2 Material and Methods

4.2.1 Preparation for GnP papers

GnP R10 powder (with average diameter of 10 μm, and surface area varies from 30 to 60 m^2 g^{-1}) was obtained from XG Science [32] and used as received. 0.4 g GnP was dispersed into water with aid of 1 mg ml^{-1} polyethyleneimine (PEI, surfactant) to make the GnP suspension. The weight ratio between GnP and PEI is 1:1. The suspension was ultrasonicated for 3 min with output power of 120 W, then stirred overnight. The GnP suspension was filtered slowly and the resulting GnP paper with its support membrane filter was kept at room temperature overnight, then peeled off the membrane filter and further dried in a vacuum oven at 75 °C for 24 h to produce the GnP paper before further usage.

Four different kinds of hybrid paper were made: GnP R10 /cellulose nanocrystal (CNC) hybrid paper; barium titanate (BT) particle coated GnP R10 paper; GnP R10/C750 hybrid paper; and potassium permanganate microwave treated GnP R10 paper (porous GnP paper).

The GnP/cellulose nanocrystal(CNC) hybrid paper, 10wt% of cellulose nanocrystal (based on GnP) was added drop-wise into the GnP R10 suspension under stirring for 24 h, then the hybrid paper was processed by filtration of the suspension under room temperature, the paper was peeled from the filter and further dried in the vacuum oven under 75 °C for 24 h.

Barium titanate (BT) particles were coated on the GnP R10 paper. 10 g of barium titanate particles were dispersed into 150 ml isopropanol under ultrasonication for 1 h. 10 ml of the barium titanate dispersion were diluted into 50 ml isopropanol for better spreading on the GnP paper before filtration. The suspension was placed on the dried GnP R10 paper, which was supported on a glass filter. The diluted barium titanate solution was filtered through it, forming a thin white layer on the surface of the GnP paper. This hybrid paper was dried at room temperature overnight, peeled from the filter membrane and then placed it into a vacuum oven for further drying to remove residue isopropanol.

The GnP R10/C750 (with average diameter less than 1 μm and surface area around 750 $m^2 g^{-1}$) hybrid paper was produced by a layer-by-layer method with a goal to create a GnP R10-C750-R10 sandwich structure. This sandwich structure was necessary since the C750 has the larger surface area, which would be important in increasing the capacitance, but does not form a self-supporting 'paper' structure because of its aggregate shape. 0.4 g GnP C750 was dispersed into 80g NMP, using a Flaktech mixer at 3000 rpm for 3 minutes followed by sonication under 175 W for 1 h 15 min. After centrifugation at 750 rpm for 30 minutes, the upper 75% of the suspension was used in the paper making process. Half of the as made GnP R10 suspension was filtered first, followed by the C750 suspension, and then by the remaining GnP R10 suspension. The filtered paper was dried with the same process and its final weight content of C750 was 10wt% (based on GnP R10).

The potassium permanganate treated GnP paper (Porous GnP paper), 1 g $KMnO_4$ was added into the GnP R10 suspension, stirred for 10 min, then placed into a microwave oven (1200 W) for 3 min, after cooling down to room temperature, an excess of hydrochloric acid (0.5 mol L^{-1}) was used to remove MnO_2 particles attached on the surface of the GnP platelets, followed by RO water

to wash and neutralize the treated sample. After the acid wash to remove the attached MnO_2, pores were formed in the GnP nanoplatelets (shown in Figure 4.3), which were then processed in water for making GnP paper following the same procedures [33].

$$4MnO_4^- + 3C + H_2O \leftrightarrow 4MnO_2 + CO_3^{2-} + 2HCO_3^- \quad (2)$$

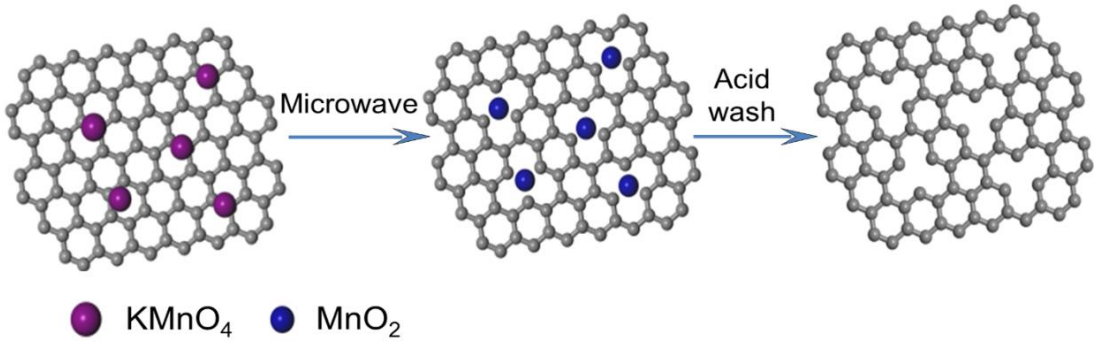

Figure 4.3. The mechanisms for GnP react with KMnO4 under microwave irradiation [33]

4.2.2 Preparation for actuating electrodes

All the GnP based papers were compressed with a Carver press at 500 pounds (3.4 psi). The pressed GnP paper was placed on the Teflon sheet and transferred to the doctor blade workstation. A copper electrode tape was attached to each GnP paper as the conductive electrode and the mixture of Epon828 and curing agent Jeffamine D2000 (at the stoichiometry ratio) was applied to the GnP paper with the doctor blade gap set to ~0.45 mm, producing an epoxy insulating GnP paper with fixed thickness epoxy layer on both sides. The coated electrode was placed into the vacuum oven to degas for 10min before curing. The curing process was 80 ˚C for 2 h and 125 ˚C for 3 h.

4.2.3 Actuating performance test

All the tested composite papers were cut into rectangular shapes 50 mm in length and 12 mm in width. Two copper tapes were clamped on the GnP paper to form one electrode at high voltage output, and the other electrode was connected to ground (the length of the copper tape and clamped position were fixed). Actuating voltage were selected as 6.5 kV, 7.5 kV, 10 kV and 12.5 kV (the actuation was shown in Figure 4.4). The separation distance between the free ends (bottom and top) of two GnP composite papers was recorded through reading from digital photos and summarized in Figure 4.7 After each run, the voltage was turned off and the composite paper electrodes were grounded to dissipate the residual charge left on the surface of the paper. The cross-section morphology of the GnP hybrid paper was examined using a ZEISS Focused Ion Beam Scanning Electron Microscope operated at 12 kV. The flexural properties were determined using Dynamic Mechanical Analyzer, 3-point bending mode, which was performed at a load speed of 0.1 N min^{-1}.

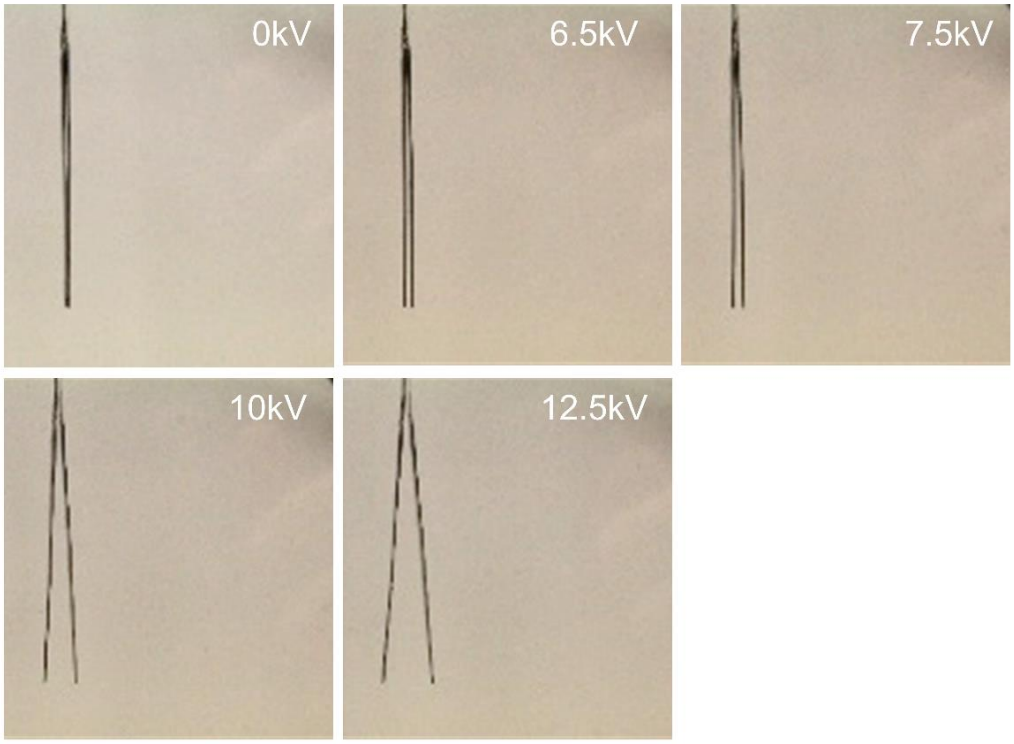

Figure 4.4. Actuating process under different voltages (Sample: Porous GnP R10 paper)

4.3 Results and Discussion

4.3.1 SEM characterization of GnP papers

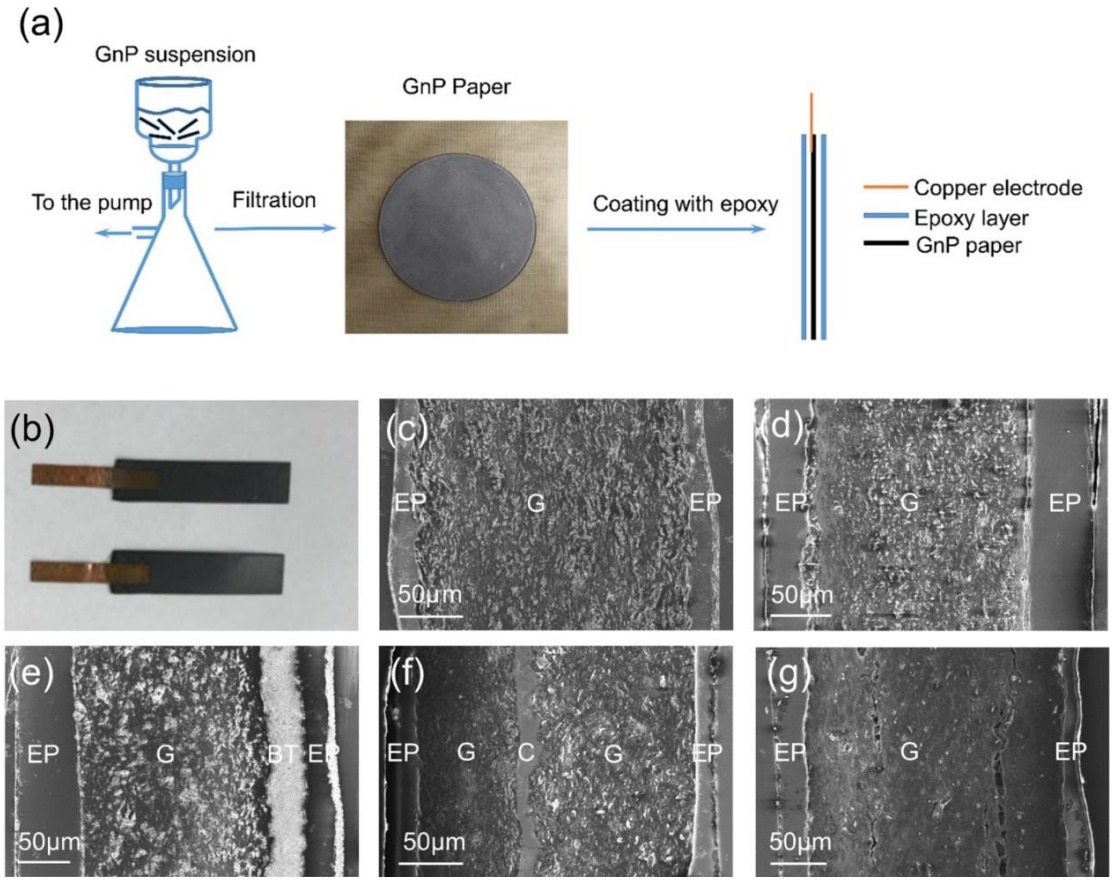

Figure 4.5. SEM images: (a) Schematic of GnP composite paper preparation; (b) Digital photo of GnP composite paper; (c)-(g) Cross-section images for GnP R10, GnP R10/CNC, GnP R10/BT particles, GnP R10/C750, Porous GnP R10 composite paper (EP: epoxy; G: GnP layer; BT: Barium titanate; C: GnP C750)

Figure 4.5 summarizes the process for making the GnP paper and using a doctor blade to coat both sides with epoxy. Figure 4.5 (c) to (g) represented the cross-section for five different kinds of the hybrid GnP papers. All the papers have a 3-layer structures, one GnP layer insulated by two epoxy layers. For Figure 4.5(e) and (f), barium titanate particles have been added as a layer and a GnP C750 layer were created at the outside or in the center of GnP R10 layer in order

to improve the relative permittivity or surface area of the electrode. During the coating process, epoxy will penetrate the GnP paper, which leads to some slight thickness variation of the epoxy layer, but epoxy layers with similar thicknesses were selected to eliminate that effect.

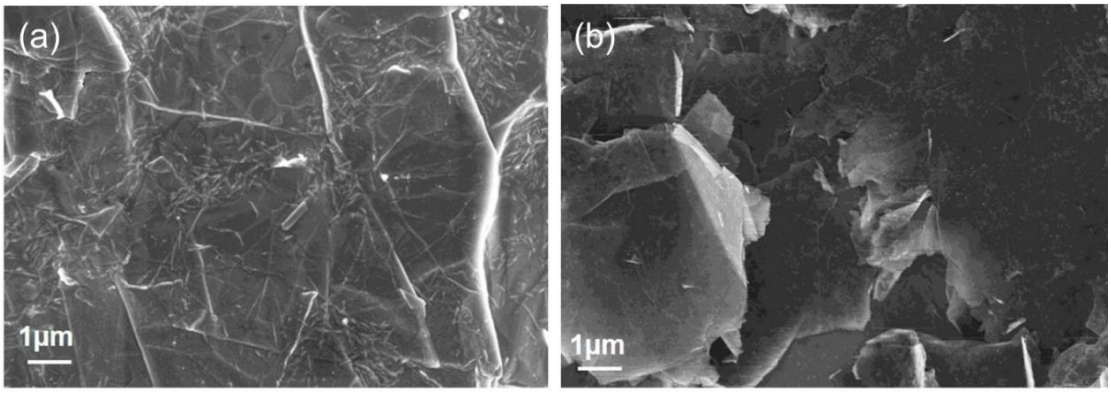

Figure 4.6. Micro-structure of functionalized GnP: (a) Cellulose-GnP; (b) KMnO4 treated GnP

Figure 4.6 represents the microstructures for GnP under two different treatments, in Figure 4.6 (a), it is clear that a large amount of cellulose nanocrystals have attached to the surface of the GnP nanoplatelets. These nanocrystals served as spacers to keep the GnP from aggregating during filtration/drying process and also increased the dielectric properties for the cellulose-GnP composite paper. For Figure 4.6 (b) represents the GnP nanoplatelets after $KMnO_4$ treatment. The $KMnO_4$ reacted with GnP which led to porous structure and even after several washings with of hydrochloric acid, there were some residual MnO_2 particles left after reaction. Other publications proposed that MnO_2 will increase the capacitance of the GnP based electrode, which agreed well with improved performance of this material based GnP paper actuator.

4.3.2 Analysis for actuating performance

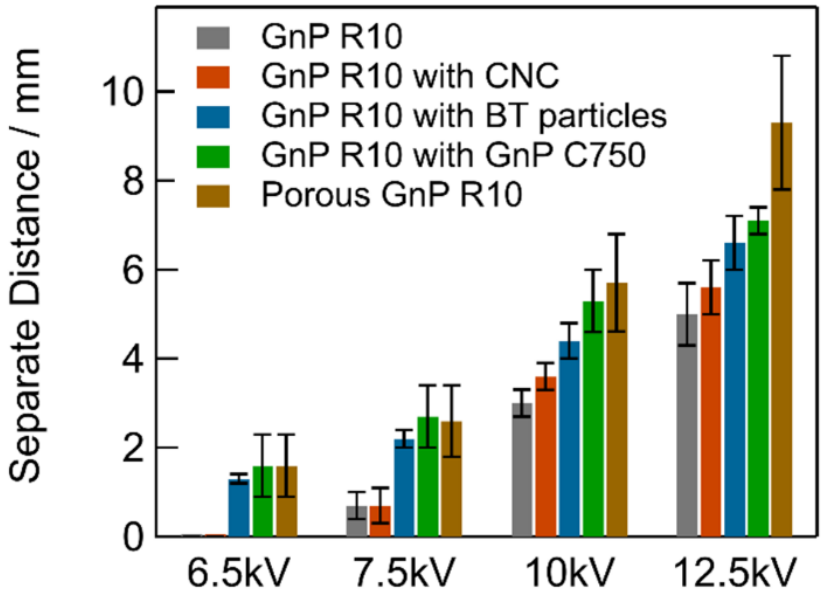

Figure 4.7. Separation distance between the bottom free ends of two composite paper electrodes

The actuating performance of the separate distance between bottom free ends was summarized in Figure 4.7. The GnP based composite paper free ends immediately separated as the voltage was applied. The composite paper did not deform during the test and the length of the GnP composite paper was the same for all of the different samples. As the final weight for each composite paper was different, the potential energy was calculated to compare the electrode performance rather than the separation distance. The potential energy represents the output work for each actuator. When a voltage of 12.5 kV was applied, the composite paper which produced the largest separation distance, was selected for calculation and comparison. In Figure 4.8 (b) the potential energy change was summarized under 12.5 kV.

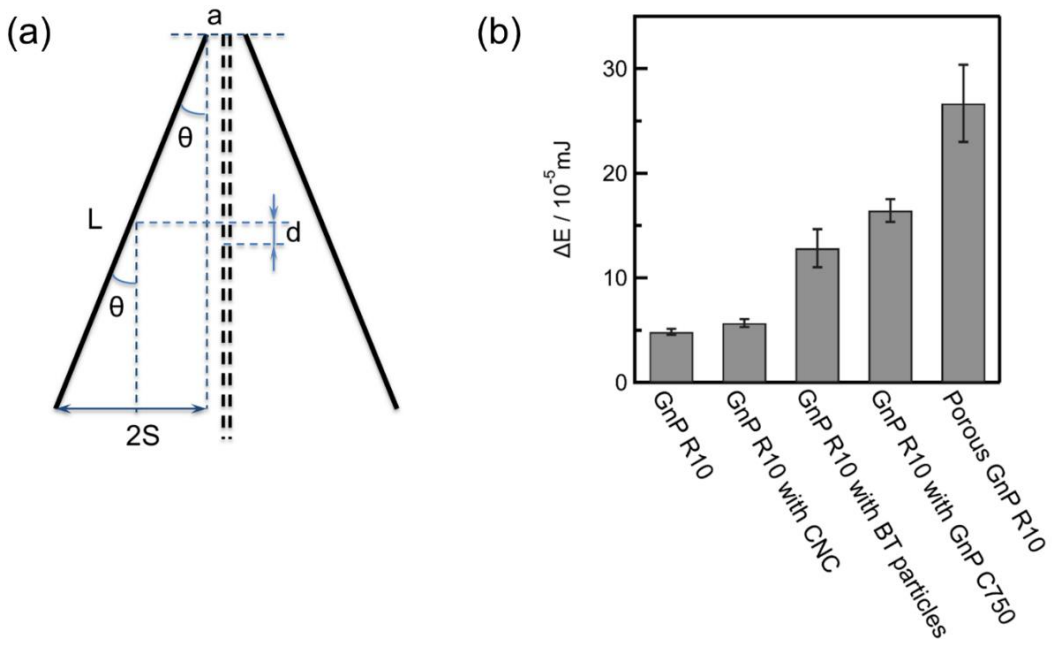

Figure 4.8. The potential energy changes (ΔE) for each hybrid GnP paper under 12.5kV: (a) Schematic illustration for calculation; (b) Calculated results

The potential energy was calculated based on the mechanism shown in Figure 4.8 (a), L is the length of GnP composite paper, 2a is separation distance on the top part. 4S plus 2a is the separation distance at the bottom (K). Both '2a' and 'K' could be read from digital photographs.

$$\sin\theta = {}^{2S}/_{L} = {}^{(K-2a)}/_{2L} \tag{3}$$

For the lift distance calculated from the gravity center

$$d = {}^{L(1-\cos\theta)}/_{2} \tag{4}$$

And the potential energy is calculated as

$$E = mgd \tag{5}$$

Based on the results, it shown that GnP R10 with 10wt% CNC hybrid paper, GnP R10 coated with BT particles hybrid paper, GnP R10 with 10wt% C750 sandwich structure hybrid paper,

porous GnP R10 paper all gave improvements in the potential energy change (output work) by 17.6%, 165.6%, 240.1% and 451.9%.

The GnP R10 based electrode with initial surface area of 14.5 $m^2 g^{-1}$ increased in surface area to 46.2 $m^2 g^{-1}$ (BET result) after the $KMnO_4$ microwave treatment. Adding GnP C750 into the GnP R10, the surface area increased to 31.2 $m^2 g^{-1}$. The combination of GnP R10 and C750, increased the surface area allowing a higher charge to accumulate, which improved the electrostatic repulsive force and led to a larger separation distance. For the GnP R10/BT particles hybrid paper, a thin BT layer with thickness around 25 μm was added, calculations show that the effective relative permittivity increased from 3.5 to 7.7, which leads to an improvement in capacitance due to a higher accumulation of electrons on the surface of electrodes. GnP R10 with 10wt% CNC hybrid composite paper also showed a 17.6% improvement. This could be attributed to two aspects. First the cellulose nanocrystals act as spacer between adjacent GnP nanoplatelets during the filtration and drying process, which result in a more accessible surface area. Second the cellulose has a higher relative permittivity (~7.5) than the epoxy matrix (~3.5), which would also increase the relative permittivity for the insulating layer between two electrodes. However, these two factors, either the increase in surface area or relative permittivity results in only 17.6% improvement.

Table 4.1. Surface area and relative permittivity of GnP paper and its derivatives

Surface area ($m^2 g^{-1}$)		**Relative permittivity**	
GnP R10	14.5	Epoxy	3.5
Porous GnP R10	46.2	GnP R10-BT particles	7.7
GnP R10-C750	31.2	Cellulose	7.5

4.3.3 Flexural properties of GnP based papers

Figure 4.9 summarizes the flexural properties of the GnP hybrid composite papers. The largest improvements were measured for the GnP R10/CNC composite paper, which increased ~440% in modulus and ~93% in strength. It was found that the cellulose nanocrystals attached to the GnP nanoplatelets, which reinforces the mechanical properties of the GnP paper and improves the interfacial bonding between GnP paper and epoxy matrix. The GnP R10/C750 composite paper produced a smaller ~15% increase in modulus and ~19% in strength, which was attributed to the formation of the dense GnP C750 layer between two R10 layers. The mechanical properties of the composite paper can be easily modified by varying the epoxy matrix properties via using different curing agents. In this paper, curing agent Jeffamine D2000(Mw~2000 g mol^{-1}) was used, as this cured epoxy was very low in modulus and flexible to produce an actuator with flexible properties. The matrix can be adjusted to over 3 GPa in modulus and 125 MPa in strength by changing the curing agent alone.

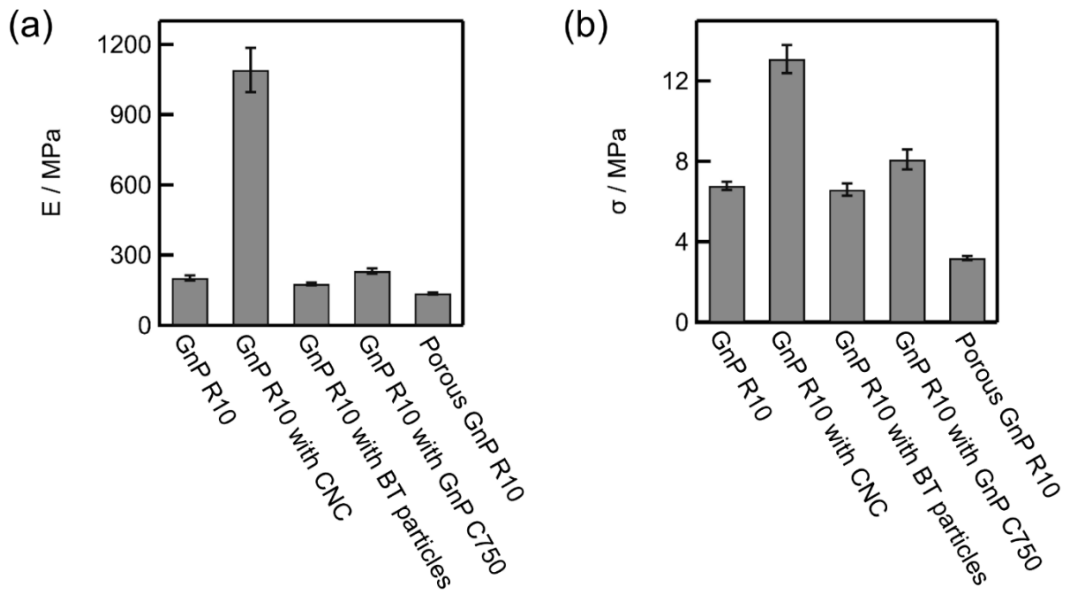

Figure 4.9. The Flexural properties for GnP composite paper: (a). Flexural modulus; (b). Flexural Strength

4.4 Structure design for improving the actuator performance

From the above results, it can be seen that after modification of the GnP paper with various surface treatments, the performance of GnP paper based actuator improved and output energy increased, however, there a high actuating voltage was required and actuating separate distance was not satisfying. Other possible modifications besides treatments of electrode materials, was design of the actuator structure, i.e. combining multiple small actuators and accumulating the stroke and output force.

Designs based on comb drive [34] and multi-layer [35] designs have been proposed.

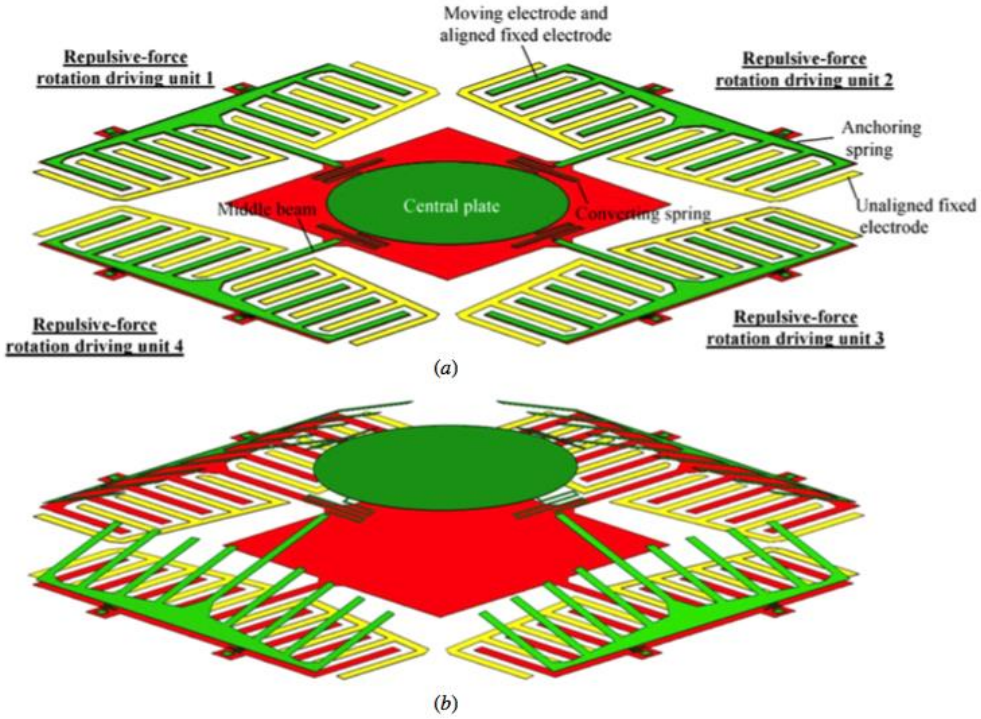

Figure 4.10. Principle of operation of the large stroke actuator. (a) No voltage is applied to the actuator. (b) A voltage is applied to all driving units [34]

As shown in Figure 4.10, the actuator was consisted of moving finger electrodes, aligned fixed finger electrodes and unaligned fixed finger electrodes. When the voltage was applied, the moving fingers and aligned fixed fingers have the same potentials while the unaligned fingers were subjected to different potentials. The horizontal force is balanced but a net force in the vertical direction is produced which pushes the center mass plate upward

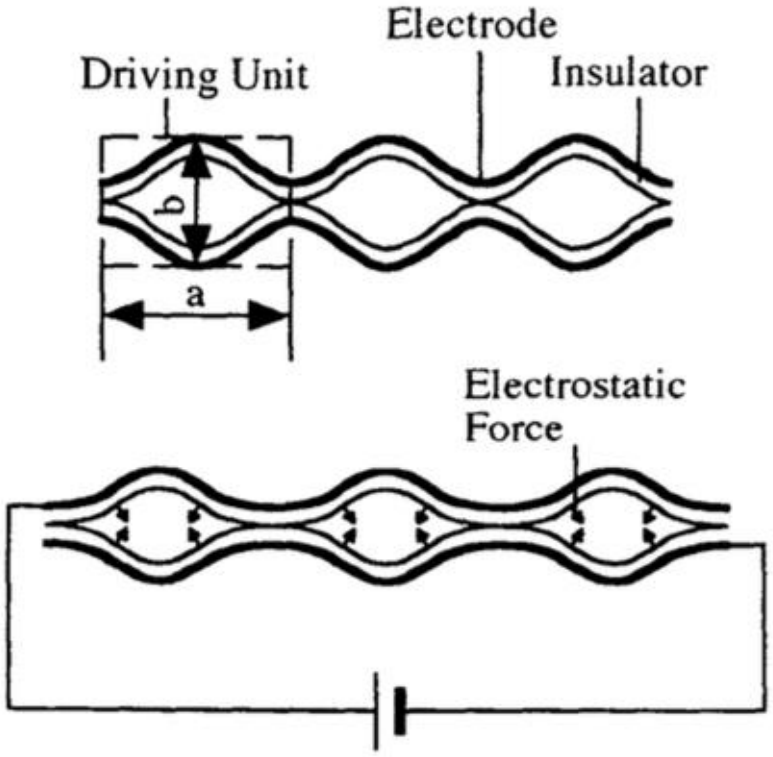

Figure 4.11. Driving units of the actuator [36]

Another design example is the distributed electrostatic actuator [36], as shown in Figure 4.11, this kind of actuator consists of several driving units. Each unit has wave-like electrodes, which are insulated; each unit had two connecting points as the starting position of deformation. When the voltage was applied at these points, the electrostatic force can be generated, and since there were many small units connected in series and parallel, the force and stroke could be increased to achieve a high value.

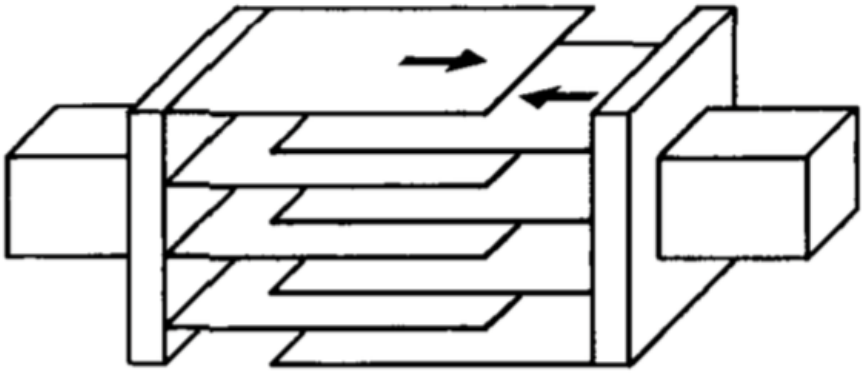

Figure 4.12. Schematic figure of multi-layered film actuator [35]

Based on a similar idea, a multi-layered film actuator was developed, shown in Figure 4.12. The key concept is that theoretically, the total force can be increased by reducing the size of each elements and increasing the number of the elements. In this film actuator, numerous films were connected to a multitude of electrodes and stacked together to form the entire actuator, which achieved increased surface area per unit volume and when the voltage was applied, the accumulated capacitance increases the output force.

The basic GnP paper actuator could be used as the electrode in these designs would improve actuating performance, and as a result, lower the actuating voltage and increasing the actuating stroke.

4.5 Conclusion

Currently, the performance of electrostatic actuators is limited due to small actuating distance and the high voltage required for the actuating motion. This research has shown that a graphene

nanoplatelet composite paper could be utilized as an electrode in a macro-actuator with significant improvements in actuating distance. The actuator distance can produce a large increase from micrometer to millimeter displacement. And the potential energy change (output work) could be improved up to over 400%. The actuator performance is improved based on the surface area of the electrode materials and the value of the relative permittivity of the insulating layer.

REFERENCES

REFERENCES

[1] O'Halloran A, O'malley F, McHugh P. A review on dielectric elastomer actuators, technology, applications, and challenges. Journal of Applied Physics. 2008 Oct 1;104(7):9.

[2] Mohamed A, Elsimary H, Ismail M. Analysis, and optimization of a CMOS vertical thermal actuator. InSymposium on Design, Test, Integration and Packaging of MEMS/MOEMS 2003. 2003 May 5 (pp. 214-217). IEEE.

[3] Popa DO, Kang BH, Wen JT, Stephanou HE, Skidmore G, Geisberger A. Dynamic modeling and input shaping of thermal bimorph MEMS actuators. In2003 IEEE International Conference on Robotics and Automation (Cat. No. 03CH37422) 2003 Sep 14 (Vol. 1, pp. 1470-1475). IEEE.

[4] Syms RR. Long-travel electrothermally driven resonant cantilever microactuators. Journal of Micromechanics and Microengineering. 2002 Mar 22;12(3):211.

[5] Zou Q, Sridhar U, Lin R. A study on micromachined bimetallic actuation. Sensors and Actuators A: Physical. 1999 Dec 14;78(2-3):212-9.

[6] Yang Y, Zhou Z, Ye X, Jiang X. Bimetallic thermally actuated micropump. InThe 1996 ASME International Mechanical Engineering Congress and Exposition, Atlanta, GA, USA, 11/17-22/96 1996 (pp. 351-354).

[7] Dosch JJ, Inman DJ, Garcia E. A self-sensing piezoelectric actuator for collocated control. Journal of Intelligent material systems and Structures. 1992 Jan;3(1):166-85.

[8] Trolier-McKinstry S, Muralt P. Thin film piezoelectrics for MEMS. Journal of Electroceramics. 2004 Jan 1;12(1-2):7-17.

[9] Kim SG, Priya S, Kanno I. Piezoelectric MEMS for energy harvesting. MRS bulletin. 2012 Nov;37(11):1039-50.

[10] Choi WJ, Jeon Y, Jeong JH, Sood R, Kim SG. Energy harvesting MEMS device based on thin film piezoelectric cantilevers. Journal of Electroceramics. 2006 Dec 1;17(2-4):543-8.

[11] Hung ES, Senturia SD. Extending the travel range of analog-tuned electrostatic actuators. Journal of microelectromechanical systems. 1999 Dec;8(4):497-505.

[12] Zhang WM, Yan H, Peng ZK, Meng G. Electrostatic pull-in instability in MEMS/NEMS: A review. Sensors and Actuators A: Physical. 2014 Aug 1;214:187-218.

[13] Mitcheson PD, Miao P, Stark BH, Yeatman EM, Holmes AS, Green TC. MEMS electrostatic micropower generator for low frequency operation. Sensors and Actuators A: Physical. 2004 Sep 21;115(2-3):523-9.

[14] Donald BR, Levey CG, McGray CD, Paprotny I, Rus D. An untethered, electrostatic, globally controllable MEMS micro-robot. Journal of microelectromechanical systems. 2006 Feb;15(1):1-5.

[15] Wright JA, Tai YC, Chang SC. A large-force, fully-integrated MEMS magnetic actuator. InProceedings of International Solid State Sensors and Actuators Conference (Transducers' 97) 1997 Jun 16 (Vol. 2, pp. 793-796). IEEE.

[16] Miller RA, Tai YC, Xu G, Bartha J, Lin F. An electromagnetic MEMS 2/spl times/2 fiber optic bypass switch. InProceedings of International Solid State Sensors and Actuators Conference (Transducers' 97) 1997 Jun 16 (Vol. 1, pp. 89-92). IEEE.

[17] Wang P, Tanaka K, Sugiyama S, Dai X, Zhao X, Liu J. A micro electromagnetic low level vibration energy harvester based on MEMS technology. Microsystem technologies. 2009 Jun 1;15(6):941-51.

[18] Cho IJ, Song T, Baek SH, Yoon E. A low-voltage and low-power RF MEMS series and shunt switches actuated by combination of electromagnetic and electrostatic forces. IEEE Transactions on Microwave Theory and Techniques. 2005 Jul;53(7):2450-7.

[19] Kulkarni S, Koukharenko E, Torah R, Tudor J, Beeby S, O'Donnell T, Roy S. Design, fabrication and test of integrated micro-scale vibration-based electromagnetic generator. Sensors and Actuators A: Physical. 2008 Jul 1;145:336-42.

[20] Ho CM, Tai YC. Micro-electro-mechanical-systems (MEMS) and fluid flows. Annual review of fluid mechanics. 1998 Jan;30(1):579-612.

[21] Srikar VT, Spearing SM. Materials selection for microfabricated electrostatic actuators. Sensors and Actuators A: physical. 2003 Jan 1;102(3):279-85.

[22] Judy JW. Microelectromechanical systems (MEMS): fabrication, design and applications. Smart materials and Structures. 2001 Nov 26;10(6):1115.

[23] Ito M, Saneyoshi K. An attempt to make a large-scale stacked-type electrostatic actuator for artificial muscles of robots. In2012 IEEE International Conference on Robotics and Biomimetics (ROBIO) 2012 Dec 11 (pp. 1182-1187). IEEE.

[24] Madou MJ. Fundamentals of microfabrication: the science of miniaturization. CRC press; 2002 Mar 13.

[25] Novoselov KS, Geim AK, Morozov SV, Jiang D, Zhang Y, Dubonos SV, Grigorieva IV, Firsov AA. Electric field effect in atomically thin carbon films. science. 2004 Oct 22;306(5696):666-9.

[26] Lee C, Wei X, Kysar JW, Hone J. Measurement of the elastic properties and intrinsic strength of monolayer graphene. science. 2008 Jul 18;321(5887):385-8.

[27] Balandin AA, Ghosh S, Bao W, Calizo I, Teweldebrhan D, Miao F, Lau CN. Superior thermal conductivity of single-layer graphene. Nano letters. 2008 Feb 20;8(3):902-7.

[28] Geim AK, Novoselov KS. The rise of graphene. Nature materials. 2007 March; 6:183-191.

[29] Fukushima H. Graphite nanoreinforcements in polymer nanocomposites. Michigan State University; 2003.

[30] Park S, An J, Suk JW, Ruoff RS. Graphene-based actuators. Small. 2010 Jan 18;6(2):210-2.

[31] Liang J, Xu Y, Huang Y, Zhang L, Wang Y, Ma Y, Li F, Guo T, Chen Y. Infrared-triggered actuators from graphene-based nanocomposites. The Journal of Physical Chemistry C. 2009 May 11;113(22):9921-7.

[32] XG Science Inc, 3101 Grand Oak Drive, Lansing, MI. http://xgsciences.com

[33] Fan Z, Zhao Q, Li T, Yan J, Ren Y, Feng J, Wei T. Easy synthesis of porous graphene nanosheets and their use in supercapacitors. Carbon. 2012 Apr 1;50(4):1699-703.

[34] He S, Mrad RB, Chong J. Repulsive-force out-of-plane large stroke translation micro electrostatic actuator. Journal of Micromechanics and Microengineering. 2011 Jun 1;21(7):075002.

[35] Egawa S, Higuchi T. Multi-layered electrostatic film actuator. InIEEE Proceedings on Micro Electro Mechanical Systems, An Investigation of Micro Structures, Sensors, Actuators, Machines and Robots. 1990 Feb 11 (pp. 166-171). IEEE.

[36] Yamaguchi M, Kawamura S, Minami K, Esashi M. Distributed electrostatic micro actuator. In[1993] Proceedings IEEE Micro Electro Mechanical Systems 1993 Feb 7 (pp. 18-23). IEEE.

CHAPTER 5 - SUMMARY AND FUTURE WORK

5.1 Summary

The research presented in this thesis focused on using graphene nanoplatelets (GnP) as filler to make polymer nanocomposites and investigated their multiple applications. The GnP possesses remarkable mechanical property, high thermal and electrical conductivity, and based on its unique 2D structure, it can be used to modify the gas barrier property of polymers. Two types of polymers, thermoplastic polyurethane (TPU) and epoxy, were selected to analyze and determine the multiple properties of GnP - polymer composites were improved.

In Chapter 2, a stretchable, thermally conductive polymer composite film was prepared by incorporating 25wt% graphene nanoplatelets into the thermoplastic polyurethane matrix through an industrial extrusion process. The influence of GnP dispersion and alignment on thermal conductivity, oxygen barrier properties, and static and dynamic mechanical properties of the composite films were investigated. The dispersion and alignment of GnP were adjusted through controlling the film extrusion speed. Three speeds were selected: 2FPM, 3FPM and 5FPM. Scanning electron microscopy was used to investigate the dispersion and alignment of GnP. When the materials exited the die, the GnPs were randomly distributed in the TPU matrix, after elongation and compression by passing through the rollers, the GnPs tended to be aligned along the film extrusion direction. With higher film extrusion speed, GnPs were better aligned and concentrated along the center line of the extrusion film as a result of the Poisson effect which caused shrinkage in the transverse direction. At the higher roller speed, more gaps formed between the GnPs and the matrix. However, compared to the neat TPU, the extruded film having the best results showed a 350% increase in thermal conductivity and a 75% reduction for oxygen

barrier property. Two consequent stress-strain cycles were conducted to analyze the Mullins effect and ability of the composite films to maintain their mechanical properties after each cycle. At 25 °C, the 2FPM sample produced ~950% and ~470% improvements in tensile modulus and strength in the extrusion direction compared to the neat TPU. The properties in the transverse direction decreased ~38% in modulus and strength. The tensile modulus and strength calculated from second stress-strain curve were ~35%, 6% lower compared to the results from first cycle. A temperature sweep produced with the DMA from -80 °C to 80 °C showed that below ~-40 °C, the storage modulus of the composite films had much higher values compared to neat TPU. At -80 °C the storage modulus of the composite films at least improved ~260% and ~180% in the extrusion and transverse directions. The glass transition temperature of the composite films was only ~ 4 °C higher than neat TPU, which could be improved by an increase in the interfacial bonding between the GnPs and TPU and is a subject for additional research.

Chapter 3 focused on modifying the interfacial properties between GnP fillers and the epoxy matrix. Graphene oxide (GO) was prepared using the Improved Hummers' method, which created oxygen based functional groups on its basal plane. GO was considered to act as a coupling agent with the basal plane of GO attracted to the GnP surface, while the oxygen functional group could bond with the epoxy resin. GnP was sonicated in the GO suspension to make the GO-GnP couple in the presence of two diamines with different chain length (p-phenylenediamine (PPDA) and Jeffamine D2000) to achieve functionalized GO-GnP couple (f-(GO-GnP)). Composites prepared with two weight ratio of GO and GnP, 1:10 and 1:50. The GO-GnP couple or the f-(GO-GnP) couple were added to the epoxy to produce composites with two loadings, 0.43wt% and 0.86wt%. The tensile modulus of the PPDA-f-(GO-GnP: 1:10) sample exhibited a ~40% improvement at the 0.43wt% concertation which increased to ~60% at

the 0.86wt% loading. All the composites using the GO-GnP couple or the f-(GO-GnP) couple produced up to a 110% enhancement in toughness compared to simply using GnP at 0.86wt%. These results suggested GO/f-GO functioned as a coupling agent which improved the dispersion and interfacial properties between GnP and epoxy matrix which in turn increased the tensile modulus/strength of the composite and the resistance to crack growth.

In chapter 4, the novel application of GnP paper used as electrostatic actuator was investigated. GnP paper was prepared through a filtration of a GnP suspension. Electrodes were fabricated from the compressed GnP paper which were then coated with epoxy on both sides. The electrostatic actuator was constructed from two parallel-aligned composite GnP papers fixed at the anode of a high power supply and the cathode was connected to ground. The two composite paper electrodes would separate when applying the voltage, then returned to their original position when the voltage was reduced. This actuator could be used as small motor, robot finger or switch. Traditional electrostatic actuators were manufactured in micrometer size, the research goal here was to improve the actuating range and lower the actuating voltage. The modifications investigated were: increasing the surface area of the electrode; improving the relative permittivity of insulating layer; or combining these two factors together. Porous GnP paper of two sizes of GnPs (R10 and C750), were used to prepare the electrode. In order to enhance the relative permittivity, barium titanate particles (BT) were coated on the GnP paper surface; and cellulose nanocrystals (CNC) was added in the composition of the GnP paper. The CNC provided space between the GnPs during the filtration process, maintaining the surface area of GnP paper and improving the relative permittivity. After these modifications, the separation distance of the electrode ends was recorded, and the potential energy was calculated to compare the electrode performance. Compared to GnP R10 paper based actuator, GnP R10 with 10wt%

CNC hybrid paper, GnP R10 coated with BT particles hybrid paper, GnP R10 with 10wt% C750 sandwich structure hybrid paper, porous GnP R10 paper gave improvements in the potential energy of 17.6%, 165.6%, 240.1% and 451.9%. Although the best result showed an over 400% improvement, the actuating voltage was still in kilovolt range. Future improvements could be made based on these results such as fabricating a comb drive or multi-layer structure. In these designs, several actuating units can be assembled together to accumulate the output force, distance and lower the actuating voltage.

The overall results of this work helped to demonstrate that GnPs added to polymers can greatly improve the mechanical properties, thermal conductivity, and gas barrier performance of the polymer matrix.

5.2 Future Work

5.2.1 Modify the interfacial property between GnP and the polymer

The interfacial property plays an important role in reinforcing a polymer composite. For the GnP-TPU composite investigated here, low interfacial properties lead to mechanical property reduction after several stress-strain cycles. During the manufacturing process, higher film extrusion speeds also cause delamination happened which limits the minimum thickness that the composite film can reach. The glass transition temperature and the gas barrier property also depends on the interfacial properties between GnP and the polymer requiring more modification in the future, such as surface treatment of GnP or using GO as the coupling agent. In reviewing the results from chapter 3, even though the tensile modulus improved significantly using the diamine functionalized GO-GnP couple as filler, the tensile strength was maintained at the same

level as neat epoxy. Several more modifications can be considered, like the optimal ratio between GO and GnP; using different length of diamines to treat the filler surface; using other polymer chains to do the surface treatment and if possible.

5.2.2 Synergistic effect between different carbon materials

For GnP-TPU composite film, the goal was to improve its through-plane thermal conductivity, the 2D structure of GnP limits the number of conductive paths formed between adjacent GnPs. Other carbon materials with different shape factors can be combined with GnPs such as carbon fiber or carbon nanotubes. These 1D materials can easily bridge between two neighboring GnPs and enhance the through plane thermal conductivity. Also, the GO has been shown to be an effective coupling agent for improving properties of GnP/epoxy composite.

5.2.3 Improving the thermal convection for composite film

GnP was incorporated into the TPU matrix to improve the thermal conductivity. Improvements in thermal convection is another factor for improving the heat transfer efficiency. Features can be created onto the surface of the composite film through placing the composite film onto a topographically designed positive mold and heating above the softening point of the composite film and compressively forming this material. Since the addition of these features on the surface can improve the turbulence of a heat transfer fluid, the density, alignment, shape of features, can be optimized through a computational approach. Since GnP possesses high thermal conductivity, a topographically modified GnP paper can be used to attach to the surface of a heat releasing device and integrated into a cooling system. Roll to roll or 3D printing are candidate processes for industrial scale production.

5.2.4 Structure design of a GnP electrostatic actuator

Investigation of the design of electrodes for electrostatic actuators identified modifications of the electrode materials. Comb drive and multi-layer actuators can be utilized to amplify the electrostatic actuator performance. However, additional improvements in the surface area of electrode materials, relative permittivity of the insulating layer and creating a better way to combine several actuating units together, in order to lower the actuating voltage and enhance the actuating stroke will be required.

5.2.5 Large scale production of graphene oxide

Graphene with its outstanding mechanical property, thermal and electrical conductivity and gas barrier property is considered as an optimal filler for the polymer in the past several years. Graphene oxide produced through treating graphene with strong acid and oxidant to add multiple oxygen based functional groups on its surface has been shown to be a possible coupling agent between the GnP and the polymer. However, the large scale production of GO needs to be developed. A fast, clean, less toxic and cost effective way is waiting to be put forward.